HHS Public Access

Author manuscript

Prog Retin Eye Res. Author manuscript; available in PMC 2021 January 01.

Published in final edited form as:

Prog Retin Eye Res. 2020 January ; 74: 100773. doi:10.1016/j.preteyeres.2019.100773.

Scleral structure and biomechanics

Craig Boote[1,2,3], **Ian A. Sigal**[4], **Rafael Grytz**[5], **Yi Hua**[4], **Thao D. Nguyen**[6], **Michael J. A. Girard**[2,7]

[1]Structural Biophysics Research Group, School of Optometry & Vision Sciences, Cardiff University, UK.

[2]Ophthalmic Engineering & Innovation Laboratory, Department of Biomedical Engineering, National University of Singapore, Singapore.

[3]Newcastle Research & Innovation Institute, Singapore.

[4]Laboratory of Ocular Biomechanics, Department of Ophthalmology, University of Pittsburgh, USA.

[5]Department of Ophthalmology & Visual Sciences, University of Alabama, USA.

[6]Department of Mechanical Engineering, Johns Hopkins University, USA.

[7]Singapore Eye Research Institute, Singapore National Eye Centre, Singapore.

Abstract

As the eye's main load-bearing connective tissue, the sclera is centrally important to vision. In addition to cooperatively maintaining refractive status with the cornea, the sclera must also provide stable mechanical support to vulnerable internal ocular structures such as the retina and optic nerve head. Moreover, it must achieve this under complex, dynamic loading conditions imposed by eye movements and fluid pressures. Recent years have seen significant advances in our knowledge of scleral biomechanics, its modulation with ageing and disease, and their relationship to the hierarchical structure of the collagen-rich scleral extracellular matrix (ECM) and its resident cells. This review focuses on notable recent structural and biomechanical studies, setting their findings in the context of the wider scleral literature. It reviews recent progress in the development of scattering and bioimaging methods to resolve scleral ECM structure at multiple scales. In-vivo and ex-vivo experimental methods to characterize scleral biomechanics are explored, along with computational techniques that combine structural and biomechanical data to simulate ocular behaviour and extract tissue material properties. Studies into alterations of scleral structure and biomechanics in myopia and glaucoma are presented, and their results reconciled with associated findings on changes in the ageing eye. Finally, new developments in scleral surgery and emerging non-invasive therapies are highlighted that could offer new hope in the fight against escalating scleral-related vision disorder worldwide.

Correspondence: Craig Boote, PhD, Structural Biophysics Research Group, School of Optometry & Vision Sciences, Cardiff University, Maindy Road, Cardiff CF24 4HQ, UK, Tel: +44 (0)2920 874859, bootec@cardiff.ac.uk.

Keywords

sclera; connective tissue structure; biomechanics; myopia; glaucoma; ageing

1. Introduction

Forming around 85% of the outer tunic of the human eyeball, the sclera is a remarkably resilient and structurally complex connective tissue that performs multiple functions critical to vision. Derived from the Greek word “skleros” (meaning “hard”), the sclera’s primary role is to provide a firm and stable substrate for the retina and to protect the other mechanically vulnerable internal structures of the eye, while its opacity prevents off-axial light transmission that could otherwise degrade the retinal image. Scleral and corneal geometry are cooperatively regulated to accurately focus light onto the retina. Although under normal conditions the sclera can be considered metabolically quiescent, it is far from inert in a biomechanical sense. Indeed, it is required to maintain optical stability under highly dynamic loading conditions imposed externally and internally by, amongst other factors, eye movements and a continually fluctuating intraocular pressure (IOP). The sclera’s ability to resist deformations that might otherwise impair vision through distortion of the retina or the lens-iris diaphragm relies on biomechanical characteristics imparted by regional specializations of its connective tissue organization. In recent years, widening collaboration between clinicians, scientists and engineers has led to significant advances in our understanding of dynamic scleral behaviour. Naturally it follows that we are beginning to perceive with more clarity the central role that the sclera plays in conditions that deteriorate vision. This article aims to summarize and reconcile the findings of these studies as it reviews our current knowledge of scleral structure and biomechanics, their implications in ageing and disease, and explores some promising therapeutic avenues in search of novel scleral treatments.

1.1 Basic scleral anatomy and function

At its anterior boundary the sclera merges with the corneal perimeter at the limbus and extends backward to form an approximate sphere of vertical diameter ~24mm. The axial length of the emmetropic adult human eye is 24–25mm. At the back of the eye, the scleral connective tissue fuses with the dural sheath of the optic nerve, whose entry pierces the sclera about 3mm nasally and 1mm downward of the posterior pole. Scleral thickness varies with anatomical position, decreasing from 1–1.3mm at the posterior pole to ~0.5mm at the equator, before increasing again to ~0.8mm in the perilimbal sclera. (Fig 1A).

1.1.1 Tenon’s capsule—Tenon’s capsule (*fascia bulbi*) is a compact layer of radial collagen bundles that lie parallel to the scleral surface. At its anterior origin, Tenon’s capsule is anchored firmly to the underlying episclera and the overlying conjunctiva, before becoming more loosely bound to the episclera further back as the capsule coalesces with the perimysium of the recti muscles. Biomechanically, the Tenon’s capsule fulfils an important function in acting as a pulley system to transfer forces from the ocular muscles to the sclera during eye movements (Roth et al., 2002).

1.1.2 Episclera—Lying directly beneath Tenon's capsule, the episclera is a thin but dense layer of connective tissue consisting mainly of collagen bundles sparsely populated with elastic fibres, melanocytes and macrophages (Watson and Young, 2004). In contrast to the neighbouring Tenon's capsule, collagen bundles of the episclera run largely circumferentially, and render the episclera more difficult to distinguish as a distinct layer by their gradual merging into the connective tissue of the underlying stroma.

1.1.3 Stroma—As the major scleral tissue layer, the stroma (*substantia propria*) dominates the sclera's biomechanical performance. Stromal material properties can be summarized as non-linear viscoelastic, and stem from its collagen-rich extracellular matrix (ECM) composition and organization. Bundles of parallel-aligned individual collagen fibrils of diameter 25–230nm, interspersed in places with elastic microfibrils and fibres, form 0.5–6μm thick lamellae that lie roughly in the plane of the eyeball surface (Fig 1B). Scleral lamellae overall demonstrate far more branching and interweaving than those of the corneal stroma, and the extent of this varies with both tissue depth and anatomical location (Komai and Ushiki, 1991). Superficially, the scleral collagen fibril bundles merge with tendon fibres at the extraocular muscles insertion sites, while in the deepest stromal layers adjacent to the uvea (the *lamina fusca*) they taper and branch to intermingle with the underlying choroidal connective tissue, co-localizing with increased numbers of elastic fibres (Marshall, 1995). Unlike the eyes of humans and other primates, the scleral stroma of many non-eutherian vertebrates comprises an inner cartilage layer in addition to an outer fibrous layer (Walls, 1942). Further, the anterior sclera of many birds, reptiles and teleost fish contains a ring of bony plates (ossicles) (Franz-Odendaal, 2008) that are thought to provide leverage for the ciliary muscles in facilitating corneal accommodation (Glasser et al., 1994), and into which meridional fibril bundles of the anterior sclera insert (Boote et al., 2008). In the human sclera, regional specializations of the stromal architecture, as described below, are of particular biomechanical influence.

1.1.4 Perilimbal sclera, scleral spur and trabecular meshwork—On approaching the limbus, the collagen bundles of the deep scleral stroma form a circumcorneal ring-like structure at the scleral spur. Together with the circumferential limbal pseudo-annulus of collagen residing in the posterior one-third of the corneal stroma (Kamma-Lorger et al., 2010; Newton and Meek, 1998), the spur probably helps to maintain the corneal contour in an area of heightened tissue stress imposed by the differing radii of curvature of the cornea and sclera (Boote et al., 2009). Indeed, the use of partial thickness limbal incisions is an established clinical procedure for inducing controlled flattening of the cornea as a means of correcting mild corneal astigmatism. However not all the scleral collagen appears to end its frontward course at the limbus, and there is evidence that a significant number of perilimbal scleral collagen bundles continue on into the corneal periphery (Boote et al., 2011), some of which probably originate in the deep sclera (Winkler et al., 2013). At its anterior aspect, the collagen fibrils of the scleral spur taper and become continuous with the connective tissue beams of the corneoscleral trabecular meshwork (Watson and Young, 2004). Here, the innermost layers of the spur, the so-called scleral roll, form a bordering substrate for the Schlemm's canal (SC), from whose posterior end an extension of the spur in the direction of the anterior chamber provides an anchor point for attachment of the meridional fibres of the

ciliary muscle to facilitate opening of the trabecular beams during aqueous drainage (Hamanaka, 1989). The corneoscleral trabecular beams are further notable for containing significant amounts of elastin (Marshall, 1995; Umihira et al., 1994) and these are probably continuous with the elastin networks observed in the deep limbus (Kamma-Lorger et al., 2010) and the pre-Descemet's stroma of the corneal periphery (Lewis et al., 2016). The possibility of the corneo-limbal elastin network forming a continuous system with elastic fibres in the sclera is an open question warranting further research.

1.1.5 Peripapillary sclera and lamina cribrosa—

On approaching the optic nerve, superficial layers of the stromal connective tissue merge with the dural sheath of the nerve while the remaining deeper scleral fibres become continuous with the lamina cribrosa (LC) - the highly fenestrated stack of interconnected plates that support the exiting retinal ganglion cell (RGC) nerve axons and central retinal artery (Anderson, 1969). The LC and peripapillary sclera (PPS - the 1–2mm wide region of sclera bordering the nerve canal opening) collectively form the connective tissue of the optic nerve head (ONH) (Fig 1D) - a region of key biomechanical interest in glaucoma (Downs, 2015). Here the scleral collagen fibrils are more uniform in diameter, show greater spatial order and associate with increased numbers of elastin fibres compared to other regions of the posterior segment (Quigley et al., 1991). A key biomechanical feature of the PPS is the circumferential pseudo-annulus of collagen that surrounds the LC (Gogola et al., 2018b; Pijanka et al., 2012; Winkler et al., 2010) that is probably necessary to limit canal expansion under IOP-loading (Girard et al., 2009a; Grytz et al., 2011).

1.2 Scleral composition

The composition of the sclera follows that of other connective tissues in being primarily a scaffold of fibrous collagen in a hydrated interfibrillar matrix of proteoglycans and glycoproteins (Table 1). Notwithstanding notable increases in the lamina fusca, perilimbal sclera and PPS, the overall content of elastin fibres in the sclera is small at around 2% of the dry weight (Watson and Young, 2004). Understandably from a metabolic perspective, the quiescent sclera displays low cellularity with transient increases shown in response to pathology or physical insult.

1.2.1 Collagens—

In the sclera, type I collagen is by far the major contributor at around 95%, with types III , V and VI making up the remaining 5% (Keeley et al., 1984; Thale and Tillmann, 1993). Scleral collagen structure is hierarchical (Fig 2). Tropocollagen molecules of length ~300nm are composed of three polypeptide alpha-helix chains of repeating Gly-X-Y amino acid sequences (Bailey et al., 1998). Five such molecules assemble to form ~4nm diameter collagen microfibrils, in which adjacent molecules are axially staggered by 67nm (the D-period – see Fig 1C and Fig 2) (Piez and Miller, 1974). Parallel arrays of microfibrils assemble into fibrils, such that individual microfibrils are slightly inclined (about 5°) to the fibril axis (Yamamoto et al., 2000). Collagen fibrils, in turn, assemble into irregular bundles that ultimately form the scleral lamellae. Scleral collagen fibrils are heterotypic: studies of macular sclera indicated interstitial collagen fibrils of co-polymerized types I/III, with type V residing at the fibril surface and type VI forming inter-bundle filament structures (Marshall et al., 1993). The presence of types V and VI at and between fibril surfaces

suggests likely roles in fibril assembly and diameter regulation, as envisaged in other tissues (Izu et al., 2011; Linsenmayer et al., 1993; Wenstrup et al., 2004). In contrast to some other connective tissues, such as tendon, collagen in the sclera does not assemble into discrete structures of a regular size beyond the fibril level. However, the general term “fibre” is used widely in the biomechanics literature to refer to the suprafibrillar collagen arrangement of the sclera and will also be used in this review. It should also be noted that some techniques that utilize visible light to examine suprafibrillar scleral microstructure (see s2.1.2 and s2.1.4) will contain both collagen and elastin components in their “fibre” signal.

1.2.2 Proteoglycans—Proteoglycans (PGs) inhabit the collagen interfibrillar space and help to mediate fibril size and organization. PGs consist of a protein core with one or more attached glycosaminoglycan (GAG) sidechains of repeating disaccharide units of either chondroitin sulfate, dermatan sulfate, keratan sulfate or heparin sulfate. The main sulfated PGs present in sclera are aggrecan, decorin and biglycan (Rada et al., 2000; Rada et al., 1997). Sulfate residues on the GAG chains impart negative charge that binds water and creates an incompressible “gel” that is ideal for mediating load transfer between the embedded scleral collagen fibrils. Evidence for the importance of PGs in maintaining scleral structure and biomechanics includes findings from research in knock-out mouse models (Austin et al., 2002; Chakravarti et al., 2003) and from enzyme digestion studies in pig (Murienne et al., 2015; Zhuola et al., 2018) and human (Murienne et al., 2016) sclera. The presence and role of aggrecan in the sclera is not well understood. Aggrecan is a large proteoglycan normally found in cartilage. Due to its many attached glycosaminoglycan sidechains, aggrecan provides osmotic properties that produce a swelling pressure. In cartilage, this swelling pressure plays a critical role in withstanding compression forces, but the importance of this swelling pressure in the sclera is unclear.

1.2.3 Elastic fibres—The elastic fibre network is a proportionately small but functionally important part of the scleral ECM, in particular in the deep tissues of the perilimbal sclera/trabecular meshwork (Marshall, 1995) and throughout the ONH (Quigley et al., 1991) where concentrations are notably increased. Mature scleral elastic fibres consist of an amorphous elastin core sheathed by an aligned scaffold of fibrillin-rich microfibrils. The significance of scleral elastic fibres to the structural integrity, shape and viscoelastic behaviour of the eyeball is not fully understood, but is coming under increasing scrutiny motivated by identified links between systemic microfibril disorders and ocular pathologies such as myopia and glaucoma (Kuchtey and Kuchtey, 2014; Robinson and Booms, 2001).

1.2.4 Fibroblasts—With the exception of the lamina fusca, most regions of the sclera are sparsely populated by cells until challenged by pathology, injury or infection. The resident cell of the scleral stroma is the fibrocyte, which undergoes transformation into the active fibroblast upon insult. Fibroblasts are responsible for synthesis of all scleral ECM components. They respond to mechanical stimuli from their surrounding ECM and there is growing interest in understanding the extent of the role that fibroblasts might play in dynamically regulating scleral biomechanics via matrix remodeling and contractile responses (Harper and Summers, 2015; McBrien et al., 2009) (see s3.3.2). In addition to mechanical stimuli, fibroblasts control scleral remodeling and alter tissue-level

biomechanics in response to a signaling cascade from the retina to the sclera that is ultimately stimulated by vision. This vision-guided response plays a critical role during eye development, determining the final size of the eye (see s4.3).

2. Scleral ECM structure at multiple scales

2.1 Microstructure

Influential studies into the fine structure of the sclera began over eighty years ago with the work of Kokott, who used histological preparations to interpret the gross directions of collagen lamellae across the ocular coat (Kokott, 1934) (Fig 3). While his methods were undoubtedly crude, Kokott's work has largely stood up to scrutiny by more sophisticated techniques and can be considered something of a landmark in beginning the enduring notion that scleral ECM structure is mechanically adapted to regional tensions in the ocular coat. However, the past decade or so has seen significant progress in the development of more quantitative methods to determine scleral microstructure, driven in large part by advances in numerical simulation of ocular biomechanics and the need to optimize models for clinical use by the inclusion of more physiologically accurate data.

2.1.1 Wide-angle X-ray scattering—Wide-angle X-ray scattering (WAXS) is an ex-vivo diffraction-based technique that does not yield an image of the tissue, but instead produces a Fourier transform (WAXS pattern) from which collagen structure parameters can be extracted (Meek and Boote, 2009) (Fig 4A). The main collagen WAXS peak from sclera derives from the regular ~1.6nm lateral separation of tropocollagen molecules within the fibrils (Fig 2). Calibration of the radial position of this peak can be useful to detect changes in intrafibrillar scleral collagen packing, for example as occurs in non-enzymatic cross-linking with age (Malik et al., 1992) (see s4.1). Moreover, because the constituent molecules are aligned near-axially within fibrils, WAXS can obtain a thickness-averaged measure of scleral fibril orientation and anisotropy in the tissue plane, without the need for tissue processing (Fig 4B). Due to its extremely high signal specificity for collagen and tissue averaging capabilities, WAXS has proven highly valuable in supplying extensive amounts of data for use in numerical modelling (Coudrillier et al., 2013; Coudrillier et al., 2015a, b; Coudrillier et al., 2015c; Pinsky et al., 2005).

Pijanka et al. (Pijanka et al., 2013; Pijanka et al., 2012) used WAXS to quantitatively map collagen fibril orientation in the sclera of human donors. These studies confirmed the major structural features originally identified by Kokott: strong uniaxial fibrillar orientation at the extraocular muscle insertion sites and predominantly circumferential collagen in the PPS. They further identified that the collagen anisotropy of the PPS psuedo-annulus is highly regionally variable and that this pattern is highly conserved between age-matched, normally sighted donors (Pijanka et al., 2012). Inclusion of the WAXS data in inverse finite element modelling (IFEM) indicated that disturbance of the PPS anisotropic structure could significantly impact the ONH's mechanical response to IOP fluctuation (Coudrillier et al., 2013). A further WAXS study using serial cryo-sections (Pijanka et al., 2015) showed that the human PPS psuedo-annulus is located primarily in the outer two-thirds of the stroma (aligning with the normal LC insertion depth range into the scleral flange), with the

remaining one-third exhibiting more random orientation and a preference toward radial alignment near the choroid.

While structural evidence and numerical modelling (Coudrillier et al., 2013; Girard et al., 2009b; Grytz et al., 2011) are suggestive of a potential neuroprotective role in limiting IOP-driven scleral canal expansion and LC strains, the exact functional importance of the PPS structure remains to be established. Sigal and co-workers (Gogola et al., 2018b) recently used a polarized light method (see s2.1.4) to show that the PPS circumferential structure is a primary structural component across a range of large animal species. Furthermore, recent work using WAXS indicates that the degree of PPS collagen circumferential alignment varies between species and that eyes from smaller animals generally exhibit a more poorly defined anisotropic structure (Fig 5). The marked difference between some species further suggests that PPS structure may not be principally determined by IOP-generated scleral wall stress in some eyes, and may be more strongly influenced by other biomechanically relevant factors. For example, the wall stress in the tree shrew eye (diameter: 7.8mm, avg. scleral thickness: 120μm, IOP: 13mmHg (Samuels et al., 2018; Siegwart and Norton, 1999)) is predicted to be approximately twice that of the human eye (diameter: 24.2mm, thickness: 0.9mm, IOP: 17mmHg (Bekerman et al., 2014; Kouchaki et al., 2017; Vurgese et al., 2012)), and yet the PPS circumferential structure in the tree shrew (Fig 5B) is far less evident than in humans (Fig 5F), despite the two species having similarly well-developed connective tissue LCs (Albon et al., 2007). Further interspecies studies may help to tease out possible physiological, behavioural and anatomical factors that may interact with IOP in influencing posterior scleral collagen microstructure.

2.1.2 Small-angle light scattering—Small-angle light scattering (SALS) is another ex-vivo technique that can be used to quantitatively map protein fibre organization in collagenous soft tissues. Similar to WAXS, SALS also produces diffraction patterns from the interaction of light with a tissue patch; but instead of X-rays SALS uses laser light. Because of the higher wavelength (usually 632.8 μm from a HeNe laser), SALS is thought to be capable of mapping the organization and orientation of larger structures such as collagen fibril bundles (~ 1–10 μm in size), but cannot distinguish between collagen and elastin fibres. For the eye, SALS was first used to map scleral fibre orientation in normal rat sclera. The rat sclera was found to be structurally anisotropic with several consistent features. At the limbus, collagen fibres were highly aligned and organized primarily into a distinct ring surrounding the cornea. In the equatorial region, the fibres were primarily meridionally aligned. In the posterior sclera and PPS, the scleral fibres were mostly circumferential but less aligned than those in the anterior and equatorial regions (Girard et al., 2011a). SALS has also been used extensively to study the microstructure of the human sclera from healthy and glaucoma donors. Interestingly, in humans PPS collagen fibres were also circumferential, consistent with the aforementioned scheme envisaged to shield the optic nerve, but they exhibited the highest alignment (i.e. degree of anisotropy) not immediately adjacent to, but at a distance (400–500 μm) away from the scleral canal (Zhang et al., 2015a). Using computational modeling, such an arrangement (i.e. heterogenous collagen fibre organization) was found to minimize deformations at the scleral canal boundary - a transition zone prone to disinsertion of the LC, focal LC defects, and optic disc hemorrhages

in glaucoma (Fig 6). In humans, SALS was also used to identify key differences in scleral microstructure with age and with glaucoma (Danford et al., 2013; Jones et al., 2015). In one study, collagen fibres in the PPS were found to be more aligned in elderly healthy eyes (average age: 82 years old) than in young healthy eyes (average: 20 years old), and also more aligned than in elderly glaucoma eyes (average age: 82 years old) (Jones et al., 2015) (see also s4.2). Scleral anisotropy was also found to change significantly as a function of depth (Danford et al., 2013). However, it is still unclear how a disrupted collagenous ring in the PPS could predispose an individual to glaucoma.

2.1.3 Multiphoton microscopy—Multiphoton microscopy (MPM) is an optical imaging technique that utilizes high penetration pulsed lasers (usually infrared) and nonlinear optics to achieve fine optical sectioning through biological tissues several hundred microns thick, without the need for exogenous labelling. Second harmonic generation (SHG) imaging exploits the coherent scattering event whereby two incident photos are converted into a single photon of half the original wavelength. SHG signal emission is an intrinsic property of biological materials containing large repetitive, non-centrosymmetric units that include collagen, and indeed SHG has been used extensively to probe the organization of scleral collagen fibril bundles (Brown et al., 2007; Cone-Kimball et al., 2013; Jones et al., 2015; Keyes et al., 2011; Pijanka et al., 2012; Teng et al., 2006; Zyablitskaya et al., 2018) (Fig 1D). The ability of SHG to image large tissue volumes has enabled full 3D reconstructions of the ex-vivo human ONH to be built (Winkler et al., 2010), while its application in monitoring real-time pressure-induced LC and PPS deformations (Midgett et al., 2018; Sigal et al., 2014a) is enhancing our understanding of the role of IOP in glaucoma biomechanics. Increasingly, other MPM imaging modalities are being combined with SHG to colocalize scleral collagen with cells and other ECM components. The most notable example is two-photon fluorescence (TPF), in which the additive absorption of two incident photons results in the emission of an autofluorescence photon of a higher energy. Amongst other structures, TPF can be used to visualize elastin fibre networks over large scleral tissue volumes (Park et al., 2016) (Fig 7).

2.1.4 Polarized Light Microscopy—Collagen in the sclera is birefringent (Chakraborty et al., 2016; Jan et al., 2015) - the optical property of a material having a refractive index that depends on the polarization and propagation direction of light. Jan et al. have demonstrated that polarized light microscopy (PLM) is a powerful technique for the study of the collagen microstructure in the sclera (Jan et al., 2015). PLM can produce accurate, repeatable, and robust measurements of collagen fibre orientation with μm-scale resolution over a broad (cm) field of view, unaffected by formalin fixation, without requiring tissue dehydration, labeling or staining. PLM has been shown to be in good agreement with other measurements of collagen, such as those from autofluorescence (Jan et al., 2017b). However current PLM techniques do not measure elastin, and it remains unclear if it is at all possible. Using PLM, Jan et al. identified three distinct regions of scleral collagen fibre organization, with circumferential, radial (sometimes called meridional) or interweaving fibres (Fig 8). They reported these first in the sheep (Jan et al., 2017b), then in human, monkey, pig, cow and goat eyes (Gogola et al., 2018b). The consistency in scleral

microstructure across species suggests that these three regions are primary organizational components whose functions should be better understood.

Although there is consensus that circumferential fibres protect neural tissues by resisting canal expansion, the role of the interweaving fibres remains unclear. Wang and colleagues hypothesized that the fibre interweaving increases tissue stiffness (Wang et al., 2018). Their computational models suggest that a region of sclera with interwoven fibres can be more than twice as stiff as another region with the same amount of collagen organized with the same angular distribution but with no interweaving. This suggests that characterizing fibre interweaving may be of critical importance to understand how the sclera bears loads.

PLM has been further used to characterize the micron-scale waviness, or crimp, of the collagen fibres in the sclera. Crimp is important because it is a major determinant of tissue biomechanical behavior (Fig 9) (Grytz and Meschke, 2009). Using PLM, Jan et al. quantified the collagen crimp period in the LC and PPS in sheep eyes at low and normal IOP levels (Jan et al., 2017a). They found that the crimp period was smaller and less variable in the LC than in the PPS (Fig 10), suggesting a configuration that prevents large or heterogeneous deformations that insult the neural tissues within the canal (Fig 11). In addition, the crimp period in the PPS increased nonlinearly with distance from the canal, which is believed to provide a smooth transition of mechanical properties that minimizes stress and strain concentrations. This technique was then extended to quantify the collagen crimp morphology across the corneoscleral shell in sheep (Jan et al., 2018) and human (Gogola et al., 2018a) eyes. In these studies, it was found that crimp tortuosity, amplitude and waviness are not uniform over the globe, exhibiting distinct patterns that were similar across species (Fig 12).

The traditional PLM used in the studies mentioned above shares an important limitation with SALS and WAXS: it only quantifies in-plane fibre orientation (in the plane perpendicular to the light beam). A more advanced technique, 3DPLM, allows quantifying both in-plane and out-of-plane fibre orientation (Fig 13) (Yang et al., 2018b). This is potentially crucial given the complex 3D architecture of ocular collagen (Komai et al., 1991), where 2D projections could lead to inaccurate interpretations and conclusions (Yang et al., 2018b). Similar to SALS and WAXS, traditional PLM is a transmitted signal technique. This means that the measurements obtained are an aggregate of properties across the sample thickness. As mentioned (see s2.1.1), this can offer important advantages in enabling collection of effective structural data for use in numerical simulations. On the other hand, obtaining finely depth-resolved information using transmitted-light techniques requires the use of thin sections which, in turn, precludes or complicates analysis of dynamic events such as pressure-induced tissue deformations. For PLM, scattering, absorption and retardance limit usable sections to under 50 μm in thickness, and best data to 30 μm or less. To overcome this limitation, Yang et al. introduced structured polarized light microscopy (SPLM) imaging, a reflected light imaging technique that combines structured light illumination with PLM (Yang et al., 2018a). SPLM effectively rejects diffuse background light interfering with the polarization analysis and preserves light encoded with useful tissue birefringence information, thus enabling the visualization and quantification of collagen fibres of thick tissues while under realistic loading conditions, such as during inflation (Fig 14).

As a full-field imaging technique, PLM is generally faster than scanning-based techniques. However, it still requires multiple image acquisitions with various filter configurations. This limits the acquisition speed, and thus the range of experiments in which it can be used. To overcome this, Yang and colleagues developed snapshot PLM (Yang et al., 2019), which allows real time visualization of the scleral bundles and the constitutive collagen fibres with sub-micron resolution in fresh, unlabeled samples (Fig 15).

2.1.5 Magnetic Resonance Imaging—Magnetic resonance imaging (MRI) has been used to image the corneoscleral shell and obtain details of the ocular anatomy, such as the globe shape and tissue thickness (Norman et al., 2010a; Voorhees et al., 2017; Wang et al., 2016a). However, MRI studies of the collagen microstructure in the sclera have been limited, partly due to the intrinsically fast transverse magnetic resonance relaxation of the fibrous tissues and the resulting low MRI signal intensities (Luan et al., 2006). Ho et al. demonstrated the use of the magic-angle enhancement effect to improve MRI sensitivity for detecting the collagen microstructure in the sclera (Ho et al., 2014). They found that, at the magic angle (approximately 55° relative to the direction of the main magnetic field), MRI can reveal the distinct lamellae fibres in the ovine sclera, and the light/dark bands indicative of collagen fibre crimps (Fig 16). Magic angle-enhanced MRI can also reveal sub-voxel microstructural changes of collagen fibres with IOP elevation. Using diffusion tensor MRI, Ho et al. found that the fractional anisotropy of the ovine sclera increased with IOP, consistent with uncrimping and straightening of microstructural fibres (Ho et al., 2016). Magic angle-enhanced MRI technique has the potential to enable cross-sectional and longitudinal monitoring of the functional microstructures of the eye and their relationship with aging and diseases involving the sclera, such as acute and chronic ocular hypertension, glaucoma, and myopia. However, before this can be realized, important technical challenges remain, particularly the resolution and the long scan times (often over 12h in the studies mentioned above).

2.2 Nanostructure

2.2.1 Scanning electron microscopy—Study of the interaction of incident electrons with the atoms of a target specimen allows the direct imaging of structure at resolutions beyond 1nm. For biological specimens this generally comes at the price of invasive tissue preparation involving dehydration, chemical fixation and heavy metal staining/coating to stabilize and preserve tissue structure and enhance image contrast. Scanning electron microscopy (SEM) produces images of a sample surface at <1nm resolution by scanning it with a focused electron beam and detecting (usually) the emission of secondary electrons from target atoms excited by the incident beam. Alternatively, an SEM image can be obtained from the reflected/transmitted incident electrons. As documented in several landmark papers (Komai and Ushiki, 1991; Thale and Tillmann, 1993; Yamamoto et al., 2000) SEM has made central contributions to our fundamental knowledge of scleral collagen hierarchical structure and organization. In recent years the advent of volume SEM methods have made it possible to image tissue ultrastructure in 3D over specimen volumes of hundreds of cubic microns (Bushby et al., 2011) and these methods are currently providing insight into how the elastin fibre network of the anterior sclera might integrate with that of the peripheral cornea (Lewis et al., 2016).

2.2.2 Transmission electron microscopy—In transmission electron microscopy (TEM) an electron beam is transmitted through an ultrathin (~100nm) section of a specimen and can image nanostructure at unparalleled resolution (Fig 1B,C). With modern aberration corrected electron microscopes, it is now possible to resolve structures of dimensions <0.1nm. TEM has made many major contributions in scleral research, in particular in the use of cationic dyes (Quantock and Meek, 1988; Young, 1985) and immunogold particulate markers (Kimura et al., 1995; Marshall et al., 1993) to elucidate collagen-collagen and collagen-proteoglycan interactions, and in defining ECM alterations in scleral pathology (Cone-Kimball et al., 2013; Funata and Tokoro, 1990; McBrien et al., 2001; Quigley et al., 1991). Recent years have seen notable progress in tissue cryopreservation methods that significantly reduce structural artifacts induced by post-processing in conventional TEM, allowing high resolution imaging of the sclera that is closer to the physiological situation (Costa et al., 2016; Ismail et al., 2017). Current bioimaging trends towards 3D visualization of ECM ultrastructure are reflected in recently documented electron tomography (Luesma et al., 2013) and quick-freeze/deep-etch (QFDE) electron microscopy (Ismail et al., 2017) (Fig 17) studies of the sclera.

2.2.3 AFM—In atomic force microscopy (AFM) contact scanning of a sample surface is performed with a fine mechanical probe. As an imaging technique, AFM can produce topographic surface images of a specimen with in-plane and depth resolutions of respectively ~2nm and ~0.1nm. An advantage of AFM over electron microscopy is that it does not require any artifact-inducing treatments and thus can provide a more physiological view of the tissue. However, the scanning area in AFM (typically a few hundred microns across) is an order of magnitude below that achievable with SEM. AFM has been used to visualize and quantify scleral collagen fibril diameter, D-period (Fullwood et al., 1995) (Meller et al., 1997) and microfibrillar tilt angle (Yamamoto et al., 2000). Importantly, AFM provides a unique link between tissue ultrastructure and mechanics by being able to measure forces between the probe and specimen surface in parallel with imaging. This has been exploited to determine the contribution of different tissue layers (Grant et al., 2011) and ECM components (Zhuola et al., 2018) of the sclera to its mechanical performance. A further strength of AFM is that it can also be used for precision manipulation of the local sample environment. For example it can mechanically stimulate individual cells and monitor the effects in real-time by synchronization with other imaging modalities (e.g. fluorescence imaging), as demonstrated in work with cultured immune cells (Cazaux et al., 2016). However, the potential for using AFM in mechanotransduction studies of the sclera is yet to be realized.

3. Scleral biomechanics

3.1 Ex-vivo biomechanical characterization methods

3.1.1 Tensile strip testing—Much of what we know about the fundamental material properties of the sclera has come from tensile strip testing of scleral stress-strain behavior. A large body of work using enucleated eyes from humans (Eilaghi et al., 2010; Elsheikh et al., 2010; Geraghty et al., 2012; Shin et al., 2018), monkeys (Downs et al., 2005), chicks (Phillips et al., 2000), pigs (Lari et al., 2012), tree shrews (Levy et al., 2018), rabbits (Shin et

al., 2018), cows (Shin et al., 2018) and dogs (Palko et al., 2011) have established that the sclera is a non-linear material, exhibiting a strain-stiffening response as crimped collagen fibrils become gradually recruited to bear load (see Fig 11). These studies have also confirmed that the sclera is viscoelastic and displays significant hysteresis. They have shown us that the healthy sclera displays considerable mechanical anisotropy that varies with anatomical position, consistent with the regional microstructural variations in tissue ECM structure discussed in s2.1. Furthermore, strip testing has been used to uncover important biomechanical changes of the sclera with ageing, glaucoma and myopia that will be described in Section 4.

While strip testing has long been a standard method of scleral biomechanical measurement, there are recognized limitations with the technique. Firstly, the scleral tissue strips required for testing are unavoidably curved and demonstrate variations in thickness and structural anisotropy along their length. This can lead to large errors in measured material behaviour that require mathematical back-correction to solve (Elsheikh and Anderson, 2005). Secondly, obtaining repeatable measurements with strip testing requires preconditioning cycles that fundamentally alter the stress-strain response. These limitations have led, in recent years, to a move towards the more physiological technique of inflation testing (see s3.1.2), which significantly reduces the above problems (Lari et al., 2012; Tonge et al., 2013). Nevertheless, strip testing continues to make important contributions to the scleral literature, with notable recent studies reporting its use to assess the effects of crosslinking treatment for myopia (Levy et al., 2018) and its combination with emergent polarization-sensitive optical coherence tomography (PSOCT) imaging to determine scleral mechanical response to dynamic loading (Shin et al., 2018).

3.1.2 Inflation testing—Although inflation testing cannot measure the stressed state of the sclera directly, it can be used to extract material properties by the applying a suitable constitutive model (with some inherent assumptions) to the experimental pressure-displacement data. Scleral inflation studies have been performed across a range of mammalian species from mice to humans (Coudrillier et al., 2012; Cruz Perez et al., 2016; Fazio et al., 2014a; Girard et al., 2009c; Myers et al., 2010a; Myers et al., 2010b; Nguyen et al., 2013; Palko et al., 2016; Tang and Liu, 2012). While the experimental details vary across these studies, the key components of the basic inflation set-up are common to all.

The first component needed is a controllable pressurization module. A fluid injection system is required that allows adjustment of both target pressure and pressure-rate, usually achieved via a combination of a syringe pump and a pressure transducer with feedback control. The scleral specimen (usually the transected posterior hemisphere or thereabouts of the eye globe) is glued/clamped to the pressure chamber with separate inlets for fluid injection and pressure measurement. The second component required is a deformation tracking module. Tracking the surface displacement of the internally pressurized sclera at sufficiently high resolution, and with enough precision, is the most challenging aspect of inflation testing, and researchers have adopted various approaches. Girard et al. (Girard et al., 2009c) and Fazio et al. (Fazio et al., 2014a) used electronic speckle pattern interferometry (ESPI) to track posterior scleral surface displacements in monkeys and humans, respectively. ESPI works on the principle that a rough surface illuminated with a coherent light beam (i.e. a laser) creates

a random speckle light field. Interference of this field with a reference field then produces an interference pattern that is dependent on the surface displacement and can thus be used to indirectly determine the latter in three dimensions. Coudrillier et al. (Coudrillier et al., 2012) adopted a more direct approach in their inflation tests of human sclera, using graphite powder to create contrast markers on the scleral surface. These markers were then tracked in 3D directly with a combination of CCD cameras and digital image correlation (DIC) software. A DIC approach was also used by Myers et al. (Myers et al., 2010a), and developed further by Nguyen et al. (Nguyen et al., 2013) in inflation tests of mouse sclera. However, the small size of the mouse eye facilitated only 2D tracking of the scleral surface profile. Tang and Liu (Tang and Liu, 2012) developed an alternative system, in which ultrasound speckle tracking was used to obtain cross-sectional profiles of scleral displacements in a porcine model. This was subsequently adapted successfully for studies in human (Pavlatos et al., 2016) and canine (Palko et al., 2016) sclera.

Going forward there is likely to be an emphasis on whole eye biomechanical modelling, and there have already been associated developments in inflation testing methods. Lari et al (Lari et al., 2012) developed a method to test intact eyeballs by using a combination of a skewer and mineral oil bath to support and image cannulated pig eyes under inflation conditions. Whitford et al. (Whitford et al., 2016) later developed a further variation on the whole eye inflation/DIC approach, in which they placed intact eyeballs in a gelatin suspension to further reduce external forces on the sclera (Fig 18). These kind of approaches have moved inflation testing closer to the in-vivo situation by reducing non-physiological stress concentrations and boundary conditions unavoidably imposed when clamping excised scleral specimens in standard inflation regimens (Lari et al., 2012; Whitford et al., 2016).

3.1.3 Indentation testing—Indentation testing studies of the sclera are relatively sparse, but can be traced back more than three decades to the work of Battaglioli and Kamm. They tested samples of sclera from cow and human eyes in compression and found that the radial compressive stiffness of the sclera (i.e. its ability to resist indentation forces perpendicular to the tissue plane) was approximately 100 times less than its circumferential (i.e. in-plane) stiffness (Battaglioli and Kamm, 1984). The results of this study highlight an important fundamental material property of the sclera – that it is an essentially incompressible tissue. In their study, Battaglioli and Kamm used a relatively simple custom-made air piston indenter and optical displacement probe apparatus capable of sub-micron resolution. However, the commercial release of the first AFM instrument some five years later made more sophisticated nanoindentation studies possible. Braunsmann et al. evaluated elasticity alterations in cryosections of LC and PPS in eyes with psuedoexfoliation (PEX) disorder, reporting a marked softening of the ONH tissues in PEX affected eyes that could possibly render them more vulnerable to glaucoma damage (Braunsmann et al., 2012). Later Leung et al. measured ex-vivo scleral load-displacement response in porcine eyes as a function of IOP using a universal indentation testing machine in combination with a DLSR camera fitted with a stereomicroscope (Leung et al., 2014). They found that scleral stiffness correlated positively with IOP. These studies indicate the possibility for indentation testing technology to perhaps one day provide valuable clinical measures of scleral stiffness in-vivo, however this potential remains largely unrealized.

3.2 In-vivo biomechanical characterization methods

Ex-vivo studies have shown that the biomechanical properties of the sclera change with age (s4.1), race (s4.1), glaucoma (s4.2), and myopia (s4.3). In-vivo measurements of these properties could therefore potentially serve as valuable biomarkers to detect the earliest stages of glaucoma damage and progressive myopia, helping to profile patients at risk of developing these pathologies. At present, in-vivo measurements of scleral biomechanical properties are, in principle, achievable through inverse methods that will be described below.

To fully assess the biomechanical behavior of the sclera in-vivo, one would need to alter one of the known loads acting on the sclera while continuously monitoring the scleral tissue and measuring its resulting local deformations. Only then can the stiffness (or biomechanical properties) of the sclera – roughly speaking the ratio of load changes to deformations – be estimated. It is important to realize that these ‘in-vivo biomechanical tests’ need to be performed within a safe physiological range in order avoid further progression of visual field loss. Furthermore, and as for any controlled mechanical test, only one load should be altered at a time while all others should remain constant. This last point represents a significant clinical challenge.

Girard et al. developed a 3D tracking algorithm that can track displacements and strains of the PPS following a change in IOP (Girard et al., 2013). This algorithm requires two optical coherence tomography (OCT) volumes of the ONH: one is captured before a change in IOP (referred to as the ‘undeformed’ volume) and the other is captured after a change in IOP (referred to as the ‘deformed’ volume). Briefly, the tracking algorithm defines regions of interest (ROIs or groups of voxels) in the undeformed OCT volume and then subjects them to mechanical transformations (rigid translation, rigid rotation, stretch/compression and shear) until they best match their co-localized ROIs in the deformed OCT volume (Fig 19). The output is a 3D displacement field from which tensile, compressive, and effective (average) strain components can be derived and mapped. Using such a technique, Girard et al. have reported in-vivo local displacement/strain mapping of the PPS following IOP lowering by trabeculectomy in glaucoma subjects (Girard et al., 2016). They demonstrated that the PPS was the tissue that exhibited the highest compressive strain relief (on average 10% for an IOP decrease of 12 mmHg) following IOP-lowering surgery by trabeculectomy. This suggests that trabeculectomy is efficient at relieving a significant amount of PPS stress that may otherwise fasten glaucoma progression.

Once scleral deformations (and the corresponding loads) are measured in-vivo, inverse computational approaches can be used to assess the biomechanical properties of the sclera, such as IFEM (Coudrillier et al., 2013), the virtual fields method (VFM) (Zhang et al., 2017), or the pre-fitting method (Sigal et al., 2014b), each having its own pros and cons. However, in-vivo scleral biomechanics is still in its infancy, and the most pressing concern is to further demonstrate and validate that the biomechanical properties of the sclera are indeed measurable in-vivo with enough sensitivity and accuracy. Improvements in OCT hardware (Sigal et al., 2014c), including adaptive optics, swept source, multiple wavelengths, phase-sensitive technology, micro-imaging, and image processing techniques such as compensation (Girard et al., 2011b), are likely to push the quality and availability of in-vivo biomechanical measurements to the next level. Furthermore, other new imaging approaches such as

Brillouin microscopy (Scarcelli et al., 2012; Yun and Chernyak, 2018) and shear wave elastography (Dikici et al., 2016) may hold great promise if they can be successfully applied to the sclera, but they also exhibit limitations as the reported elastic moduli are typically off by several orders of magnitude.

3.3 Scleral response to IOP

3.3.1 ECM response—Studies of the scleral ECM response to IOP can be divided into two groups: response to acute and chronic IOP elevations. Following acute IOP elevations, posterior bowing of the PPS and expansion of the scleral canal were observed in human (Ma et al., 2019; Pavlatos et al., 2018), monkey (Girard et al., 2009a; Yang et al., 2009), porcine (Pavlatos et al., 2018) and sheep (Voorhees et al., 2017) eyes. The effects were nonlinear, with larger deformations at normal or sub-normal IOPs than at elevated IOPs, consistent with a nonlinear deformation-induced stiffening resulting from inhomogeneously crimped collagen fibres (Fig 11). Although crimp had been postulated as the microstructural basis of the nonlinear mechanical behavior of sclera (Grytz and Meschke, 2009), it is only recently that it has been confirmed experimentally (Jan and Sigal, 2018). Jan et al. used PLM to quantify and characterize how the collagen fibre crimp waviness (standard deviation of the fibre orientation along a fibre bundle) of the LC and PPS in sheep eyes changes with IOP (Jan and Sigal, 2018). It was found that the crimp waviness decreased with IOP. Interestingly, at a normal IOP of 15 mmHg, both LC and PPS had about 75% recruited fibres, with 25% ostensibly in reserve. Whether this applies to human eyes remains unknown.

Posterior bowing of the PPS and expansion of the scleral canal were observed as well in monkey eyes exposed to chronic IOP elevations (Bellezza et al., 2003; Yang et al., 2007). Girard et al. estimated the scleral tangent modulus (a measure of scleral stiffness) of monkey eyes in which chronic IOP elevation was induced. They found that the tangent modulus decreased at the earliest stage of IOP elevation but increased at moderate stages (Girard et al., 2011c). Age-related decreases in collagen crimp are likely one of the mechanisms underlying age-related stiffening of the sclera. Using PLM, Gogola et al. quantified collagen crimp morphology (waviness, tortuosity, and amplitude) in 20 normal eyes of 20 human donors, ranging in age from 0.08 (1 month) to 97 years (Gogola et al., 2018a). They found that all crimp parameters decreased significantly with age, with significantly different age-related decreases between regions. The crimp morphology of the limbus changed the most drastically with age, such that it had the largest crimp in neonates, and among the smallest in the elderly, suggesting that crimp in this region may play a role in eye development. Stiffening of the sclera may also be caused by alterations in the content of scleral glycosaminoglycan (Murienne et al., 2016; Murienne et al., 2015). The scleral ECM response to chronic IOP elevation in glaucoma has also been studied from both a biomechanical and microstructural perspective by groups using scattering methods and inflation testing in various combinations (Coudrillier et al., 2013; Coudrillier et al., 2012; Danford et al., 2013; Jones et al., 2015; Pijanka et al., 2012). These studies are described in detail in s4.2.

3.3.2 Cellular response—In comparison to ECM less is known of the response of cells to eye pressure fluctuation, yet scleral mechanotransduction is an area of growing interest, driven in major part by the need to clarify the sclera's dynamic role in myopia and glaucoma development. Fibroblasts have the potential to impact tissue-level mechanics by two routes: (i) a slow, indirect route via their expression of ECM molecules (tissue remodeling), and (ii) a faster, direct route through force-transduction to ECM from intracellular cytoskeletal protein networks. Cultured human scleral fibroblasts have been shown to be sensitive to their mechanical environment. Applied load alters the expression levels of ECM molecules (Cui et al., 2004; Shelton and Rada, 2007) and promotes phenotypic changes (Qu et al., 2015) in-vitro. Notably, high-magnitude and/or high-frequency load was shown to promote differentiation of cultured human PPS fibroblasts into contractile myofibroblasts (Qu et al., 2015), indicating that IOP fluctuations may have an important impact on fibroblast activity in-vivo (Fig 20).

Meanwhile, in-vivo animal studies have reported increased myofibroblast cell numbers in the sclera of mice with experimental glaucoma (Oglesby et al., 2016) and tree-shrews with induced myopia (Phillips and McBrien, 2004). It has been suggested that the latter observation could explain recovery from axial elongation in the shrew eye that is too rapid to be attributable to matrix remodeling (Phillips and McBrien, 2004). A role for scleral myofibroblasts in regulation of eye size through tissue-level mechanical influence is further supported by the identification of collagen-binding integrins in human (Hu et al., 2011) and tree shrew (McBrien et al., 2006) derived scleral cell lines, and their demonstrated modulation of tissue creep in collagen gels seeded with human fibroblasts in-vitro (Hu et al., 2011). In light of these observations, it is interesting to note that, in contrast to the adult eye, there is an absence of contractile scleral cells in primate eyes undergoing ocular growth (fetal and neonatal stages) (Poukens et al., 1998).

3.4 Scleral influence on ONH biomechanics

The scleral influence on ONH biomechanics has been studied using both generic and specimen-specific models. An example of early generic numerical modeling is the work of Bellezza et al., who studied the effects of the scleral canal size and shape and scleral thickness on the biomechanical response of the ONH (Bellezza et al., 2000). They found that, for a given level of IOP, a thinner sclera with a larger and more elliptical canal induced higher stresses within the load-bearing connective tissues of the ONH. Expanding on this early work, Sigal et al. developed a more realistic generic model that incorporated pre- and post-laminar neural tissues, as well as the central retinal vessel and the pia mater (Sigal et al., 2004). They found that the mean laminar strain was more sensitive to the scleral stiffness than to the laminar stiffness, and was only weakly dependent on the stiffness of the neural tissues and pia mater. A schematic illustration of how the stiffness of the sclera affects the IOP-induced ONH deformations is shown in Fig 21 (Sigal et al., 2011b).

To determine which anatomic and biomechanical factors most influenced the biomechanical response of the ONH to acute changes in IOP, Sigal et al. parameterized the generic model into 21 factors representing ONH tissue anatomies and material properties (Sigal et al., 2005). The biomechanical response of the ONH tissues was quantified through a set of 29

outcome measures, including peak and mean stress and strain within each tissue, and measures of geometric changes in ONH tissues, such as the cup to disc ratio. The five most important determinants of ONH biomechanics (in rank order) were identified as: the stiffness of the sclera, the size of the eye, IOP, the stiffness of the LC, and the thickness of the sclera. This study was the first to highlight the importance of scleral stiffness on ONH stress and deformation. However, it was performed with the simple, but limited, method of varying one parameter at a time. Sigal et al. then extended this work by varying the geometric and material parameters simultaneously (Sigal et al., 2009). They found that independently increasing either the stiffness or thickness of the sclera leads to reduced deformations being transmitted to the ONH. However, if the sclera is already quite stiff, then changing its thickness has relatively little effect on ONH biomechanics and vice versa.

Girard et al. developed a generic model to investigate the effects of scleral collagen fibre alignment on scleral and ONH mechanics (Girard et al., 2009b). The influence of the fibre concentration factor, a parameter used to control collagen fibre alignment along a preferred fibre orientation, was also evaluated. Results showed that a circumferential fibre organization in the sclera reduced scleral canal expansion, whereas the opposite was observed with a meridional fibre organization. Perez et al. developed a generic model of the corneoscleral shell to simulate the viscoelastic responses of the eye during micro-volumetric changes (Perez et al., 2013). The viscoelastic properties of the cornea and the sclera, including the instantaneous modulus, equilibrium modulus, and relaxation time constants, were parameterized to examine their effects on IOP elevations at different rates of volumetric changes. Results showed that all viscoelastic properties influenced the profile of the dynamic IOP due to volumetric changes, and the relative significance of a specific parameter was highly dependent on the rate of change. From this, they concluded that it is necessary to better characterize the viscoelastic properties of ocular tissues. Ayyalasomayajula et al. developed a porohyperelastic model of the ONH to discern the effects of interstitial and intracellular fluid pressure on the biomechanical response to IOP (Ayyalasomayajula et al., 2016). A generic model of human eye was constructed and the fluid permeabilities of the retina-Bruch’s-choroid complex, sclera, uveoscleral pathway, and trabecular meshwork were parameterized. IOP, translaminar pressure gradient and strains in the lamina were considered as computational outputs. As tissue permeability increased, both IOP and translaminar pressure gradient decreased, resulting in decreased strains in the lamina.

Specimen-specific models, which are based on the geometry and/or mechanical properties of an individual eye, have been developed to more accurately evaluate ONH biomechanics. Sigal et al. developed models of human posterior poles with specimen-specific geometries to explore the IOP-induced deformation of the ONH (Sigal et al., 2007, 2009; Sigal et al., 2011a; Sigal et al., 2010). They found that the scleral stiffness was the most important material parameter in determining the biomechanical insult to the lamina, matching the findings from generic models (Sigal et al., 2005; Sigal et al., 2004, 2009). Norman et al. developed human globe models that combined specimen-specific corneo-scleral shells and generic ONHs to determine the effects of globe shape and size on ONH biomechanics (Norman et al., 2010b). They found that the PPS thickness was the largest determinant of

ONH biomechanics, with decreased thickness resulting in increased maximum strains in the LC and increased scleral canal radial displacement.

The state of the art in eye models now includes experimental measurements of collagen microstructure. Coudrillier et al. developed a model with human specimen-specific scleral geometry including specimen-specific details of sclera collagen anisotropy derived from WAXS data, but with a generic lamina (Coudrillier et al., 2013). The non-linear material stiffness used in this study was also specimen-specific and was determined through inverse modeling. This model implemented a distributed fibre-based constitutive equation that allowed them to study the influence of collagen fibre alignment and anisotropy through an elegant parametric variation. They found that increasing fibre anisotropy in the PPS resulted in a decrease in LC strains and scleral canal expansion, but also resulted in a posterior deformation of the LC. Campbell et al. created a finite element model with a generic geometry but non-linear and anisotropic material properties based on specimen-specific measurements of connective tissue volume fraction and collagen beam orientation obtained from a μCT scan of a porcine eye (Campbell et al., 2015). They compared their full model to a model of a homogenous isotropic lamina and an inhomogeneous isotropic lamina. They found that the structure of the LC homogenizes the strain field within the lamina and that the anisotropy of the collagen beams had little influence on the lamina strains. Zhang et al. incorporated fibre organization information from postmortem human eyes within the ONH models (Zhang et al., 2015a). The models predicted that the circumferential collagen fibres in the PPS were effective in limiting LC strains and was able to reduce strain levels at the scleral canal boundary. Instead, Voorhees et al. proposed an alternative fibre architecture for the PPS, in which the scleral canal is supported primarily by long-running fibres oriented tangentially to the canal (Voorhees et al., 2018). They found that the tangential arrangement of fibres afforded better mechanical support to the tissues within the scleral canal as compared to a simple circumferential ring of fibres (Fig 22).

Importantly, the long fibre arrangement can also explain clinically observed behaviors of the ONH that otherwise have found no explanation in other theories of PPS mechanics and behavior, such as a contraction of the scleral canal under elevated IOP (or its counterpart, the expansion under a decrease in IOP) (Poostchi et al., 2010; Strouthidis et al., 2011; Yang et al., 2009; Yang et al., 2011). The precise nature of the PPS fibre organization remains an issue of debate and intense study. However some consensus may be found across recent studies. For example the presence of a subpopulation of long straight fibres (as postulated by Vorhees et al.) that contribute to ONH canal support would be consistent with previous WAXS studies that reported tangential linear “bands” emanating from the PPS pseudo-annulus into the mid-posterior sclera (see s2.1.1) (Pijanka et al., 2012). Interestingly, more than a decade earlier Meek and Boote had envisaged a similar linear tangential model as one possible explanation of the circumferential collagen fibrils in the corneo-scleral limbus (Meek and Boote, 2004), although its biomechanical implications were not studied. The model by Vorhees et al. suggests that long tangential fibres in the limbus would play a major role in anterior segment mechanics.

3.5 Scleral response to optic nerve traction

The ‘standard’ biomechanical theory of glaucoma hypothesizes that elevated (or fluctuating) IOP deforms the ONH tissues, including the LC, and that these deformations drive RGC injury and death (resulting in blindness). However, IOP is not the only load deforming the eye tissues. Studies that used OCT (Chang et al., 2017; Sibony, 2016; Wang et al., 2016a), finite element modeling (FEM) (Wang et al., 2017b; Wang et al., 2016c) and MRI (Demer, 2016) all converge to the conclusion that horizontal eye movements considerably deform/shear the ONH tissues (through the “strong” optic nerve [including its sheath] traction imposed on the ONH), and that these deformations can be as large (or significantly larger) than those induced by a substantial IOP elevation (Wang et al., 2016a; Wang et al., 2016c) (Fig 23). Using FEM, Wang et al. were able to predict relatively large optic nerve traction forces during eye movements, i.e., between 90 (abduction) and 150 mN (adduction), in the same order of magnitude as extraocular muscle forces (Wang et al., 2017b). These forces are directly transmitted to the PPS and scleral flange via the dura, and may have important consequences on the growth & remodeling behaviour of the posterior sclera and surrounding tissues. For instance, optic nerve traction forces may partially explain: 1) the development and progression of myopia; 2) the development of staphylomas (i.e. weak spots within the scleral shell); 3) the presence of tilted discs in myopia; 4) intrachoroidal cavitations; and 5) peripapillary atrophy (Jonas et al., 2016a; Wang et al., 2016b). Interestingly, these findings may also relate to recently reported microstructural alterations found in the PPS in human high myopia eyes (Markov et al., 2018) (see s4.3). Further, Wang et al. showed using simulations that the presence of a stiff sclera (or a weaker, or more tortuous, optic nerve) would, in theory, considerably reduce gaze-induced ONH deformations and may thus limit the development of such conditions. This awaits experimental support.

3.6 Scleral influence on the ocular pulse during the cardiac cycle

IOP is not a constant value, but instead is pulsatile in nature. The difference between systolic and diastolic IOP has been defined as the ocular pulse amplitude (OPA) that ranges between 0.9 and 7.2 mm Hg in healthy subjects (Kaufmann et al., 2006). Generally, it has been well accepted that the OPA is mainly caused by acute choroidal expansion due to the pulsatile blood flow, and changes in the mechanical properties of the sclera could strongly influence the OPA, which might in turn have implications for the development and progression of glaucoma. To better understand how the sclera could influence the OPA, Jin et al. built a comprehensive FEM of the eye that took into account blood pressure and choroidal swelling during the cardiac cycle (Jin et al., 2018). The authors found that, during the cardiac cycle, a change in arterial pressure resulted in choroidal expansion, which in turn induced a change in IOP (the OPA) and ONH deformations. From diastole to systole, they found that choroidal expansion made the peripapillary retina move anteriorly, but both choroidal expansion and the OPA made the prelamina and LC move posteriorly. The net result was shearing of neural tissues in the neuroretinal rim. Interestingly, a stiffer sclera was shown to result in a higher OPA, smaller pulse volume, larger diastole-to-systole ONH strains, and larger neural tissue shear in the neuroretinal rim. This study is one of the first to suggest that a stiff sclera may have generally negative medical consequences.

3.7 Scleral response to cerebrospinal fluid pressure

While several studies have addressed the effects of cerebrospinal fluid pressure (CSFP) on the biomechanical environment within the scleral canal and the LC (Feola et al., 2017; Feola et al., 2016; Hua et al., 2017; Jonas, 2011; Morgan et al., 1995; Sibony et al., 2011; Wang et al., 2017a), little is known about the scleral response to CSFP. Fazio et al. used OCT angiography to image and quantify the CSFP-induced ONH deformations in the living human eye (Fazio et al., 2018). They found that the CSFP-induced strains in the PPS were higher than those in the LC and retina. In addition, their results showed that the PPS strain was negatively correlated with the retinal nerve fibre layer (RNFL) thickness. Hua et al. extended a previously published numerical model of the ONH (Sigal et al., 2005) to include CSFP and 23 other factors representing IOP, central retinal artery blood pressure, tissue anatomy and mechanical properties, and constraints on the optic nerve (Hua et al., 2018). A total of 8340 models were studied to predict factor influences on ONH deformations. The models predicted that the strongest influence of CSFP, more than twice that of IOP, was on the rotation of the PPS. Fig 24 illustrates how increases in CSFP cause deformation of the ONH.

4. Scleral changes with ageing and disease

4.1 Ageing

Numerous studies have shown that the structure and composition of the sclera change with age, though the findings are sometimes conflicting, depending on the experimental methods, age range, and animal species examined. Thickness measurements of fresh enucleated, monkey eyes (Girard et al., 2009c), mouse eyes older than 1 year (Nguyen et al., 2013), and human donor eyes (Coudrillier et al., 2012) have shown that the sclera thins with age. However, other histological thickness measurements of fixed human eyes did not vary with age (Vurgese et al., 2012). In the human sclera, the number of elastin fibres decreases after 20 years of age (Watson and Young, 2004), while decorin and biglycan levels decrease after age 40 (Rada et al., 2000). The cross-sectional area of scleral collagen fibrils increases with age (Malik et al., 1992), which may be caused by age-related accumulation of advanced glycation end-products (AGEs) (Schultz et al., 2008). Moreover, the mean collagen fibril radius and intermolecular lateral spacing in the sclera also increases with age (Daxer et al., 1998). Taken together, these findings point to both an accumulation of intermolecular, non-enzymatic crosslinks and an increase in the number of tropocollagen molecules per fibril as important mechanistic determinants of the observed stiffening of the sclera as it ages. WAXS measurements of the collagen fibre structure by Coudrillier et al. in the posterior sclera of human donor eyes measured a significant degree of collagen fibre alignment but no changes in the dominant collagen fibre orientation of the tissue with age (Coudrillier et al., 2015b) (Coudrillier et al., 2015a). In contrast, SALS measurements by Vande Geest and coworkers did not find age-related variations in the fibre structure of the human sclera (Danford et al., 2013; Yan et al., 2011). The contrasting results may be associated with differences in the way that these studies defined the degree of fibre alignment and in the specific regions of the sclera they examined. Moreover, as mentioned, unlike WAXS measurements using SALS are not specific to collagen and may include the alignment of elastin fibres.

The mechanical behavior of the sclera has been measured using a variety of methods in human, monkey and mouse eyes, and the studies have consistently found a stiffening effect with age. Uniaxial strip tests of human sclera reported that the elastic modulus increased with age and is different in the anterior and posterior regions (Friberg and Lace, 1988) (Geraghty et al., 2012). Inflation tests of the posterior scleral shell of monkey eyes (Girard et al., 2009c), canine eyes (Palko et al., 2016) and human eyes (Coudrillier et al., 2012; Fazio et al., 2014a) all observed an increased stiffness of the pressure-strain response with older age. The stiffness increases more rapidly with age for eyes from donors of African descent (Fazio et al., 2014b). How this latter observation might link to racial differences in susceptibility to scleral-involved ocular diseases such as myopia and glaucoma remains an important unanswered question. Pressure-displacement response measured in inflation tests of mouse eyes was also significantly stiffer in older compared to younger mouse eyes (Myers et al., 2010a).

Various studies have applied computational modeling to analyze the inflation tests to estimate the mechanical properties of the sclera and collagen fibres and their variations with age. The stress-strain relationship of the sclera was described by anisotropic hyperelastic models that represent the tissue as a distribution of stiff collagen and elastin fibres in a compliant isotropic matrix. The latter represents contributions from the non-fibrous components of the tissue, such as proteoglycans, and the effects of crosslinking. Girard et al. (Girard et al., 2009c) and Grytz et al. (Grytz et al., 2014) applied the models to fit the elastic properties of the fibres and matrix, and the parameters for the distribution of fibre orientation to the full-field measurements of the inflation tests of monkey and human eyes. Coudrillier et al. (Coudrillier et al., 2013) applied WAXS measurements directly to describe the collagen fibre structure and fit the elastic properties of the collagen fibres and matrix to the inflation tests of human eyes. All three studies showed that the shear modulus of the soft matrix material increased with age. The increase in matrix stiffness may be caused by the accumulation of AGEs with age and other age-related changes in the matrix microstructure that may affect the collagen interfibrillar interactions. For example, Murienne et al. (Murienne et al., 2016) showed that removing glycosaminoglycans in the posterior sclera of human donor eyes decreased the scleral thickness and increased its stiffness under inflation testing. Grytz et al. (Grytz et al., 2014) also reported a smaller collagen crimp angle parameter in the model employed by decreased with age. Both the larger matrix stiffness and smaller collagen crimp angle lead to a stiffer stress-strain response in the low-pressure region of an inflation test, resulting in a more linear stress-strain response. The findings for the collagen fibre stiffness were more varied. Girard et al. (Girard et al., 2009c) found that the strain-stiffening behavior of the scleral collagen fibres in monkeys increases with age, indicating that the sclera stiffens more quickly with strain in older animals. Grytz et al. (Grytz et al., 2014) reported that the collagen fibre modulus decreased with age in European-derived donor eyes, while there was no statistically significant age effects in fibre modulus of African-derived donor eyes. Furthermore, Coudrillier et al. found that the fibre modulus increased with age in human diabetic donors but not in those without diabetes (Coudrillier et al., 2015a, b). However, the precise relationship between ageing, diabetes and glaucoma remains to be established.

The gross shape of the sclera is also altered by ageing. Recently, using OCT, Tun et al. found that the shape of the sclera at its boundary with the ONH changes as a function of age (Tun et al., 2018). On average, the anterior surface of the PPS had a characteristic v-shaped configuration with its peak pointing towards the orbit. The range, however, varied from an inverted v-shaped (but with a relatively flat profile) to a more pronounced v-shaped configuration. Interestingly, the v-shaped configuration was more prominent with increasing age, worse vision, thinner cornea, greater axial length, thinner peripapillary choroid, and deeper anterior LC (Fig 25). Such changes in PPS shape with age could have a significant impact on the overall biomechanical environment of the ONH, and therefore warrant further investigation.

4.2 Glaucoma

Multiple studies have shown that the collagen structure and mechanical behavior of the PPS is different in glaucoma human donor eyes and animal models subjected to long-term IOP elevation. Significant regional differences have been measured in the collagen fibre organization in human eyes by WAXS (Coudrillier et al., 2015c; Pijanka et al., 2012) and SALS (Danford et al., 2013). Using WAXS, Pijanka et al. reported a decrease in the degree of fibre alignment in the superior/temporal and inferior/nasal quadrants of the human PPS, while the remaining two quadrants showed an increase (Pijanka et al., 2012). A later study with a larger number of specimens showed that the collagen structure in the PPS overall becomes more uniform as the level of optic nerve damage changed from normal to glaucoma undamaged to glaucoma damaged (Coudrillier et al., 2015c). SALS measurements showed that a parameter related to the degree of collagen alignment of the PPS of glaucoma eyes was greater than in normal eyes in the nasal region but smaller in the superior region (Danford et al., 2013). The collagen structure of the PPS also became less organized in mouse eyes with glaucoma. Pijanka et al. measured a lower degree of collagen alignment in bead-injected glaucoma mouse eyes compared to the contralateral control eye (Pijanka et al., 2014). Cone-Kimball et al. performed detailed TEM evaluation of the collagen structure in bead-glaucoma mouse eyes and reported an increase in the number and the cross-section area of collagen fibrils. There was also an increase in the number smaller diameter fibrils and fewer larger diameter fibrils (Cone-Kimball et al., 2013).

The mechanical behavior of the PPS becomes stiffer with glaucoma. Nguyen et al. developed an inflation test method for mouse eyes that used two-dimensional DIC to track the deformation of the scleral edge (Nguyen et al., 2013). They observed a stiffer pressure-strain response in the PPS, in both the meridional and circumferential directions, in bead-glaucoma mouse eyes compared to the contralateral controls. Downs et al. used uniaxial strip tests to measure the stress relaxation behavior of the PPS of normal and early-glaucoma monkey eyes and found a stiffer equilibrium (long-time) elastic modulus in the early-glaucoma group (Downs et al., 2005). The increased scleral stiffness in early-glaucoma monkey eyes was later confirmed by Girard et al. in more detailed inflation tests with ESPI to measure the full three-dimensional deformation field of the posterior sclera (Girard et al., 2011c). The authors applied IFEM to fit the parameters of a hyperelastic distributed fibre model to the surface deformation field and reported a larger elastic modulus and structural stiffness. Coudrillier et al. applied inflation testing with DIC to measure the full-field

deformation response of the posterior sclera of human donor eyes and found that diagnosed glaucoma patients, both with and without optic nerve damage, exhibited a stiffer pressure-strain response in the meridional direction and a smaller ratio of meridional to circumferential strain in the PPS (Coudrillier et al., 2012). These findings were consistent with WAXS measurements indicating a less aligned fibre structure in the various regions of the PPS (Pijanka et al., 2012). IFEM showed that the matrix shear modulus and collagen fibre stiffness on average increased as the level of optic nerve damage changed from undamaged to glaucoma undamaged and finally glaucoma damaged (Coudrillier et al., 2015c). However, the effect was not statistically significant because of the large variability.

Taken together, experimental studies suggest that a chronic increase in IOP from the homeostatic baseline causes remodeling of the collagen structure of the sclera at the same time as optic nerve damage. The effect is individually variable and may be influenced by the baseline structure and mechanical properties of the eye. The pressure-strain inflation response of the peripapillary sclera are stiffer in C57BL/6 (B6) than in albino CD1 mouse strain, which has a longer and wider eye and thinner PPS. In bead-injected glaucoma experiments, the optic nerve of CD1 mice were more susceptible than B6 to RGC axonal death and the sclera of bead-glaucoma CD1 eyes exhibited a significantly larger stiffening effect than those of C57BL6 (Cone et al., 2010). It remains unclear, however, whether a stiffer scleral response to pressure is protective of glaucoma. Mice with a mutation in collagen 8A2 exhibited a larger eye and stiffer scleral response to IOP and were less susceptible to RGC axon death than the wild-type B6 control (Steinhart et al., 2012). However, stiffening the sclera of CD1 mice by collagen crosslinking with glyceraldehyde led to greater susceptibility of RGC damage (Kimball et al., 2014). Efforts to directly measure strains in the ONH in mouse models may show the combined effects of variations in eye length, regional scleral thickness and scleral stiffness on the ONH strains (Nguyen et al., 2018; Nguyen et al., 2017). More detailed modeling is needed to evaluate the combined effects of these factors on the stresses experienced by the glial and axonal tissues of the ONH (Myers et al., 2011).

4.3 Myopia

Myopia is the most common refractive condition, affecting about 22% of the current world population (Holden et al., 2016). In a normal emmetropic eye with clear vision, light rays entering the eye focus precisely on the retina (Fig 26A). However, in a myopic eye light rays focus in front of the retina, causing the typical blurry vision in myopia (Fig 26B). Generally, myopia first occurs in school-age children and typically progresses until age 20. Juvenile-onset myopia is typically characterized by an elongated posterior scleral shell (Fig 26C).

Human and animal studies have confirmed the existence of a common mechanism across species that uses visual cues to actively match the axial length of the eye to its focal length (Howlett and McFadden, 2007; Norton and Siegwart, 1995; Siegwart and Norton, 2011; Wallman and Winawer, 2004; Wildsoet, 1997). This vision-guided, active process is called emmetropization. Similar to humans, many animals are hyperopic at birth (i.e. the light focuses behind the eye) and the refractive error diminishes as the eye emmetropizes. In animals, eye size can be experimentally modulated by shifting the focal plane posterior or

anterior to the retina using negatively or positively powered lenses, making the eye respectively myopic or hyperopic (Norton et al., 2010; Schaeffel et al., 1988; Siegwart and Norton, 2010). Increasing evidence from animal studies suggests that the emmetropization process relies on a feedback mechanism that alters scleral remodeling to match the axial length of the eye to its optical system. Fig 27 illustrates the emmetropization process as a mechanism involving the detection of the visual stimuli at the retina, signaling from retina to the sclera and modulation of scleral remodeling and axial elongation; which in turn modulates the visual stimulus and closes the loop.

The prevalence of myopia has dramatically increased over the past 60 years and has risen from 20% to nearly 90% in some Asian populations (Dolgin, 2015). Several visual stimuli have been identified that alter the refractive development the eyes including axial defocus, peripheral defocus, form deprivation, light intensity, contrast and light chromaticity (Ashby et al., 2009; Gawne et al., 2017; Liu and Wildsoet, 2011; Ohlendorf and Schaeffel, 2009; Rucker and Wallman, 2012; Sherman et al., 1977; Wallman et al., 1978). While the exact cause of the epidemic increase in myopia is still unclear, accelerated scleral remodeling is thought to be a common factor across all visual stimuli that may cause myopia (Grytz, 2018).

Several changes in scleral composition and structure have been identified in human myopia and experimental animal myopia. In terms of composition, notable changes reported include lower hyaluronan and sulfated glycosaminoglycan levels (Moring et al., 2007), upregulated enzymatic degradation (Guggenheim and McBrien, 1996; Guo et al., 2013), downregulated collagen type I synthesis (Gentle et al., 2003) and downregulation of aggrecan (Siegwart and Strang, 2007). While myopia occurs early in life and is characterized by an elongated eye size, accelerated tissue growth is not the cause of myopia. Scleral growth ceases very early during axial development of the eye. Scleral volume increases from birth to the end of the second year of life but remains unchanged thereafter in both normal eyes (Shen et al., 2016) and eyes that develop myopia (Jonas et al., 2014, 2016b). Similar to human myopia, the amount of sclera changes little (3–5% reduction in dry weight) during experimental myopia in tree shrews (McBrien et al., 2001; McBrien et al., 2000; Moring et al., 2007). In human eyes, scleral thickness decreases significantly with increasing axial length (Shen et al., 2015a). In severe cases of high myopia, the sclera thickness was reported to be only 31% of a normal sclera (Cheng et al., 1992). Severe scleral thinning in high myopia can lead to the formation of posterior scleral staphyloma. Animal studies have confirmed that the sclera thins during experimental myopia (McBrien et al., 2001; Norton and Rada, 1995). These tissue-level observations suggest that not accelerated scleral growth, but another distinct mechanism underlies axial elongation in myopia: scleral remodeling. Scleral remodeling is understood as a mechanism that involves the rearrangement of existing material due to micro-deformations that are (nearly) volume-conserving at the tissue-scale, while scleral growth is a mechanism that changes the amount (volume) of the sclera.

Animal studies have revealed changes in scleral ultrastructure during myopia development. After experimental myopia induction, a significant diameter thinning of scleral collagen fibrils has been observed in rabbits (Lin et al., 2018) and tree shrews (McBrien et al., 2001). While these ultrastructural changes occur quickly (2 weeks) in rabbits with lens induced

myopia, no significant changes were seen in a similar time frame in tree shrews. Instead, only after prolonged lens-induced myopia (~3 months) was a significant reduction in collagen fibril diameter seen in the shrew. This reduction in collagen fibril diameter is consistent with ultrastructural observations in highly myopic human eyes (Curtin et al., 1979). Based on inverse computational models, Grytz and Siegwart reported that the crimp of scleral collagen fibres increases during the development of myopia (Grytz and Siegwart, 2015). Meanwhile, experimental evidence of changes to the bulk fibre organization of scleral collagen in human high myopia has recently come from WAXS studies. Markov et al. reported changes in the posterior collagen fibre alignment, in which the normally well-conserved circumferential PPS fibre structure unravels towards a more radial alignment (Markov et al., 2018) (Fig 28). Further studies are required to ascertain whether these changes reflect tissue remodeling relating directly to axial lengthening of the sclera. A further possibility is that they could point to a mechanical adaption to fluid pressure/eye movement forces that will be larger in an elongated myopic eye (Markov et al., 2018). If and how such scleral microstructural changes might relate to optic nerve traction forces (see s3.5) and increased risk of retinal atrophy and staphyloma in highly myopic eyes is unknown.

Siegwart and Norton reported the first vision-induced change in scleral biomechanics, showing that the scleral creep rate increases during experimentally induced myopia (Siegwart and Norton, 1999). The creep rate represents the rate by which the sclera stretches while it is subjected to a constant load. The creep rate was found to respectively increase/decrease while the axial elongation rate was experimentally increased/decreased and myopia induced/recovered (Fig 29). Similar to the changes in scleral creep rate, the so-called transition or locking strain was found to increase/decrease during myopia development/recovery (Grytz and Siegwart, 2015). The transition strain is directly related to the collagen fibre crimp and represents the strain level at which the scleral collagen fibres straighten (Jan and Sigal, 2018) (see Fig 11). Interestingly a similar increase in scleral transition strain was found by Murienne et al. after the digestion of glycosaminoglycans in pig sclera (Murienne et al., 2015). Collectively, these finding illustrate the tight connection between changes in scleral composition, ultrastructure, biomechanics and scleral remodeling. More recently, Levy et al. identified a profound cyclic softening effect in tree shrew sclera after inducing experimental myopia (Levy et al., 2018). They also reported that scleral crosslinking using genipin inhibits the process, providing support for the notion of scleral crosslinking as a potential myopia control therapy (see s5.2).

5. Scleral therapies

5.1 Surgical treatments

In the context of this review, relevant surgical treatments may be broadly divided into two groups: (i) those that justify surgery of the sclera as a means to access and/or biomechanically alter neighboring ocular structures for clinical benefit (referred to here as “collateral scleral surgeries”); and (ii) those involving deliberate and targeted mechanical alteration of the sclera itself (classified here as “primary scleral surgeries”).

5.1.1 Collateral scleral surgeries—Scleral surgery to treat presbyopia (loss of focal range) has been explored for more than two decades (reviewed in (Hipsley et al., 2018)). Surgical approaches include anterior ciliary sclerotomy (radial incisions in the sclera overlying the ciliary muscle) (Hamilton et al., 2002), implantation of scleral expansion bands (Davidson et al., 2016; Malecaze et al., 2001), and anterior scleral laser ablative surgeries (Hipsley et al., 2017; Lin and Mallo, 2003). All these approaches have been shown to be effective in reversing presbyopia to varying degrees by increasing the elasticity of the eye's accommodative apparatus. However inconsistent clinical outcomes, treatment effect regression and incidences of anterior ischemia have led to the justification of scleral surgery as a presbyopia treatment being called into question. Nevertheless, while controversial it remains an active area of research (Glasser, 2008; Hipsley et al., 2018). Scleral buckle (SB) treatment to repair retinal detachment is another example of an enduring scleral surgical procedure that continues to evolve. A silicon sponge, rubber or plastic "buckle" element is strapped to the eyeball to indent the sclera at the retinal detachment site, promoting reattachment and healing (Park et al., 2018). Over the past decade, the burgeoning of ocular biomechanics as a scientific discipline has positively impacted SB technique development. For example, computational modelling approaches are continuing to guide surgeons on buckle design and usage through the identification of factors (e.g. buckle size/shape, strap tightness, ocular biometry, IOP) that most strongly influence the clinical outcome (Ge et al., 2017; Lanchares et al., 2016; Wang et al., 2007). Increasingly, SB is being combined with pars plana vitrectomy (PPV), a procedure where a small number of scleral holes (typically three) are created to facilitate vitreous removal (Park et al., 2018).

Anterior scleral surgery in the form of trabeculectomy, scleral laser trabeculoplasty (SLT) and drainage shunt implantation has long been a clinical mainstay of IOP reduction in treatment of medically uncontrolled glaucoma (Bovee and Pasquale, 2017), and here too techniques are progressing. The recent adoption of micropulse lasers for SLT (Yu et al., 2019), new shunt implant designs and materials (Chen and Gedde, 2018) and adjunct tools such as collagen matrix implants, fibrin adhesives, and amniotic membrane transplants (Lu et al., 2018) are all examples of emerging strategies to suppress fibrosis, scarring and other side-effects of glaucoma drainage surgery.

5.1.2 Primary scleral surgeries—Surgical reinforcement of the posterior sclera is a viable but highly debated option to manage pathologic myopia, and is usually indicated in eyes with associated macular changes and/or staphyloma (Ohno-Matsui and Jonas, 2018). The procedure involves inserting a strip of (usually) donor sclera material under the separated extraorbital muscles and pushing it down deeply towards the posterior pole. The ends of the strip are then crossed over the medial rectus muscle and sutured to the sclera on the medial aspect of the superior and inferior recti (Thompson, 1990). One source of controversy stems from difficulty in obtaining and storing donor tissue, and this is driving current efforts to develop biocompatible artificial materials and devices (Yuan et al., 2016). Meanwhile, established and emerging adjunct procedures such as patching therapy (Shen et al., 2015b) and collagen crosslinking (Xue et al., 2018) (see s5.2) are being combined with surgical reinforcement in an effort to improve efficacy and safety. Mechanical alteration of the posterior sclera is also being considered as an alternative neuroprotective strategy for

glaucoma patients who respond poorly to IOP lowering (Quigley and Cone, 2013; Strouthidis and Girard, 2013). One possible surgical approach could be to locally stiffen the scleral tissue around the ONH, for example by the insertion of a biocompatible (e.g. titanium) ring implant into the PPS and/or adjacent tissues. While there is not yet any experimental evidence to support the viability of such an approach, recent computational modelling results (Soh, 2016) show that, theoretically at least, it could be one effective route to reducing IOP-driven scleral canal expansion and LC strain (Fig. 30).

5.2 Scleral crosslinking

Collagen crosslinking has been used in multiple settings to mechanically stabilize collagenous tissues and hydrogels (Lima et al., 2009). It is thought that biomechanical weakening of the cornea is the underlying cause of keratoconus (Hayes et al., 2007). Corneal crosslinking using riboflavin and ultraviolet A light has been proposed and successfully used to mechanically stabilize the cornea in keratoconus patients since 1998 (Raiskup et al., 2015; Wollensak et al., 2003). A single treatment session of corneal crosslinking has been shown to slow or arrest keratoconus progression and achieve long-term stabilization of the condition (10 years) with a good safety profile (Raiskup et al., 2015). In section 4.3 we discussed several structural and biomechanical changes that occur during the development of myopia, including scleral creep rate, collagen fibre crimping and re-alignment, and cyclic softening (Grytz and Siegwart, 2015; Levy et al., 2018; Markov et al., 2018; Siegwart and Norton, 1999). These changes suggest that the sclera is biomechanically weakened during the development of myopia. Collagen crosslinking has therefore been proposed as a potential treatment for myopia, in particular, as a treatment for progressive myopia (Wollensak and Iomdina, 2008a). Progressive myopia is one of the leading causes of blindness worldwide without an accepted treatment option that can slow or halt progressive scleral remodeling (Buch et al., 2004; Cotter et al., 2006; Green et al., 1986; Krumpaszky et al., 1999; Munier et al., 1998). Given the lack of treatment options available and the morbidity of progressive myopia, an effective clinical solution is becoming increasingly necessary.

Collagen crosslinks accumulate naturally in the sclera during throughout life (Schultz et al., 2008). Based on computational model predictions, Grytz and El Hamdaoui proposed that the natural accumulation of collagen crosslinks decreases the susceptibility to scleral remodeling and myopia with age (Grytz and El Hamdaoui, 2017). McBrien and Norton have shown that preventing natural collagen crosslinking doubles the axial elongation rate during lens-induced myopia in juvenile tree shrews, suggesting that collagen crosslinks modulate scleral remodeling in myopia (McBrien and Norton, 1994). Wollensak and colleagues reported that the biomechanical changes introduced by scleral crosslinking remain effective for up to 8 months in rabbits (Wollensak and Iomdina, 2008b, 2009). Scleral crosslinking was shown to reduce collagen fibril crimping (Zyablitskaya et al., 2017) supporting the idea that crosslinking can counteract biomechanical changes that were seen in experimental myopia (see s4.3). Wang and Corpuz demonstrated that weekly scleral crosslinking using sub-Tenon’s injections of genipin can slow experimental myopia over 21 days in guinea pig eyes (Wang and Corpuz, 2015). However, that study did not incorporate a sham injected group. Garcia et al. have shown that sham injection behind the sclera can a have a significant

effect on axial development and should, therefore, be considered when delivering crosslink agent via sub-Tenon's injections (Garcia et al., 2017). Two groups have reported that scleral crosslinking using riboflavin and ultraviolet-A radiation can also slow progression of experimental myopia by increasing scleral biomechanical strength in guinea pigs (Dotan et al., 2016; Liu et al., 2016). Recently, Lin et al. showed successful slowing of experimental myopia using glyceraldehyde for scleral crosslinking in rabbits (Lin et al., 2019). Interestingly, Chu et al. had earlier also performed sub-Tenon's injection using glyceraldehyde in the guinea pig model of myopia (Chu et al., 2016) but, in contrast to the study by Lin et al., they reported that scleral crosslinking had no effect on the development of myopia despite biomechanical strengthening of the sclera. Chu et al. (similar to most studies) used only one dose of their crosslink agent, which may explain the controversial result. Recently, Grytz et al. reported the first investigation of dose-dependent effects of scleral crosslinking on myopia development (Grytz et al., 2018). This study used sub-Tenon's injections of genipin in tree shrews, confirming that scleral crosslinking can slow axial elongation in myopia and that the effect is dose dependent. Furthermore, a sham effect of sub-Tenon's injections on axial elongation was also seen in the study of Grytz et al., confirming the previous finding of Garcia et al. (Garcia et al., 2017).

Artificial crosslinking can be induced in multiple ways, where each method has its benefits and disadvantages. Maintaining a balance between minimizing cytotoxic effects and invasive operative procedures, while preserving treatment efficacy, will be essential to identify and optimize a clinically deliverable method of scleral crosslinking. The classical approach is based on using ultraviolet A light-activated riboflavin. The clear advantage of a light activated crosslink agent is the ability to use the light to localize the treatment to the area of interest. A major challenge of this strategy remains the safe delivery of the light to the sclera, which currently requires the operative exposure of the sclera (Wollensak and Iomdina, 2009; Wollensak et al., 2005). Current scleral crosslinking techniques using riboflavin/ultraviolet A light were found to be not safe enough (Wang et al., 2015). To improve efficacy and reduce retinal toxicity, other light wavelengths such as blue light (Zhang et al., 2015b) have been proposed and continue to be evaluated.

An alternative approach is to use crosslink agents that don't require light activation. The most commonly used scleral crosslinking agents from this category are two low-cytotoxic compounds: glyceraldehyde and genipin. Both agents have been successfully used to slow myopia progression, as mentioned above. Genipin is a naturally occurring organic compound and one of the best characterized low-cytotoxic crosslinking agents (Campbell et al., 2017; Fessel et al., 2014). Campbell et al. have shown that a much lower concentration of genipin is required to achieve a comparable scleral stiffening effect to that obtainable using alternative lowcytotoxicity agents such as glyceraldehyde (7-fold) or methylglyoxal (30-fold) (Campbell et al., 2017). The main advantage of using a crosslink agent that doesn't require light activation is the less invasive delivery of the agent via sub-Tenon's injections. However, there are also disadvantages in using non-light activated agents. For example, currently there is no method to limit the crosslinking procedure to the sclera alone. Grytz et al. reported that the genipin solution can diffuse across the limbal boundary during the sub-Tenon's injections, crosslinking not only the sclera but also the cornea (Grytz et al., 2018). All studies that showed successful slowing of myopia progression using glyceraldehyde or

genipin required repeated injections of the crosslink agents (typically 3 to 5 times or weekly injections). The development of an improved and sustained delivery strategy will be essential for a potential application in the clinic. Moreover, while no study has reported any major safety concerns or alarming adverse effects, the safety of these agents is still under evaluation.

Scleral crosslinking has also been proposed as a potential treatment strategy for glaucoma, but was found to increase glaucoma damage in a mouse model when the entire sclera was crosslinked (Kimball et al., 2014). However, Coudrillier et al. have shown that restricting scleral crosslinking to the PPS region has a beneficial effect by reducing the magnitude of biomechanical strains within the LC (Coudrillier et al., 2016). Consequently, localized scleral crosslinking may find utilization in glaucoma axonal neuroprotection, but this potential treatment modality requires further investigation and remains unproven.

6. Future directions and conclusions

The structure and biomechanical performance of the sclera is coming under increasing focus by researchers whose work is defining with more clarity the tissue's central importance in common, sight-threatening ocular pathologies such as glaucoma and progressive myopia. Classical views of the sclera as a largely static, quiescent tissue are being replaced by a growing awareness of its dynamic nature in terms of ECM growth and remodeling mechanisms and cellular biomechanical responses over wide-ranging time scales. Increasingly comprehensive understanding of the multiple, interacting biomechanical loads on the sclera (including eye movement forces and fluid pressures) is leading to more physiologically relevant combined experimental and computational models. Such models are required to investigate scleral-related disease and its association with ageing - a need that will become more pressing as the global population continues to age.

Going forward it is certain that we will see more notable advances in the broad and fertile area of scleral research. It is likely that new imaging modalities will be leveraged to visualize further aspects of scleral hierarchical structure and cell-ECM interactions, similar to what we are seeing in corneal research with the recent application of methods such as third harmonic generation (Jay et al., 2015) and coherent anti-Stokes Raman scattering (Kaji et al., 2017) multiphoton imaging. We can also expect to see bioimaging methods increasingly combined with quantitative tools such as Fourier methods (Pijanka et al., 2018) to provide more representative ECM and cellular structural inputs for computational modeling (Fig 31).

In the future there will likely be a continuation of the current trend towards 3D imaging techniques (Feneck et al., 2018; Yang et al., 2018b) and the unification of ocular structure data in an effort to gain a more holistic view of ocular behaviour through whole eye biomechanical modelling (Voorhees et al., 2017; Whitford et al., 2016; Zhou et al., 2019a; Zhou et al., 2019b). It is possible that we will also see a future shift towards in-vivo biomechanical modelling approaches, particularly if urgently needed progress can be made on characterization of ECM structure in the living eye. Indeed, quantitatively mapping collagen fibre organization in-vivo in human subjects may prove critical to improve

glaucoma diagnosis and management. Recently, PSOCT has been used to evaluate the volumetric microstructural tissue organization in rat PPS in-vivo (Fig 32). This was done by taking advantage of the birefringence caused by collagen fibres (Baumann et al., 2014). In that study, a PPS fibre ring was observed, which was validated against conventional histology and found consistent with other ex-vivo studies (Girard et al., 2011a). Translating PSOCT to the clinic could become feasible in the future, however significant challenges such as loss of signal quality when imaging deep tissues must be overcome.

The rise of artificial intelligence (AI) computing and its pervasion into vision research will likely accelerate in future, and this could result in further clinical benefits for scleral-related disease diagnosis and prognosis – perhaps most immediately in the glaucoma clinic. For instance, AI algorithms have already been developed to enhance, denoise, and automatically segment the PPS (along with other connective and neural tissues) in OCT images of the ONH in order to extract important in-vivo structural information. The performance of such algorithms is already on a par with that of human experts (Fig 33). Other AI algorithms have used the textural and structural information (Devalla et al., 2018a; Devalla et al., 2018b; Girard et al., 2011b) of the sclera (along that of other tissues) in OCT images of the ONH to provide a glaucoma diagnostic power that could challenge current gold-standard glaucoma parameters such as RNFL thickness (Girard et al., 2018). In the future, we are likely to see the emergence of other AI algorithms that will use structural and biomechanical information about the sclera to help predict which patients are at risk of developing visual field loss from glaucoma.

In terms of scleral treatments, an increasing emphasis on non-invasive therapies is probable. The success of collagen crosslinking to treat corneal biomechanical problems (e.g. keratoconus) has provided much incentive for research into scleral crosslinking (see s5.2). However, while notable progress has been made using animal models there remain many unanswered questions in terms of safety, efficacy and mode of delivery that are currently blocking clinical translation. Another potentially productive scleral therapeutic route currently still in its infancy is stem cell treatment. Scleral reinforcement via the application of mesenchymal stem cells is being evaluated as a potential treatment for progressive myopia (Janowski et al., 2015). Cell-mediated strategies involving both direct structural enhancement of the scleral stroma and indirect routes via stimulation of dopamine are being considered (Fig 34). Meanwhile, increasing success in the search for novel myopia genes is coming from the widening use of big data analyses (Flitcroft et al., 2018). These studies are already providing potential targets that could be leveraged in future towards gaining control of myopic scleral elongation through, for example, gene therapy. Given the already substantial and growing burden of scleral-related eye disorder worldwide, the success of such approaches will become even more important in the future.

Acknowledgements

The assistance of Petar Markov in preparation of figures for this document is gratefully acknowledged. The authors are thankful for funding support under the following grant numbers. CB: Fight For Sight Project Grant 1360, NIH Grant R01EY021500 (subaward 2003284605), MRC Program Grant MR/K000837/1 and various STFC Facility Access Awards; IAS: NIH grants R01-EY023966, R01-EY028662 and P30-EY008098; RG: NIH grants R01-EY026588, R01-EY027759, Eye Sight Foundation of Alabama and Research to Prevent Blindness; TDN: Public Health Service Research Grant EY021500 and NSF Grant CMMI-1727104; MJAG: MOE Singapore Academic

Research Funds (Tier 2: R-397-000-280-112 & R-397-000-308-112, Tier 1: R-397-000-294-114), NMRC Grant NMRC/STAR/0023/2014.

List of abbreviations

AFM	Atomic Force Microscopy
AI	Artificial Intelligence
CCD	Charge-Coupled Device
CCT	Central Corneal Thickness
CSFP	Cerebrospinal Fluid Pressure
DIC	Digital Image Correlation
ECM	Extracellular Matrix
ESPI	Electronic Speckle Pattern Interferometry
FEM	Finite Element Modelling
GAG	Glycosaminoglycan
IFEM	Inverse Finite Element Modelling
IOP	Intraocular Pressure
LC	Lamina Cribrosa
MPM	Multiphoton Microscopy
MRI	Magnetic Resonance Imaging
OCT	Optical Coherence Tomography
ONH	Optic Nerve Head
OPA	Ocular Pulse Amplitude
PG	Proteoglycan
PLM	Polarized Light Microscopy
PPS	Peripapillary Sclera
PPV	Pars Plana Vitrectomy
PSOCT	Polarization-Sensitive Optical Coherence Tomography
QFDE	Quick Freeze Deep Etch
RGC	Retinal Ganglion Cell
RNFL	Retinal Nerve Fibre Layer

ROI	Region of Interest
SALS	Small-Angle Light Scattering
SAS	Subarachnoid Space
SB	Scleral Buckle
SC	Schlemm's Canal
SEM	Scanning Electron Microscopy
SHG	Second Harmonic Generation
SPLM	Structured Polarized Light Microscopy
SLT	Scleral Laser Trabeculoplasty
TEM	Transmission Electron Microscopy
TPF	Two-Photon Fluorescence
VFM	Virtual Fields Method
WAXS	Wide-Angle X-ray Scattering

References

Albon J, Farrant S, Akhtar S, Young R, Boulton ME, Smith G, Taylor M, Guggenheim J, Morgan JE, 2007 Connective tissue structure of the tree shrew optic nerve and associated ageing changes. Invest Ophthalmol Vis Sci. 48, 2134–2144. [PubMed: 17460272]

Anderson DR, 1969 Ultrastructure of human and monkey lamina cribrosa and optic nerve head. Arch Ophthalmol 82, 800–814. [PubMed: 4982225]

Ashby R, Ohlendorf A, Schaeffel F, 2009 The effect of ambient illuminance on the development of deprivation myopia in chicks. Invest Ophthalmol Vis Sci 50, 5348–5354. [PubMed: 19516016]

Austin BA, Coulon C, Liu CY, Kao WW, Rada JA, 2002 Altered collagen fibril formation in the sclera of lumican-deficient mice. Invest Ophthalmol Vis Sci 43, 1695–1701. [PubMed: 12036967]

Ayyalasomayajula A, Park RI, Simon BR, Vande Geest JP, 2016 A porohyperelastic finite element model of the eye: the influence of stiffness and permeability on intraocular pressure and optic nerve head biomechanics. Computer methods in biomechanics and biomedical engineering 19, 591–602. [PubMed: 26195024]

Bailey AJ, Paul RG, Knott L, 1998 Mechanisms of maturation and ageing of collagen. Mech Ageing Dev 106, 1–56. [PubMed: 9883973]

Battaglioli JL, Kamm RD, 1984 Measurements of the compressive properties of scleral tissue. Invest Ophthalmol Vis Sci 25, 59–65. [PubMed: 6698732]

Baumann B, Rauscher S, Glosmann M, Gotzinger E, Pircher M, Fialova S, Groger M, Hitzenberger CK, 2014 Peripapillary rat sclera investigated in vivo with polarization-sensitive optical coherence tomography. Invest Ophthalmol Vis Sci 55, 7686–7696. [PubMed: 25352116]

Bekerman I, Gottlieb P, Vaiman M, 2014 Variations in eyeball diameters of the healthy adults. Journal of ophthalmology 2014, 503645. [PubMed: 25431659]

Bellezza AJ, Hart RT, Burgoyne CF, 2000 The optic nerve head as a biomechanical structure: initial finite element modeling. Invest Ophthalmol Vis Sci 41, 2991–3000. [PubMed: 10967056]

Bellezza AJ, Rintalan CJ, Thompson HW, Downs JC, Hart RT, Burgoyne CF, 2003 Deformation of the lamina cribrosa and anterior scleral canal wall in early experimental glaucoma. Invest Ophthalmol Vis Sci 44, 623–637. [PubMed: 12556392]

Boote C, Hayes S, Jones S, Quantock AJ, Hocking PM, Inglehearn CF, Ali M, Meek KM, 2008 Collagen organization in the chicken cornea and structural alterations in the retinopathy, globe enlarged (rge) phenotype--an X-ray diffraction study. J Struct Biol 161, 1–8. [PubMed: 17936639]

Boote C, Hayes S, Young RD, Kamma-Lorger CS, Hocking PM, Elsheikh A, Inglehearn CF, Ali M, Meek KM, 2009 Ultrastructural changes in the retinopathy, globe enlarged (rge) chick cornea. J Struct Biol 166, 195–204. [PubMed: 19258040]

Boote C, Kamma-Lorger CS, Hayes S, Harris J, Burghammer M, Hiller J, Terrill NJ, Meek KM, 2011 Quantification of collagen organization in the peripheral human cornea at micron-scale resolution. Biophys J 101, 33–42. [PubMed: 21723812]

Bovee CE, Pasquale LR, 2017 Evolving Surgical Interventions in the Treatment of Glaucoma. Seminars in ophthalmology 32, 91–95. [PubMed: 27686565]

Braunsmann C, Hammer CM, Rheinlaender J, Kruse FE, Schaffer TE, Schlotzer-Schrehardt U, 2012 Evaluation of lamina cribrosa and peripapillary sclera stiffness in pseudoexfoliation and normal eyes by atomic force microscopy. Invest Ophthalmol Vis Sci 53, 2960–2967. [PubMed: 22491409]

Brown DJ, Morishige N, Neekhra A, Minckler DS, Jester JV, 2007 Application of second harmonic imaging microscopy to assess structural changes in optic nerve head structure ex vivo. J Biomed Opt. 12, 024029. [PubMed: 17477744]

Buch H, Vinding T, La Cour M, Appleyard M, Jensen GB, Nielsen NV, 2004 Prevalence and causes of visual impairment and blindness among 9980 Scandinavian adults: the Copenhagen City Eye Study. Ophthalmology 111, 53–61. [PubMed: 14711714]

Bushby AJ, P'Ng KM, Young RD, Pinali C, Knupp C, Quantock AJ, 2011 Imaging three-dimensional tissue architectures by focused ion beam scanning electron microscopy. Nat Protoc 6, 845–858. [PubMed: 21637203]

Campbell IC, Coudrillier B, Mensah J, Abel RL, Ethier CR, 2015 Automated segmentation of the lamina cribrosa using Frangi's filter: a novel approach for rapid identification of tissue volume fraction and beam orientation in a trabeculated structure in the eye. J R Soc Interface 12, 20141009. [PubMed: 25589572]

Campbell IC, Hannon BG, Read AT, Sherwood JM, Schwaner SA, Ethier CR, 2017 Quantification of the efficacy of collagen cross-linking agents to induce stiffening of rat sclera. J R Soc Interface 14.

Cazaux S, Sadoun A, Biarnes-Pelicot M, Martinez M, Obeid S, Bongrand P, Limozin L, Puech PH, 2016 Synchronizing atomic force microscopy force mode and fluorescence microscopy in real time for immune cell stimulation and activation studies. Ultramicroscopy 160, 168–181. [PubMed: 26521163]

Chakraborty N, Wang M, Solocinski J, Kim W, Argento A, 2016 Imaging of Scleral Collagen Deformation Using Combined Confocal Raman Microspectroscopy and Polarized Light Microscopy Techniques. PLoS One 11, e0165520. [PubMed: 27806070]

Chakravarti S, Paul J, Roberts L, Chervoneva I, Oldberg A, Birk DE, 2003 Ocular and scleral alterations in gene-targeted lumican-fibromodulin double-null mice. Invest Ophthalmol Vis Sci 44, 2422–2432. [PubMed: 12766039]

Chang MY, Shin A, Park J, Nagiel A, Lalane RA, Schwartz SD, Demer JL, 2017 Deformation of Optic Nerve Head and Peripapillary Tissues by Horizontal Duction. Am J Ophthalmol 174, 85–94. [PubMed: 27751810]

Chen J, Gedde SJ, 2018 New developments in tube shunt surgery. Current opinion in ophthalmology.

Cheng HM, Singh OS, Kwong KK, Xiong J, Woods BT, Brady TJ, 1992 Shape of the myopic eye as seen with high-resolution magnetic resonance imaging. Optom Vis Sci 69, 698–701. [PubMed: 1437010]

Chu Y, Cheng Z, Liu J, Wang Y, Guo H, Han Q, 2016 The Effects of Scleral Collagen Cross-Linking Using Glyceraldehyde on the Progression of Form-Deprived Myopia in Guinea Pigs. Journal of ophthalmology 2016, 3526153. [PubMed: 27504195]

Cone-Kimball E, Nguyen C, Oglesby EN, Pease ME, Steinhart MR, Quigley HA, 2013 Scleral structural alterations associated with chronic experimental intraocular pressure elevation in mice. Mol Vis 19, 2023–2039. [PubMed: 24146537]

Cone FE, Gelman SE, Son JL, Pease ME, Quigley HA, 2010 Differential susceptibility to experimental glaucoma among 3 mouse strains using bead and viscoelastic injection. Exp Eye Res 91, 415–424. [PubMed: 20599961]

Costa D, Leiva M, Naranjo C, Rios J, Pena MT, 2016 Cryopreservation (−20 degrees C) of feline corneoscleral tissue: histologic, microbiologic, and ultrastructural study. Vet Ophthalmol 19 Suppl 1, 97–104.

Cotter SA, Varma R, Ying-Lai M, Azen SP, Klein R, 2006 Causes of low vision and blindness in adult Latinos: the Los Angeles Latino Eye Study. Ophthalmology 113, 1574–1582. [PubMed: 16949442]

Coudrillier B, Boote C, Quigley HA, Nguyen TD, 2013 Scleral anisotropy and its effects on the mechanical response of the optic nerve head. Biomech Model Mechanobiol 12, 941–963. [PubMed: 23188256]

Coudrillier B, Campbell IC, Read AT, Geraldes DM, Vo NT, Feola A, Mulvihill J, Albon J, Abel RL, Ethier CR, 2016 Effects of Peripapillary Scleral Stiffening on the Deformation of the Lamina Cribrosa. Invest Ophthalmol Vis Sci 57, 2666–2677. [PubMed: 27183053]

Coudrillier B, Pijanka J, Jefferys J, Sorensen T, Quigley HA, Boote C, Nguyen TD, 2015a Collagen structure and mechanical properties of the human sclera: analysis for the effects of age. J Biomech Eng 137, 041006. [PubMed: 25531905]

Coudrillier B, Pijanka J, Jefferys J, Sorensen T, Quigley HA, Boote C, Nguyen TD, 2015b Effects of age and diabetes on scleral stiffness. J Biomech Eng 137.

Coudrillier B, Pijanka JK, Jefferys JL, Goel A, Quigley HA, Boote C, Nguyen TD, 2015c Glaucoma-related Changes in the Mechanical Properties and Collagen Micro-architecture of the Human Sclera. PLoS One 10, e0131396. [PubMed: 26161963]

Coudrillier B, Tian J, Alexander S, Myers KM, Quigley HA, Nguyen TD, 2012 Biomechanics of the human posterior sclera: age- and glaucoma-related changes measured using inflation testing. Invest Ophthalmol Vis Sci 53, 1714–1728. [PubMed: 22395883]

Cruz Perez B, Pavlatos E, Morris HJ, Chen H, Pan X, Hart RT, Liu J, 2016 Mapping 3D Strains with Ultrasound Speckle Tracking: Method Validation and Initial Results in Porcine Scleral Inflation. Annals of biomedical engineering 44, 2302–2312. [PubMed: 26563101]

Cui W, Bryant MR, Sweet PM, McDonnell PJ, 2004 Changes in gene expression in response to mechanical strain in human scleral fibroblasts. Exp Eye Res 78, 275–284. [PubMed: 14729359]

Curtin BJ, Iwamoto T, Renaldo DP, 1979 Normal and staphylomatous sclera of high myopia. An electron microscopic study. Arch Ophthalmol 97, 912–915. [PubMed: 444126]

Danford FL, Yan D, Dreier RA, Cahir TM, Girkin CA, Vande Geest JP, 2013 Differences in the region- and depth-dependent microstructural organization in normal versus glaucomatous human posterior sclerae. Invest Ophthalmol Vis Sci 54, 7922–7932. [PubMed: 24204041]

Davidson RS, Dhaliwal D, Hamilton DR, Jackson M, Patterson L, Stonecipher K, Yoo SH, Braga-Mele R, Donaldson K, 2016 Surgical correction of presbyopia. J Cataract Refract Surg 42, 920–930. [PubMed: 27373400]

Daxer A, Misof K, Grabner B, Ettl A, Fratzl P, 1998 Collagen fibrils in the human corneal stroma: structure and ageing. Investigative Ophthalmology and Visual Science 39, 644–648. [PubMed: 9501878]

Demer JL, 2016 Optic Nerve Sheath as a Novel Mechanical Load on the Globe in Ocular Duction. Invest Ophthalmol Vis Sci 57, 1826–1838. [PubMed: 27082297]

Devalla SK, Chin KS, Mari JM, Tun TA, Strouthidis NG, Aung T, Thiery AH, Girard MJA, 2018a A Deep Learning Approach to Digitally Stain Optical Coherence Tomography Images of the Optic Nerve Head. Invest Ophthalmol Vis Sci 59, 63–74. [PubMed: 29313052]

Devalla SK, Renukanand PK, Sreedhar BK, Subramanian G, Zhang L, Perera S, Mari JM, Chin KS, Tun TA, Strouthidis NG, Aung T, Thiery AH, Girard MJA, 2018b DRUNET: a dilated-residual U-Net deep learning network to segment optic nerve head tissues in optical coherence tomography images. Biomedical optics express 9, 3244–3265. [PubMed: 29984096]

Dikici AS, Mihmanli I, Kilic F, Ozkok A, Kuyumcu G, Sultan P, Samanci C, Halit Yilmaz M, Rafiee B, Tamcelik N, Isik Hasiloglu Z, Kantarci F, 2016 In Vivo Evaluation of the Biomechanical Properties of Optic Nerve and Peripapillary Structures by Ultrasonic Shear Wave Elastography in

Glaucoma. Iranian journal of radiology : a quarterly journal published by the Iranian Radiological Society 13, e36849. [PubMed: 27703662]

Dolgin E, 2015 The myopia boom. Nature 519, 276–278. [PubMed: 25788077]

Dotan A, Kremer I, Gal-Or O, Livnat T, Zigler A, Bourla D, Weinberger D, 2016 Scleral Cross-linking Using Riboflavin and Ultraviolet-A Radiation for Prevention of Axial Myopia in a Rabbit Model. J Vis Exp, e53201. [PubMed: 27077753]

Downs JC, 2015 Optic nerve head biomechanics in aging and disease. Exp Eye Res 133, 19–29. [PubMed: 25819451]

Downs JC, Suh JK, Thomas KA, Bellezza AJ, Hart RT, Burgoyne CF, 2005 Viscoelastic material properties of the peripapillary sclera in normal and early-glaucoma monkey eyes. Invest Ophthalmol Vis Sci 46, 540–546. [PubMed: 15671280]

Eilaghi A, Flanagan JG, Tertinegg I, Simmons CA, Wayne Brodland G, Ross Ethier C, 2010 Biaxial mechanical testing of human sclera. Journal of biomechanics 43, 1696–1701. [PubMed: 20399430]

Elsheikh A, Anderson K, 2005 Comparative study of corneal strip extensometry and inflation tests. J R Soc Interface 2, 177–185. [PubMed: 16849178]

Elsheikh A, Geraghty B, Alhasso D, Knappett J, Campanelli M, Rama P, 2010 Regional variation in the biomechanical properties of the human sclera. Exp Eye Res 90, 624–633. [PubMed: 20219460]

Fazio MA, Clark ME, Bruno L, Girkin CA, 2018 In vivo optic nerve head mechanical response to intraocular and cerebrospinal fluid pressure: imaging protocol and quantification method. Scientific reports 8, 12639. [PubMed: 30140057]

Fazio MA, Grytz R, Morris JS, Bruno L, Gardiner SK, Girkin CA, Downs JC, 2014a Age-related changes in human peripapillary scleral strain. Biomech Model Mechanobiol 13, 551–563. [PubMed: 23896936]

Fazio MA, Grytz R, Morris JS, Bruno L, Girkin CA, Downs JC, 2014b Human scleral structural stiffness increases more rapidly with age in donors of African descent compared to donors of European descent. Invest Ophthalmol Vis Sci 55, 7189–7198. [PubMed: 25237162]

Feneck EM, Lewis PN, Ralphs J, Meek KM, 2018 A comparative study of the elastic fibre system within the mouse and human cornea. Exp Eye Res 177, 35–44. [PubMed: 30053442]

Feola AJ, Coudrillier B, Mulvihill J, Geraldes DM, Vo NT, Albon J, Abel RL, Samuels BC, Ethier CR, 2017 Deformation of the Lamina Cribrosa and Optic Nerve Due to Changes in Cerebrospinal Fluid Pressure. Invest Ophthalmol Vis Sci 58, 2070–2078. [PubMed: 28389675]

Feola AJ, Myers JG, Raykin J, Mulugeta L, Nelson ES, Samuels BC, Ethier CR, 2016 Finite Element Modeling of Factors Influencing Optic Nerve Head Deformation Due to Intracranial Pressure. Invest Ophthalmol Vis Sci 57, 1901–1911. [PubMed: 27088762]

Fessel G, Cadby J, Wunderli S, van Weeren R, Snedeker JG, 2014 Dose- and time-dependent effects of genipin crosslinking on cell viability and tissue mechanics - toward clinical application for tendon repair. Acta biomaterialia 10, 1897–1906. [PubMed: 24384123]

Flitcroft DI, Loughman J, Wildsoet CF, Williams C, Guggenheim JA, 2018 Novel Myopia Genes and Pathways Identified From Syndromic Forms of Myopia. Invest Ophthalmol Vis Sci 59, 338–348. [PubMed: 29346494]

Franz-Odendaal TA, 2008 Scleral ossicles of teleostei: evolutionary and developmental trends. Anatomical record (Hoboken, N.J. : 2007) 291, 161–168.

Friberg TR, Lace JW, 1988 A comparison of the elastic properties of human choroid and sclera. Exp Eye Res 47, 429–436. [PubMed: 3181326]

Fullwood NJ, Hammiche A, Pollock HM, Hourston DJ, Song M, 1995 Atomic force microscopy of the cornea and sclera. Curr Eye Res 14, 529–535. [PubMed: 7587298]

Funata M, Tokoro T, 1990 Scleral change in experimentally myopic monkeys. Graefes Arch Clin Exp Ophthalmol 228, 174–179. [PubMed: 2338255]

Garcia MB, Jha AK, Healy KE, Wildsoet CF, 2017 A Bioengineering Approach to Myopia Control Tested in a Guinea Pig Model. Invest Ophthalmol Vis Sci 58, 1875–1886. [PubMed: 28358959]

Gawne TJ, Siegwart JT Jr., Ward AH, Norton TT, 2017 The wavelength composition and temporal modulation of ambient lighting strongly affect refractive development in young tree shrews. Exp Eye Res 155, 75–84. [PubMed: 27979713]

Ge P, Bottega WJ, Prenner JL, Fine HF, 2017 On the behavior of an eye encircled by a scleral buckle. Journal of mathematical biology 74, 313–332. [PubMed: 27230781]

Gentle A, Liu Y, Martin JE, Conti GL, McBrien NA, 2003 Collagen gene expression and the altered accumulation of scleral collagen during the development of high myopia. J Biol Chem 278, 16587–16594. [PubMed: 12606541]

Geraghty B, Jones SW, Rama P, Akhtar R, Elsheikh A, 2012 Age-related variations in the biomechanical properties of human sclera. J Mech Behav Biomed Mater 16, 181–191. [PubMed: 23182387]

Girard MJ, Beotra MR, Chin KS, Sandhu A, Clemo M, Nikita E, Kamal DS, Papadopoulos M, Mari JM, Aung T, Strouthidis NG, 2016 In Vivo 3-Dimensional Strain Mapping of the Optic Nerve Head Following Intraocular Pressure Lowering by Trabeculectomy. Ophthalmology 123, 1190–1200. [PubMed: 26992836]

Girard MJ, Chin KS, Devalla SK, Aung T, Jonas JB, Wang YX, Thiery AH, 2018 Deep Learning can Exploit 3D Structural Information of the Optic Nerve Head to Provide a Glaucoma Diagnostic Power Superior to that of Retinal Nerve Fibre Layer Thickness., Association for Research in Vision and Ophthalmology, Honolulu, p. 4081.

Girard MJ, Dahlmann-Noor A, Rayapureddi S, Bechara JA, Bertin BM, Jones H, Albon J, Khaw PT, Ethier CR, 2011a Quantitative mapping of scleral fiber orientation in normal rat eyes. Invest Ophthalmol Vis Sci 52, 9684–9693. [PubMed: 22076988]

Girard MJ, Downs JC, Bottlang M, Burgoyne CF, Suh JK, 2009a Peripapillary and Posterior Scleral Mechanics-Part II: Experimental and Inverse Finite Element Characterization. J Biomech Eng 131, 051012. [PubMed: 19388782]

Girard MJ, Downs JC, Burgoyne CF, Suh JK, 2009b Peripapillary and posterior scleral mechanics-part I: development of an anisotropic hyperelastic constitutive model. J Biomech Eng 131, 051011. [PubMed: 19388781]

Girard MJ, Strouthidis NG, Desjardins A, Mari JM, Ethier CR, 2013 In vivo optic nerve head biomechanics: performance testing of a three-dimensional tracking algorithm. J R Soc Interface 10, 20130459. [PubMed: 23883953]

Girard MJ, Strouthidis NG, Ethier CR, Mari JM, 2011b Shadow removal and contrast enhancement in optical coherence tomography images of the human optic nerve head. Invest Ophthalmol Vis Sci 52, 7738–7748. [PubMed: 21551412]

Girard MJ, Suh JK, Bottlang M, Burgoyne CF, Downs JC, 2009c Scleral Biomechanics in the Aging Monkey Eye. Invest Ophthalmol Vis Sci 50, 5226–5237. [PubMed: 19494203]

Girard MJ, Suh JK, Bottlang M, Burgoyne CF, Downs JC, 2011c Biomechanical Changes in the Sclera of Monkey Eyes Exposed to Chronic IOP Elevations. Invest Ophthalmol Vis Sci.

Glasser A, 2008 Restoration of accommodation: surgical options for correction of presbyopia. Clin Exp Optom 91, 279–295. [PubMed: 18399800]

Glasser A, Troilo D, Howland HC, 1994 The Mechanism of Corneal Accommodation in Chicks. Vision research 34, 1549–1566. [PubMed: 7941363]

Gogola A, Jan NJ, Brazile B, Lam P, Lathrop KL, Chan KC, Sigal IA, 2018a Spatial Patterns and Age-Related Changes of the Collagen Crimp in the Human Cornea and Sclera. Invest Ophthalmol Vis Sci 59, 2987–2998. [PubMed: 30025116]

Gogola A, Jan NJ, Lathrop KL, Sigal IA, 2018b Radial and Circumferential Collagen Fibers Are a Feature of the Peripapillary Sclera of Human, Monkey, Pig, Cow, Goat, and Sheep. Invest Ophthalmol Vis Sci 59, 4763–4774. [PubMed: 30304458]

Grant CA, Thomson NH, Savage MD, Woon HW, Greig D, 2011 Surface characterisation and biomechanical analysis of the sclera by atomic force microscopy. J Mech Behav Biomed Mater 4, 535–540. [PubMed: 21396602]

Green JS, Bear JC, Johnson GJ, 1986 The burden of genetically determined eye disease. Br J Ophthalmol 70, 696–699. [PubMed: 3756127]

Grytz R, 2018 Scleral Remodeling in Myopia, in: Roberts C, Dupps WJ, Downs JC (Eds.), Biomechanics of the Eye, 1st ed. Kugler, Amsterdam, pp. 383–403.

Grytz R, El Hamdaoui M, 2017 Multi-Scale Modeling of Vision-Guided Remodeling and Age-Dependent Growth of the Tree Shrew Sclera During Eye Development and Lens-Induced Myopia. Journal Of Elasticity 129, 171–195. [PubMed: 28966436]

Grytz R, El Hamdaoui M, Levy AM, Girkin CA, Samuels BC, 2018 Scleral Crosslinking Using Genipin Has a Dose-Dependent Effect on Form-Deprivation Myopia in Tree Shrews, Association for Research in Vision and Ophthalmology Annual Meeting, Honolulu, p. 708.

Grytz R, Fazio MA, Libertiaux V, Bruno L, Gardiner S, Girkin CA, Downs JC, 2014 Age- and race-related differences in human scleral material properties. Invest Ophthalmol Vis Sci 55, 8163–8172. [PubMed: 25389203]

Grytz R, Meschke G, 2009 Constitutive modeling of crimped collagen fibrils in soft tissues. J Mech Behav Biomed Mater 2, 522–533. [PubMed: 19627859]

Grytz R, Meschke G, Jonas JB, 2011 The collagen fibril architecture in the lamina cribrosa and peripapillary sclera predicted by a computational remodeling approach. Biomech Model Mechanobiol 10, 371–382. [PubMed: 20628781]

Grytz R, Siegwart JT Jr., 2015 Changing material properties of the tree shrew sclera during minus lens compensation and recovery. Invest Ophthalmol Vis Sci 56, 2065–2078. [PubMed: 25736788]

Guggenheim JA, McBrien NA, 1996 Form-deprivation myopia induces activation of scleral matrix metalloproteinase-2 in tree shrew. Invest Ophthalmol Vis Sci 37, 1380–1395. [PubMed: 8641841]

Guo L, Frost MR, He L, Siegwart JT Jr., Norton TT, 2013 Gene expression signatures in tree shrew sclera in response to three myopiagenic conditions. Invest Ophthalmol Vis Sci 54, 6806–6819. [PubMed: 24045991]

Hamanaka T, 1989 Scleral spur and ciliary muscle in man and monkey. Japanese journal of ophthalmology 33, 221–236. [PubMed: 2761116]

Hamilton DR, Davidorf JM, Maloney RK, 2002 Anterior ciliary sclerotomy for treatment of presbyopia: a prospective controlled study. Ophthalmology 109, 1970–1976; discussion 1976–1977. [PubMed: 12414400]

Harper AR, Summers JA, 2015 The dynamic sclera: extracellular matrix remodeling in normal ocular growth and myopia development. Exp Eye Res 133, 100–111. [PubMed: 25819458]

Hayes S, Boote C, Tuft SJ, Quantock AJ, Meek KM, 2007 A study of corneal thickness, shape and collagen organisation in keratoconus using videokeratography and X-ray scattering techniques. Experimental Eye Research 84, 423–434. [PubMed: 17178118]

Hipsley A, Hall B, Rocha KM, 2018 Scleral surgery for the treatment of presbyopia: where are we today? Eye and vision (London, England) 5, 4.

Hipsley A, Ma DH, Sun CC, Jackson MA, Goldberg D, Hall B, 2017 Visual outcomes 24 months after LaserACE. Eye and vision (London, England) 4, 15.

Ho LC, Sigal IA, Jan NJ, Squires A, Tse Z, Wu EX, Kim SG, Schuman JS, Chan KC, 2014 Magic angle-enhanced MRI of fibrous microstructures in sclera and cornea with and without intraocular pressure loading. Invest Ophthalmol Vis Sci 55, 5662–5672. [PubMed: 25103267]

Ho LC, Sigal IA, Jan NJ, Yang X, van der Merwe Y, Yu Y, Chau Y, Leung CK, Conner IP, Jin T, Wu EX, Kim SG, Wollstein G, Schuman JS, Chan KC, 2016 Noninvasive MRI Assessments of Tissue Microstructures and Macromolecules in the Eye upon Biomechanical or Biochemical Modulation. Scientific reports 6, 32080. [PubMed: 27561353]

Holden BA, Fricke TR, Wilson DA, Jong M, Naidoo KS, Sankaridurg P, Wong TY, Naduvilath TJ, Resnikoff S, 2016 Global Prevalence of Myopia and High Myopia and Temporal Trends from 2000 through 2050. Ophthalmology 123, 1036–1042. [PubMed: 26875007]

Howlett MH, McFadden SA, 2007 Emmetropization and schematic eye models in developing pigmented guinea pigs. Vision research 47, 1178–1190. [PubMed: 17360016]

Hu S, Cui D, Yang X, Hu J, Wan W, Zeng J, 2011 The crucial role of collagen-binding integrins in maintaining the mechanical properties of human scleral fibroblasts-seeded collagen matrix. Mol Vis 17, 1334–1342. [PubMed: 21647271]

Hua Y, Tong J, Ghate D, Kedar S, Gu L, 2017 Intracranial Pressure Influences the Behavior of the Optic Nerve Head. J Biomech Eng 139.

Hua Y, Voorhees AP, Sigal IA, 2018 Cerebrospinal Fluid Pressure: Revisiting Factors Influencing Optic Nerve Head Biomechanics. Invest Ophthalmol Vis Sci 59, 154–165. [PubMed: 29332130]

Ismail EN, Ruberti JW, Malek G, 2017 Quick-freeze/deep-etch electron microscopy visualization of the mouse posterior pole. Exp Eye Res 162, 62–72. [PubMed: 28629927]

Izu Y, Ansorge HL, Zhang G, Soslowsky LJ, Bonaldo P, Chu ML, Birk DE, 2011 Dysfunctional tendon collagen fibrillogenesis in collagen VI null mice. Matrix Biol 30, 53–61. [PubMed: 20951202]

Jan NJ, Brazile BL, Hu D, Grube G, Wallace J, Gogola A, Sigal IA, 2018 Crimp around the globe; patterns of collagen crimp across the corneoscleral shell. Exp Eye Res 172, 159–170. [PubMed: 29660327]

Jan NJ, Gomez C, Moed S, Voorhees AP, Schuman JS, Bilonick RA, Sigal IA, 2017a Microstructural Crimp of the Lamina Cribrosa and Peripapillary Sclera Collagen Fibers. Invest Ophthalmol Vis Sci 58, 3378–3388. [PubMed: 28687851]

Jan NJ, Grimm JL, Tran H, Lathrop KL, Wollstein G, Bilonick RA, Ishikawa H, Kagemann L, Schuman JS, Sigal IA, 2015 Polarization microscopy for characterizing fiber orientation of ocular tissues. Biomedical optics express 6, 4705–4718. [PubMed: 26713188]

Jan NJ, Lathrop K, Sigal IA, 2017b Collagen Architecture of the Posterior Pole: High-Resolution Wide Field of View Visualization and Analysis Using Polarized Light Microscopy. Invest Ophthalmol Vis Sci 58, 735–744. [PubMed: 28146238]

Jan NJ, Sigal IA, 2018 Collagen fiber recruitment: A microstructural basis for the nonlinear response of the posterior pole of the eye to increases in intraocular pressure. Acta biomaterialia 72, 295–305. [PubMed: 29574185]

Janowski M, Bulte JW, Handa JT, Rini D, Walczak P, 2015 Concise Review: Using Stem Cells to Prevent the Progression of Myopia-A Concept. Stem cells (Dayton, Ohio) 33, 2104–2113.

Jay L, Bourget JM, Goyer B, Singh K, Brunette I, Ozaki T, Proulx S, 2015 Characterization of tissue-engineered posterior corneas using second- and third-harmonic generation microscopy. PLoS One 10, e0125564. [PubMed: 25918849]

Jin Y, Wang X, Zhang L, Jonas JB, Aung T, Schmetterer L, Girard MJA, 2018 Modeling the Origin of the Ocular Pulse and Its Impact on the Optic Nerve Head. Invest Ophthalmol Vis Sci 59, 3997–4010. [PubMed: 30098188]

Jonas JB, 2011 Role of cerebrospinal fluid pressure in the pathogenesis of glaucoma. Acta Ophthalmol 89, 505–514. [PubMed: 20456257]

Jonas JB, Dai Y, Panda-Jonas S, 2016a Peripapillary Suprachoroidal Cavitation, Parapapillary Gamma Zone and Optic Disc Rotation Due to the Biomechanics of the Optic Nerve Dura Mater. Invest Ophthalmol Vis Sci 57, 4373. [PubMed: 27557435]

Jonas JB, Holbach L, Panda-Jonas S, 2014 Scleral cross section area and volume and axial length. PLoS One 9, e93551. [PubMed: 24681550]

Jonas JB, Holbach L, Panda-Jonas S, 2016b Histologic differences between primary high myopia and secondary high myopia due to congenital glaucoma. Acta Ophthalmol 94, 147–153. [PubMed: 26695106]

Jones HJ, Girard MJ, White N, Fautsch MP, Morgan JE, Ethier CR, Albon J, 2015 Quantitative analysis of three-dimensional fibrillar collagen microstructure within the normal, aged and glaucomatous human optic nerve head. J R Soc Interface 12.

Kaji Y, Akiyama T, Segawa H, Oshika T, Kano H, 2017 Raman Microscopy: A Noninvasive Method to Visualize the Localizations of Biomolecules in the Cornea. Cornea 36 Suppl 1, S67–s71. [PubMed: 28902016]

Kamma-Lorger CS, Boote C, Hayes S, Moger J, Burghammer M, Knupp C, Quantock AJ, Sorensen T, Di Cola E, White N, Young RD, Meek KM, 2010 Collagen and mature elastic fibre organisation as a function of depth in the human cornea and limbus. J Struct Biol 169, 424–430. [PubMed: 19914381]

Kaufmann C, Bachmann LM, Robert YC, Thiel MA, 2006 Ocular pulse amplitude in healthy subjects as measured by dynamic contour tonometry. Arch Ophthalmol 124, 1104–1108. [PubMed: 16908812]

Keeley FW, Morin JD, Vesely S, 1984 Characterisation of collagen from normal human sclera. Experimental Eye Research 39, 533–542. [PubMed: 6519194]

Keyes JT, Yan D, Rader JH, Utzinger U, Vande Geest JP, 2011 A gimbal-mounted pressurization chamber for macroscopic and microscopic assessment of ocular tissues. J Biomech Eng 133, 095001. [PubMed: 22010754]

Kimball FE, Nguyen C, Steinhart MR, Nguyen TD, Pease ME, Oglesby EN, Oveson BC, Quigley HA, 2014 Experimental scleral cross-linking increases glaucoma damage in a mouse model . Exp Eye Res [In Press].

Kimura S, Kobayashi M, Nakamura M, Hirano K, Awaya S, Hoshino T, 1995 Immunoelectron microscopic localization of decorin in aged human corneal and scleral stroma. Journal of electron microscopy 44, 445–449. [PubMed: 8991920]

Kokott W, 1934 Das spaltlinienbild der sklera (Ein beitrag zum funktionellen bau der sklera) Klin Monbl Augenheilkd 92, 177–185.

Komai Y, Ushiki T, 1991 The three-dimensional organisation of collagen fibrils in the human cornea and sclera. Investigative Ophthalmology and Visual Science 32, 2244–2258. [PubMed: 2071337]

Kouchaki B, Hashemi H, Yekta A, Khabazkhoob M, 2017 Comparison of current tonometry techniques in measurement of intraocular pressure. Journal of current ophthalmology 29, 92–97. [PubMed: 28626817]

Krumpaszky HG, Ludtke R, Mickler A, Klauss V, Selbmann HK, 1999 Blindness incidence in Germany. A population-based study from Wurttemberg-Hohenzollern. Ophthalmologica. Journal international d'ophtalmologie. International journal of ophthalmology. Zeitschrift fur Augenheilkunde 213, 176–182. [PubMed: 10202291]

Kuchtey J, Kuchtey RW, 2014 The microfibril hypothesis of glaucoma: implications for treatment of elevated intraocular pressure. Journal of ocular pharmacology and therapeutics : the official journal of the Association for Ocular Pharmacology and Therapeutics 30, 170–180.

Lanchares E, Del Buey MA, Cristobal JA, Calvo B, Ascaso FJ, Malve M, 2016 Computational Simulation of Scleral Buckling Surgery for Rhegmatogenous Retinal Detachment: On the Effect of the Band Size on the Myopization. Journal of ophthalmology 2016, 3578617. [PubMed: 27413542]

Lari DR, Schultz DS, Wang AS, Lee OT, Stewart JM, 2012 Scleral mechanics: comparing whole globe inflation and uniaxial testing. Exp Eye Res 94, 128–135. [PubMed: 22155444]

Leung LK, Ko MW, Ye C, Lam DC, Leung CK, 2014 Noninvasive measurement of scleral stiffness and tangent modulus in porcine eyes. Invest Ophthalmol Vis Sci 55, 3721–3726. [PubMed: 24833738]

Levy AM, Fazio MA, Grytz R, 2018 Experimental myopia increases and scleral crosslinking using genipin inhibits cyclic softening in the tree shrew sclera. Ophthalmic Physiol Opt 38, 246–256. [PubMed: 29691925]

Lewis PN, White TL, Young RD, Bell JS, Winlove CP, Meek KM, 2016 Three-dimensional arrangement of elastic fibers in the human corneal stroma. Exp Eye Res 146, 43–53. [PubMed: 26704458]

Lima EG, Tan AR, Tai T, Marra KG, DeFail A, Ateshian GA, Hung CT, 2009 Genipin enhances the mechanical properties of tissue-engineered cartilage and protects against inflammatory degradation when used as a medium supplement. J Biomed Mater Res A 91, 692–700. [PubMed: 19025982]

Lin JT, Mallo O, 2003 Treatment of presbyopia by infrared laser radial sclerectomy. J Refract Surg 19, 465–467. [PubMed: 12899482]

Lin X, Naidu RK, Dai J, Zhou X, Qu X, Zhou H, 2019 Scleral Cross-Linking Using Glyceraldehyde for the Prevention of Axial Elongation in the Rabbit: Blocked Axial Elongation and Altered Scleral Microstructure. Curr Eye Res 44, 162–171. [PubMed: 30222005]

Lin X, Wang BJ, Wang YC, Chu RY, Dai JH, Zhou XT, Qu XM, Liu H, Zhou H, 2018 Scleral ultrastructure and biomechanical changes in rabbits after negative lens application. Int J Ophthalmol 11, 354–362. [PubMed: 29600166]

Linsenmayer TF, Gibney E, Igoe F, Gordon MK, Fitch JM, Fessler LI, Birk DE, 1993 Type V collagen: molecular structure and fibrillar organization of the chicken alpha 1(V) NH2-terminal domain, a putative regulator of corneal fibrillogenesis. The Journal of cell biology 121, 1181–1189. [PubMed: 8501123]

Liu S, Li S, Wang B, Lin X, Wu Y, Liu H, Qu X, Dai J, Zhou X, Zhou H, 2016 Scleral Cross-Linking Using Riboflavin UVA Irradiation for the Prevention of Myopia Progression in a Guinea Pig Model: Blocked Axial Extension and Altered Scleral Microstructure. PLoS One 11, e0165792. [PubMed: 27829051]

Liu Y, Wildsoet C, 2011 The effect of two-zone concentric bifocal spectacle lenses on refractive error development and eye growth in young chicks. Invest Ophthalmol Vis Sci 52, 1078–1086. [PubMed: 20861487]

Lu JL, Hall L, Liu J, 2018 Improving Glaucoma Surgical Outcomes with Adjunct Tools. Journal of current glaucoma practice 12, 19–28. [PubMed: 29861578]

Luan H, Roberts R, Sniegowski M, Goebel DJ, Berkowitz BA, 2006 Retinal thickness and subnormal retinal oxygenation response in experimental diabetic retinopathy. Invest Ophthalmol Vis Sci 47, 320–328. [PubMed: 16384980]

Luesma MJ, Gherghiceanu M, Popescu LM, 2013 Telocytes and stem cells in limbus and uvea of mouse eye. Journal of cellular and molecular medicine 17, 1016–1024. [PubMed: 23991685]

Ma Y, Pavlatos E, Clayson K, Pan X, Kwok S, Sandwisch T, Liu J, 2019 Mechanical Deformation of Human Optic Nerve Head and Peripapillary Tissue in Response to Acute IOP Elevation. Invest Ophthalmol Vis Sci 60, 913–920. [PubMed: 30835783]

Malecaze FJ, Gazagne CS, Tarroux MC, Gorrand JM, 2001 Scleral expansion bands for presbyopia. Ophthalmology 108, 2165–2171. [PubMed: 11733253]

Malik NS, Moss SJ, Ahmed N, Furth AJ, Wall RS, Meek KM, 1992 Ageing of the human corneal stroma: structural and biochemical changes. Biochim Biophys Acta 1138, 222–228. [PubMed: 1547284]

Markov PP, Eliasy A, Pijanka JK, Htoon HM, Paterson NG, Sorensen T, Elsheikh A, Girard MJA, Boote C, 2018 Bulk changes in posterior scleral collagen microstructure in human high myopia. Mol Vis 24, 818–833. [PubMed: 30713421]

Marshall GE, 1995 Human scleral elastic system: an immunoelectron microscopic study. Br J Ophthalmol 79, 57–64. [PubMed: 7533533]

Marshall GE, Konstas AGP, Lee WR, 1993 Collagens in the aged humour macular sclera. Current Eye Research 12, 143–153. [PubMed: 8449025]

McBrien NA, Cornell LM, Gentle A, 2001 Structural and ultrastructural changes to the sclera in a mammalian model of high myopia. Invest Ophthalmol Vis Sci 42, 2179–2187. [PubMed: 11527928]

McBrien NA, Jobling AI, Gentle A, 2009 Biomechanics of the sclera in myopia: extracellular and cellular factors. Optom Vis Sci. 86, E23–30. [PubMed: 19104466]

McBrien NA, Lawlor P, Gentle A, 2000 Scleral remodeling during the development of and recovery from axial myopia in the tree shrew. Invest Ophthalmol Vis Sci 41, 3713–3719. [PubMed: 11053267]

McBrien NA, Metlapally R, Jobling AI, Gentle A, 2006 Expression of collagen-binding integrin receptors in the mammalian sclera and their regulation during the development of myopia. Invest Ophthalmol Vis Sci 47, 4674–4682. [PubMed: 17065473]

McBrien NA, Norton TT, 1994 Prevention of collagen crosslinking increases form-deprivation myopia in tree shrew. Exp Eye Res 59, 475–486. [PubMed: 7859823]

Meek K, Boote C, 2004 The organisation of collagen in the corneal stroma. Experimental Eye Research 78, 503–512. [PubMed: 15106929]

Meek KM, Boote C, 2009 The use of x-ray scattering techniques to quantify the orientation and distribution of collagen in the corneal stroma. Prog Retin Eye Res 28, 369–392. [PubMed: 19577657]

Meller D, Peters K, Meller K, 1997 Human cornea and sclera studied by atomic force microscopy. Cell Tissue Res 288, 111–118. [PubMed: 9042778]

Midgett DE, Jefferys JL, Quigley HA, Nguyen TD, 2018 The Contribution of Sulfated Glycosaminoglycans to the Inflation Response of the Human Optic Nerve Head. Invest Ophthalmol Vis Sci 59, 3144–3154. [PubMed: 30025126]

Morgan WH, Yu DY, Cooper RL, Alder VA, Cringle SJ, Constable IJ, 1995 The influence of cerebrospinal fluid pressure on the lamina cribrosa tissue pressure gradient. Invest Ophthalmol Vis Sci 36, 1163–1172. [PubMed: 7730025]

Moring AG, Baker JR, Norton TT, 2007 Modulation of glycosaminoglycan levels in tree shrew sclera during lens-induced myopia development and recovery. Invest Ophthalmol Vis Sci 48, 2947–2956. [PubMed: 17591859]

Munier A, Gunning T, Kenny D, O'Keefe M, 1998 Causes of blindness in the adult population of the Republic of Ireland. Br J Ophthalmol 82, 630–633. [PubMed: 9797662]

Murienne BJ, Chen ML, Quigley HA, Nguyen TD, 2016 The contribution of glycosaminoglycans to the mechanical behaviour of the posterior human sclera. J R Soc Interface 13.

Murienne BJ, Jefferys JL, Quigley HA, Nguyen TD, 2015 The effects of glycosaminoglycan degradation on the mechanical behavior of the posterior porcine sclera. Acta biomaterialia 12, 195–206. [PubMed: 25448352]

Myers KM, Cone FE, Quigley HA, Gelman S, Pease ME, Nguyen TD, 2010a The in vitro inflation response of mouse sclera. Exp Eye Res 91, 866–875. [PubMed: 20868685]

Myers KM, Cone FE, Quigley HA, Nguyen TD, 2011 The Scleral Inflation Response of Mouse Eyes to Increases in Pressure, in: Proulx T (Ed.), Mechanics of Biological Systems and Materials. Springer, New York.

Myers KM, Coudrillier B, Boyce BL, Nguyen TD, 2010b The inflation response of the posterior bovine sclera. Acta biomaterialia 6, 4327–4335. [PubMed: 20558331]

Newton RH, Meek KM, 1998 Circumcorneal annulus of collagen fibrils in the human limbus. Investigative Ophthalmology and Visual Science 39, 1125–1134. [PubMed: 9620071]

Nguyen C, Cone FE, Nguyen TD, Coudrillier B, Pease ME, Steinhart MR, Oglesby EN, Jefferys JL, Quigley HA, 2013 Studies of scleral biomechanical behavior related to susceptibility for retinal ganglion cell loss in experimental mouse glaucoma. Invest Ophthalmol Vis Sci 54, 1767–1780. [PubMed: 23404116]

Nguyen C, Midgett D, Kimball E, Jefferys J, Nguyen TD, Schaub J, Pease M, Quigley H, 2018 Age-Related Changes in Quantitative Strain of Mouse Astrocytic Lamina Cribrosa and Peripapillary Sclera Using Confocal Microscopy in an Explant Model. Invest Ophthalmol Vis Sci 59, 5157–5166. [PubMed: 30372742]

Nguyen C, Midgett D, Kimball EC, Steinhart MR, Nguyen TD, Pease ME, Oglesby EN, Jefferys JL, Quigley HA, 2017 Measuring Deformation in the Mouse Optic Nerve Head and Peripapillary Sclera. Invest Ophthalmol Vis Sci 58, 721–733. [PubMed: 28146237]

Norman RE, Flanagan JG, Rausch SM, Sigal IA, Tertinegg I, Eilaghi A, Portnoy S, Sled JG, Ethier CR, 2010a Dimensions of the human sclera: Thickness measurement and regional changes with axial length. Exp Eye Res 90, 277–284. [PubMed: 19900442]

Norman RE, Flanagan JG, Sigal IA, Rausch SM, Tertinegg I, Ethier CR, 2010b Finite element modeling of the human sclera: Influence on optic nerve head biomechanics and connections with glaucoma. Exp Eye Res, 9 29.

Norton TT, Amedo AO, Siegwart JT Jr., 2010 The effect of age on compensation for a negative lens and recovery from lens-induced myopia in tree shrews (Tupaia glis belangeri). Vision research 50, 564–576. [PubMed: 20045711]

Norton TT, Rada JA, 1995 Reduced extracellular matrix in mammalian sclera with induced myopia. Vision research 35, 1271–1281. [PubMed: 7610587]

Norton TT, Siegwart JT Jr., 1995 Animal models of emmetropization: matching axial length to the focal plane. Journal of the American Optometric Association 66, 405–414. [PubMed: 7560727]

Oglesby EN, Tezel G, Cone-Kimball E, Steinhart MR, Jefferys J, Pease ME, Quigley HA, 2016 Scleral fibroblast response to experimental glaucoma in mice. Mol Vis 22, 82–99. [PubMed: 26900327]

Ohlendorf A, Schaeffel F, 2009 Contrast adaptation induced by defocus - a possible error signal for emmetropization? Vision research 49, 249–256. [PubMed: 19000917]

Ohno-Matsui K, Jonas JB, 2018 Posterior staphyloma in pathologic myopia. Prog Retin Eye Res.

Palko JR, Morris HJ, Pan X, Harman CD, Koehl KL, Gelatt KN, Plummer CE, Komaromy AM, Liu J, 2016 Influence of Age on Ocular Biomechanical Properties in a Canine Glaucoma Model with ADAMTS10 Mutation. PLoS One 11, e0156466. [PubMed: 27271467]

Palko JR, Pan X, Liu J, 2011 Dynamic testing of regional viscoelastic behavior of canine sclera. Exp Eye Res 93, 825–832. [PubMed: 21983041]

Park CY, Marando CM, Liao JA, Lee JK, Kwon J, Chuck RS, 2016 Details of the Collagen and Elastin Architecture in the Human Limbal Conjunctiva, Tenon's Capsule and Sclera Revealed by Two-Photon Excited Fluorescence Microscopy. Invest Ophthalmol Vis Sci 57, 5602–5610. [PubMed: 27784064]

Park SW, Lee JJ, Lee JE, 2018 Scleral buckling in the management of rhegmatogenous retinal detachment: patient selection and perspectives. Clin Ophthalmol 12, 1605–1615. [PubMed: 30214145]

Pavlatos E, Ma Y, Clayson K, Pan X, Liu J, 2018 Regional Deformation of the Optic Nerve Head and Peripapillary Sclera During IOP Elevation. Invest Ophthalmol Vis Sci 59, 3779–3788. [PubMed: 30046819]

Pavlatos E, Perez BC, Morris HJ, Chen H, Palko JR, Pan X, Weber PA, Hart RT, Liu J, 2016 Three-Dimensional Strains in Human Posterior Sclera Using Ultrasound Speckle Tracking. J Biomech Eng 138, 021015. [PubMed: 26632258]

Perez BC, Morris HJ, Hart RT, Liu J, 2013 Finite element modeling of the viscoelastic responses of the eye during microvolumetric changes. Journal of biomedical science and engineering 6, 29–37. [PubMed: 24672621]

Phillips JR, Khalaj M, McBrien NA, 2000 Induced myopia associated with increased scleral creep in chick and tree shrew eyes. Invest Ophthalmol Vis Sci 41, 2028–2034. [PubMed: 10892839]

Phillips JR, McBrien NA, 2004 Pressure-induced changes in axial eye length of chick and tree shrew: significance of myofibroblasts in the sclera. Invest Ophthalmol Vis Sci 45, 758–763. [PubMed: 14985287]

Piez KA, Miller A, 1974 The structure of collagen fibrils. J Supramol Struct 2, 121–137. [PubMed: 4437176]

Pijanka JK, Abass A, Sorensen T, Elsheikh A, Boote C, 2013 A wide-angle X-ray fibre diffraction method for quantifying collagen orientation across large tissue areas: application to the human eyeball coat. Journal of Applied Crystallography 46, 1481–1489.

Pijanka JK, Coudrillier B, Ziegler K, Sorensen T, Meek KM, Nguyen TD, Quigley HA, Boote C, 2012 Quantitative mapping of collagen fiber orientation in non-glaucoma and glaucoma posterior human sclerae. Invest Ophthalmol Vis Sci 53, 5258–5270. [PubMed: 22786908]

Pijanka JK, Kimball EC, Pease ME, Abass A, Sorensen T, Nguyen TD, Quigley HA, Boote C, 2014 Changes in scleral collagen organization in murine chronic experimental glaucoma. Invest Ophthalmol Vis Sci 55, 6554–6564. [PubMed: 25228540]

Pijanka JK, Markov PP, Midgett D, Paterson NG, White N, Blain EJ, Nguyen TD, Quigley HA, Boote C, 2018 Quantification of collagen fiber structure using second harmonic generation imaging and two-dimensional discrete Fourier transform analysis: Application to the human optic nerve head. Journal of biophotonics 12, e201800376.

Pijanka JK, Spang MT, Sorensen T, Liu J, Nguyen TD, Quigley HA, Boote C, 2015 Depth-dependent changes in collagen organization in the human peripapillary sclera. PLoS One 10, e0118648. [PubMed: 25714753]

Pinsky PM, Van der Heide D, Chernyak D, 2005 Computational modeling of mechanical anisotropy in the cornea and sclera. Journal of Cataract and Refractive Surgery 31, 136–145. [PubMed: 15721706]

Poostchi A, Wong T, Chan KC, Kedzlie L, Sachdev N, Nicholas S, Garway-Heath DF, Wells AP, 2010 Optic disc diameter increases during acute elevations of intraocular pressure. Invest Ophthalmol Vis Sci 51, 2313–2316. [PubMed: 19907027]

Poukens V, Glasgow BJ, Demer JL, 1998 Nonvascular contractile cells in sclera and choroid of humans and monkeys. Invest Ophthalmol Vis Sci 39, 1765–1774. [PubMed: 9727398]

Qu J, Chen H, Zhu L, Ambalavanan N, Girkin CA, Murphy-Ullrich JE, Downs JC, Zhou Y, 2015 High-Magnitude and/or High-Frequency Mechanical Strain Promotes Peripapillary Scleral Myofibroblast Differentiation. Invest Ophthalmol Vis Sci 56, 7821–7830. [PubMed: 26658503]

Quantock AJ, Meek KM, 1988 Axial electron density of human scleral collagen. Location of proteoglycans by x-ray diffraction. Biophys J 54, 159–164. [PubMed: 3416025]

Quigley HA, Cone FE, 2013 Development of diagnostic and treatment strategies for glaucoma through understanding and modification of scleral and lamina cribrosa connective tissue. Cell Tissue Res.

Quigley HA, Dorman-Pease ME, Brown AE, 1991 Quantitative study of collagen and elastin of the optic nerve head and sclera in human and experimental monkey glaucoma. Curr Eye Res 10, 877–888. [PubMed: 1790718]

Rada JA, Achen VR, Penugonda S, Schmidt RW, Mount BA, 2000 Proteoglycan composition in the human sclera during growth and aging. Invest Ophthalmol Vis Sci 41, 1639–1648. [PubMed: 10845580]

Rada JA, Achen VR, Perry CA, Fox PW, 1997 Proteoglycans in the human sclera. Evidence for the presence of aggrecan. Invest Ophthalmol Vis Sci 38, 1740–1751. [PubMed: 9286262]

Raiskup F, Theuring A, Pillunat LE, Spoerl E, 2015 Corneal collagen crosslinking with riboflavin and ultraviolet-A light in progressive keratoconus: ten-year results. J Cataract Refract Surg 41, 41–46. [PubMed: 25532633]

Robinson PN, Booms P, 2001 The molecular pathogenesis of the Marfan syndrome. Cellular and molecular life sciences : CMLS 58, 1698–1707. [PubMed: 11706995]

Roth A, Muhlendyck H, De Gottrau P, 2002 [The function of Tenon's capsule revisited]. Journal francais d'ophtalmologie 25, 968–976.

Rucker FJ, Wallman J, 2012 Chicks use changes in luminance and chromatic contrast as indicators of the sign of defocus. Journal of vision 12.

Samuels BC, Siegwart JT, Zhan W, Hethcox L, Chimento M, Whitley R, Downs JC, Girkin CA, 2018 A Novel Tree Shrew (Tupaia belangeri) Model of Glaucoma. Invest Ophthalmol Vis Sci 59, 3136–3143. [PubMed: 30025140]

Scarcelli G, Pineda R, Yun SH, 2012 Brillouin optical microscopy for corneal biomechanics. Invest Ophthalmol Vis Sci 53, 185–190. [PubMed: 22159012]

Schaeffel F, Glasser A, Howland HC, 1988 Accommodation, refractive error and eye growth in chickens. Vision research 28, 639–657. [PubMed: 3195068]

Schultz DS, Lotz JC, Lee SM, Trinidad ML, Stewart JM, 2008 Structural factors that mediate scleral stiffness. Investigative Ophthalmology & Visual Science 49, 4232–4236. [PubMed: 18539943]

Shelton L, Rada JS, 2007 Effects of cyclic mechanical stretch on extracellular matrix synthesis by human scleral fibroblasts. Exp Eye Res 84, 314–322. [PubMed: 17123515]

Shen L, You QS, Xu X, Gao F, Zhang Z, Li B, Jonas JB, 2015a Scleral Thickness in Chinese Eyes. Invest Ophthalmol Vis Sci 56, 2720–2727. [PubMed: 25783605]

Shen L, You QS, Xu X, Gao F, Zhang Z, Li B, Jonas JB, 2016 Scleral and choroidal volume in relation to axial length in infants with retinoblastoma versus adults with malignant melanomas or end-stage glaucoma. Graefes Arch Clin Exp Ophthalmol 254, 1779–1786. [PubMed: 27116210]

Shen ZM, Zhang ZY, Zhang LY, Li ZG, Chu RY, 2015b Posterior scleral reinforcement combined with patching therapy for pre-school children with unilateral high myopia. Graefes Arch Clin Exp Ophthalmol 253, 1391–1395. [PubMed: 25694153]

Sherman SM, Norton TT, Casagrande VA, 1977 Myopia in the lid-sutured tree shrew (Tupaia glis). Brain research 124, 154–157. [PubMed: 843938]

Shin A, Park J, Demer JL, 2018 Opto-mechanical characterization of sclera by polarization sensitive optical coherence tomography. Journal of biomechanics 72, 173–179. [PubMed: 29580690]

Sibony P, Kupersmith MJ, Rohlf FJ, 2011 Shape analysis of the peripapillary RPE layer in papilledema and ischemic optic neuropathy. Invest Ophthalmol Vis Sci 52, 7987–7995. [PubMed: 21896851]

Sibony PA, 2016 Gaze Evoked Deformations of the Peripapillary Retina in Papilledema and Ischemic Optic Neuropathy. Invest Ophthalmol Vis Sci 57, 4979–4987. [PubMed: 27661851]

Siegwart JT Jr., Norton TT, 1999 Regulation of the mechanical properties of tree shrew sclera by the visual environment. Vision research 39, 387–407. [PubMed: 10326144]

Siegwart JT Jr., Norton TT, 2010 Binocular lens treatment in tree shrews: Effect of age and comparison of plus lens wear with recovery from minus lens-induced myopia. Exp Eye Res 91, 660–669. [PubMed: 20713041]

Siegwart JT Jr., Norton TT, 2011 Perspective: how might emmetropization and genetic factors produce myopia in normal eyes? Optom Vis Sci 88, E365–372. [PubMed: 21258261]

Siegwart JT Jr., Strang CE, 2007 Selective modulation of scleral proteoglycan mRNA levels during minus lens compensation and recovery. Mol Vis 13, 1878–1886. [PubMed: 17960126]

Sigal IA, Flanagan JG, Ethier CR, 2005 Factors influencing optic nerve head biomechanics. Invest Ophthalmol Vis Sci 46, 4189–4199. [PubMed: 16249498]

Sigal IA, Flanagan JG, Tertinegg I, Ethier CR, 2004 Finite element modeling of optic nerve head biomechanics. Invest Ophthalmol Vis Sci 45, 4378–4387. [PubMed: 15557446]

Sigal IA, Flanagan JG, Tertinegg I, Ethier CR, 2007 Predicted extension, compression and shearing of optic nerve head tissues. Exp Eye Res 85, 312–322. [PubMed: 17624325]

Sigal IA, Flanagan JG, Tertinegg I, Ethier CR, 2009 Modeling individual-specific human optic nerve head biomechanics. Part I: IOP-induced deformations and influence of geometry. Biomech Model Mechanobiol 8, 85–98. [PubMed: 18309526]

Sigal IA, Grimm JL, Jan NJ, Reid K, Minckler DS, Brown DJ, 2014a Eye-specific IOP-induced displacements and deformations of human lamina cribrosa. Invest Ophthalmol Vis Sci 55, 1–15. [PubMed: 24334450]

Sigal IA, Grimm JL, Schuman JS, Kagemann L, Ishikawa H, Wollstein G, 2014b A method to estimate biomechanics and mechanical properties of optic nerve head tissues from parameters measurable using optical coherence tomography. IEEE transactions on medical imaging 33, 1381–1389. [PubMed: 24691117]

Sigal IA, Wang B, Strouthidis NG, Akagi T, Girard MJ, 2014c Recent advances in OCT imaging of the lamina cribrosa. Br J Ophthalmol 98 Suppl 2, ii34–39. [PubMed: 24934221]

Sigal IA, Yang H, Roberts MD, Burgoyne CF, Downs JC, 2011a IOP-induced lamina cribrosa displacement and scleral canal expansion: an analysis of factor interactions using parameterized eye-specific models. Invest Ophthalmol Vis Sci 52, 1896–1907. [PubMed: 20881292]

Sigal IA, Yang H, Roberts MD, Downs JC, 2010 Morphing methods to parameterize specimen-specific finite element model geometries. Journal of biomechanics 43, 254–262. [PubMed: 19878950]

Sigal IA, Yang H, Roberts MD, Grimm JL, Burgoyne CF, Demirel S, Downs JC, 2011b IOP-induced lamina cribrosa deformation and scleral canal expansion: independent or related? Invest Ophthalmol Vis Sci 52, 9023–9032. [PubMed: 21989723]

Soh YB, 2016 Development of a ring implant for glaucoma Department of Biomedical Engineering. National University of Singapore.

Steinhart MR, Cone FE, Nguyen C, Nguyen TD, Pease ME, Puk O, Graw J, Oglesby EN, Quigley HA, 2012 Mice with an induced mutation in collagen 8A2 develop larger eyes and are resistant to retinal ganglion cell damage in an experimental glaucoma model. Mol Vis 18, 1093–1106. [PubMed: 22701298]

Strouthidis NG, Fortune B, Yang H, Sigal IA, Burgoyne CF, 2011 Effect of acute intraocular pressure elevation on the monkey optic nerve head as detected by spectral domain optical coherence tomography. Invest Ophthalmol Vis Sci 52, 9431–9437. [PubMed: 22058335]

Strouthidis NG, Girard MJ, 2013 Altering the way the optic nerve head responds to intraocular pressure-a potential approach to glaucoma therapy. Curr Opin Pharmacol 13, 83–89. [PubMed: 22999652]

Tang J, Liu J, 2012 Ultrasonic measurement of scleral cross-sectional strains during elevations of intraocular pressure: method validation and initial results in posterior porcine sclera. J Biomech Eng 134, 091007. [PubMed: 22938374]

Teng S, Tan H, Peng J, Lin HC, Kim KH, Lo W, Sun Y, Lin W, Lin S, Jee S, So PTC, Dong CY, 2006 Multiphoton autoflourescence and second harmonic generation imaging of the ex-vivo porcine eye. Investigative Ophthalmology & Visual Science 47, 1216–1224. [PubMed: 16505061]

Thale A, Tillmann B, 1993 The collagen architecture of the sclera--SEM and immunohistochemical studies. Annals of anatomy = Anatomischer Anzeiger : official organ of the Anatomische Gesellschaft 175, 215–220. [PubMed: 8338219]

Thompson F, 1990 Scleral Reinforcement, Myopia Surgery. Macmillan, New York, pp. 267–297.

Tonge TK, Murienne BJ, Coudrillier B, Alexander S, Rothkopf W, Nguyen TD, 2013 Minimal preconditioning effects observed for inflation tests of planar tissues. J Biomech Eng 135, 114502. [PubMed: 23897279]

Tun TA, Wang X, Baskaran M, Nongpuir ME, Cheng CY, Strouthidis NG, Aung T, Girard MJ, 2018 Effect of Age and Glaucoma on Anterior Peripapillary Sclera Shape ARVO Annual Meeting. IOVS, Honolulu, p. 2018.

Umihira J, Nagata S, Nohara M, Hanai T, Usuda N, Segawa K, 1994 Localization of elastin in the normal and glaucomatous human trabecular meshwork. Invest Ophthalmol Vis Sci 35, 486–494. [PubMed: 8112998]

Voorhees AP, Ho LC, Jan NJ, Tran H, van der Merwe Y, Chan K, Sigal IA, 2017 Whole-globe biomechanics using high-field MRI. Exp Eye Res 160, 85–95. [PubMed: 28527594]

Voorhees AP, Jan NJ, Hua Y, Yang B, Sigal IA, 2018 Peripapillary sclera architecture revisited: A tangential fiber model and its biomechanical implications. Acta biomaterialia 79, 113–122. [PubMed: 30142444]

Vurgese S, Panda-Jonas S, Jonas JB, 2012 Scleral thickness in human eyes. PLoS One 7, e29692. [PubMed: 22238635]

Wallman J, Turkel J, Trachtman J, 1978 Extreme myopia produced by modest change in early visual experience. Science 201, 1249–1251. [PubMed: 694514]

Wallman J, Winawer J, 2004 Homeostasis of eye growth and the question of myopia. Neuron 43, 447–468. [PubMed: 15312645]

Walls GS, 1942 The vertebrate eye and its adaptive radiation. Haffner, New York.

Wang B, Hua Y, Sigal IA, 2018 Biomechanical effects of fiber interweaving, Biomedical Engineering Society (BMES) Annual Meeting, Atlanta, Georgia, USA.

Wang F, Lee HP, Lu C, 2007 Biomechanical effect of segmental scleral buckling surgery. Curr Eye Res 32, 133–142. [PubMed: 17364746]

Wang JK, Kardon RH, Ledolter J, Sibony PA, Kupersmith MJ, Garvin MK, 2017a Peripapillary Retinal Pigment Epithelium Layer Shape Changes From Acetazolamide Treatment in the Idiopathic Intracranial Hypertension Treatment Trial. Invest Ophthalmol Vis Sci 58, 2554–2565. [PubMed: 28492874]

Wang M, Corpuz CC, 2015 Effects of scleral cross-linking using genipin on the process of form-deprivation myopia in the guinea pig: a randomized controlled experimental study. BMC ophthalmology 15, 89. [PubMed: 26220299]

Wang M, Zhang F, Liu K, Zhao X, 2015 Safety evaluation of rabbit eyes on scleral collagen cross-linking by riboflavin and ultraviolet A. Clin Exp Ophthalmol 43, 156–163. [PubMed: 25070292]

Wang X, Beotra MR, Tun TA, Baskaran M, Perera S, Aung T, Strouthidis NG, Milea D, Girard MJ, 2016a In Vivo 3-Dimensional Strain Mapping Confirms Large Optic Nerve Head Deformations Following Horizontal Eye Movements. Invest Ophthalmol Vis Sci 57, 5825–5833. [PubMed: 27802488]

Wang X, Fisher LK, Milea D, Jonas JB, Girard MJ, 2017b Predictions of Optic Nerve Traction Forces and Peripapillary Tissue Stresses Following Horizontal Eye Movements. Invest Ophthalmol Vis Sci 58, 2044–2053. [PubMed: 28384725]

Wang X, Rumpel H, Lim WE, Baskaran M, Perera SA, Nongpiur ME, Aung T, Milea D, Girard MJ, 2016b Author Response: Peripapillary Suprachoroidal Cavitation, Parapapillary Gamma Zone and Optic Disc Rotation Due to the Biomechanics of the Optic Nerve Dura Mater. Invest Ophthalmol Vis Sci 57, 4374–4375. [PubMed: 27557436]

Wang X, Rumpel H, Lim WE, Baskaran M, Perera SA, Nongpiur ME, Aung T, Milea D, Girard MJ, 2016c Finite Element Analysis Predicts Large Optic Nerve Head Strains During Horizontal Eye Movements. Invest Ophthalmol Vis Sci 57, 2452–2462. [PubMed: 27149695]

Watson PG, Young RD, 2004 Scleral structure, organisation and disease. A review. Experimental Eye Research 78, 609–623. [PubMed: 15106941]

Wenstrup RJ, Florer JB, Brunskill EW, Bell SM, Chervoneva I, Birk DE, 2004 Type V collagen controls the initiation of collagen fibril assembly. J Biol Chem 279, 53331–53337. [PubMed: 15383546]

Whitford C, Joda A, Jones S, Bao F, Rama P, Elsheikh A, 2016 Ex vivo testing of intact eye globes under inflation conditions to determine regional variation of mechanical stiffness. Eye and vision (London, England) 3, 21.

Wildsoet CF, 1997 Active emmetropization--evidence for its existence and ramifications for clinical practice. Ophthalmic Physiol Opt 17, 279–290. [PubMed: 9390372]

Winkler M, Jester B, Nien-Shy C, Massei S, Minckler DS, Jester JV, Brown DJ, 2010 High resolution three-dimensional reconstruction of the collagenous matrix of the human optic nerve head. Brain Research Bulletin 81, 339–348. [PubMed: 19524027]

Winkler M, Shoa G, Xie Y, Petsche SJ, Pinsky PM, Juhasz T, Brown DJ, Jester JV, 2013 Three-dimensional distribution of transverse collagen fibers in the anterior human corneal stroma. Invest Ophthalmol Vis Sci 54, 7293–7301. [PubMed: 24114547]

Wollensak G, Iomdina E, 2008a Crosslinking of scleral collagen in the rabbit using glyceraldehyde. J Cataract Refract Surg 34, 651–656. [PubMed: 18361989]

Wollensak G, Iomdina E, 2008b Long-term biomechanical properties after collagen crosslinking of sclera using glyceraldehyde. Acta Ophthalmol 86, 887–893. [PubMed: 18537936]

Wollensak G, Iomdina E, 2009 Long-term biomechanical properties of rabbit sclera after collagen crosslinking using riboflavin and ultraviolet A (UVA). Acta Ophthalmol 87, 193–198. [PubMed: 18803623]

Wollensak G, Iomdina E, Dittert DD, Salamatina O, Stoltenburg G, 2005 Cross-linking of scleral collagen in the rabbit using riboflavin and UVA. Acta Ophthalmol Scand 83, 477–482. [PubMed: 16029274]

Wollensak G, Spoerl E, Seiler T, 2003 Riboflavin/Ultraviolet-A-induced collagen crosslinking for the treatment of keratococnus. American Journal of Ophthalmology 135, 620–627. [PubMed: 12719068]

Xue A, Zheng L, Tan G, Wu S, Wu Y, Cheng L, Qu J, 2018 Genipin-Crosslinked Donor Sclera for Posterior Scleral Contraction/Reinforcement to Fight Progressive Myopia. Invest Ophthalmol Vis Sci 59, 3564–3573. [PubMed: 30025077]

Yamamoto S, Hashizume H, Hitomi J, Shigeno M, Sawaguchi S, Abe H, Ushiki T, 2000 The subfibrillar arrangement of corneal and scleral collagen fibrils as revealed by scanning electron and atomic force microscopy. Archives of Histology and Cytology 63, 127–135. [PubMed: 10885449]

Yan D, McPheeters S, Johnson G, Utzinger U, Vande Geest JP, 2011 Microstructural differences in the human posterior sclera as a function of age and race. Invest Ophthalmol Vis Sci 52, 821–829. [PubMed: 21051726]

Yang B, Brazile B, Jan NJ, Hua Y, Wei J, Sigal IA, 2018a Structured polarized light microscopy for collagen fiber structure and orientation quantification in thick ocular tissues. Journal of biomedical optics 23, 1–10.

Yang B, Jan NJ, Brazile B, Voorhees A, Lathrop KL, Sigal IA, 2018b Polarized light microscopy for 3-dimensional mapping of collagen fiber architecture in ocular tissues. Journal of biophotonics 11, e201700356. [PubMed: 29633576]

Yang B, Lee P-Y, Brazile B, Sigal IA, 2019 Snapshot-polarized light microscopy to visualize and quantify collagenous soft tissue microstructure at 156 frames/second, SB3C - Summer Biomechanics, Bioengineering and Biotransport Conference, Seven Springs, Philadelphia, USA.

Yang H, Downs JC, Girkin C, Sakata L, Bellezza A, Thompson H, Burgoyne CF, 2007 3-D histomorphometry of the normal and early glaucomatous monkey optic nerve head: lamina cribrosa and peripapillary scleral position and thickness. Invest Ophthalmol Vis Sci. 48, 4597–4607. [PubMed: 17898283]

Yang H, Downs JC, Sigal IA, Roberts MD, Thompson H, Burgoyne CF, 2009 Deformation of the normal monkey optic nerve head connective tissue after acute IOP elevation within 3-D histomorphometric reconstructions. Invest Ophthalmol Vis Sci 50, 5785–5799. [PubMed: 19628739]

Yang H, Thompson H, Roberts MD, Sigal IA, Downs JC, Burgoyne CF, 2011 Deformation of the early glaucomatous monkey optic nerve head connective tissue after acute IOP elevation in 3-D histomorphometric reconstructions. Invest Ophthalmol Vis Sci 52, 345–363. [PubMed: 20702834]

Young RD, 1985 The ultrastructural organization of proteoglycans and collagen in human and rabbit scleral matrix. Journal of cell science 74, 95–104. [PubMed: 4030913]

Yu SW, Ma A, Wong JK, 2019 Micropulse Laser for the Treatment of Glaucoma: A Literature Review. Survey of ophthalmology.

Yuan Y, Zong Y, Zheng Q, Qian G, Qian X, Li Y, Shao W, Gao Q, 2016 The efficacy and safety of a novel posterior scleral reinforcement device in rabbits. Materials science & engineering. C, Materials for biological applications 62, 233–241. [PubMed: 26952419]

Yun SH, Chernyak D, 2018 Brillouin microscopy: assessing ocular tissue biomechanics. Current opinion in ophthalmology 29, 299–305. [PubMed: 29771749]

Zhang L, Albon J, Jones H, Gouget CL, Ethier CR, Goh JC, Girard MJ, 2015a Collagen microstructural factors influencing optic nerve head biomechanics. Invest Ophthalmol Vis Sci 56, 2031–2042. [PubMed: 25736791]

Zhang L, Thakku SG, Beotra MR, Baskaran M, Aung T, Goh JCH, Strouthidis NG, Girard MJA, 2017 Verification of a virtual fields method to extract the mechanical properties of human optic nerve head tissues in vivo. Biomech Model Mechanobiol 16, 871–887. [PubMed: 27909833]

Zhang M, Zou Y, Zhang F, Zhang X, Wang M, 2015b Efficacy of Blue-Light Cross-linking on Human Scleral Reinforcement. Optom Vis Sci 92, 873–878. [PubMed: 26099056]

Zhou D, Abass A, Eliasy A, Studer HP, Movchan A, Movchan N, Elsheikh A, 2019a Microstructure-based numerical simulation of the mechanical behaviour of ocular tissue. J R Soc Interface 16, 20180685. [PubMed: 31039694]

Zhou D, Eliasy A, Abass A, Markov P, Whitford C, Boote C, Movchan A, Movchan N, Elsheikh A, 2019b Analysis of X-ray scattering microstructure data for implementation in numerical simulations of ocular biomechanical behaviour. PLoS One 14, e0214770. [PubMed: 30934028]

Zhuola, Barrett, S., Kharaz YA, Comerford E, Akhtar R, 2018 Nanostructural and mechanical changes in the sclera following proteoglycan depletio. J Model Ophthalmol 2, 14–17.

Zyablitskaya M, Munteanu EL, Nagasaki T, Paik DC, 2018 Second Harmonic Generation Signals in Rabbit Sclera As a Tool for Evaluation of Therapeutic Tissue Cross-linking (TXL) for Myopia. J Vis Exp.

Zyablitskaya M, Takaoka A, Munteanu EL, Nagasaki T, Trokel SL, Paik DC, 2017 Evaluation of Therapeutic Tissue Crosslinking (TXL) for Myopia Using Second Harmonic Generation Signal Microscopy in Rabbit Sclera. Invest Ophthalmol Vis Sci 58, 21–29. [PubMed: 28055099]

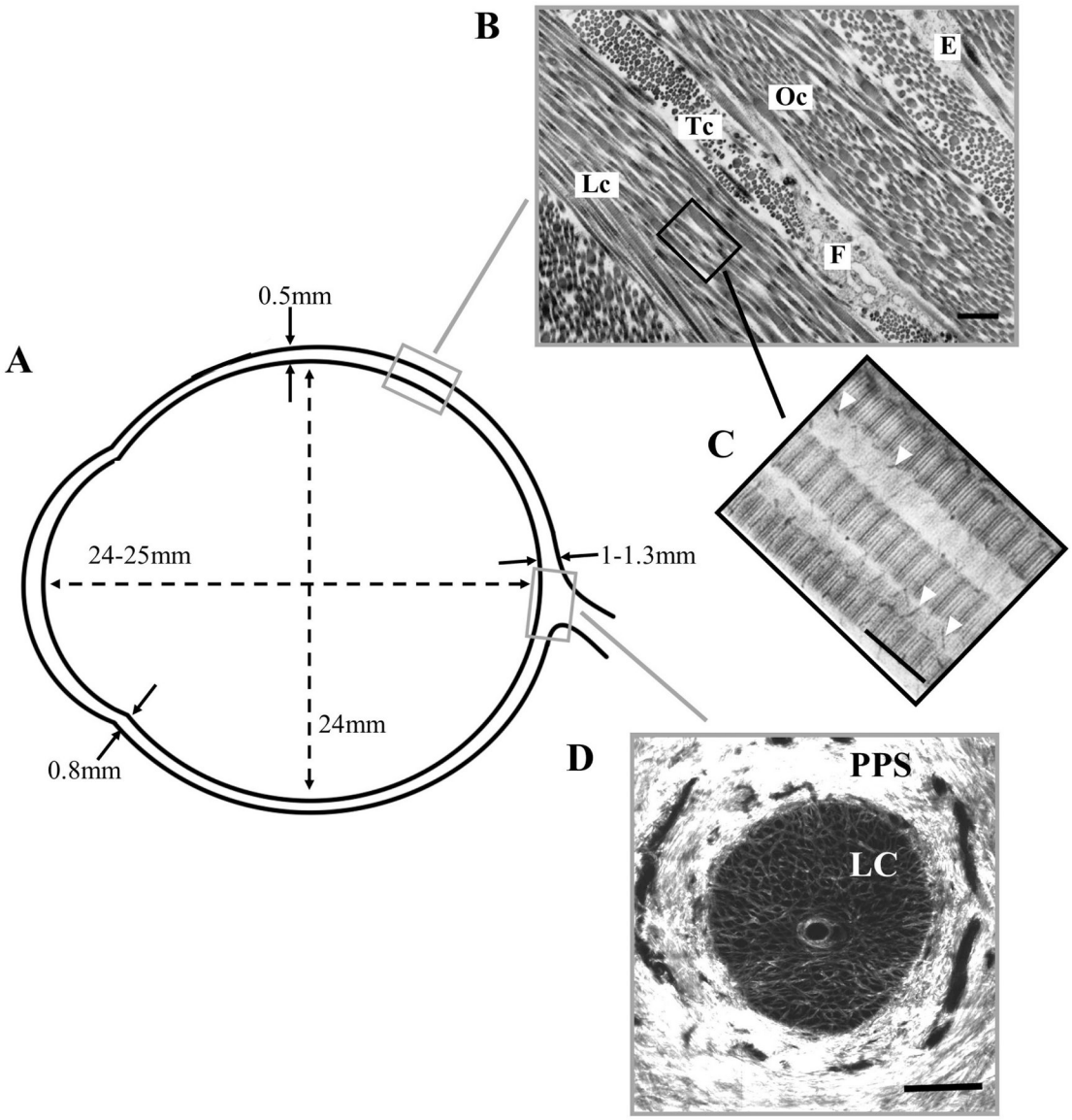

Figure 1:

Overview of scleral morphometry and connective tissue structure. **A)** Approximate wall thickness and dimensions of the normal, adult human sclera. **B)** Transmission electron microscopy (TEM) image of the outer scleral stroma, showing lamellar structure formed by collagen fibril bundles in longitudinal (Lc), transverse (Tc) and oblique (Oc) section. A fibrocyte (F) and elastin fibre (E) can also be seen. Bar: 1.5μm. **C)** TEM image of stroma from a different specimen at higher magnification, showing D-periodic banding of individual fibrils in longitudinal section. Proteoglycans are present as fine filaments (arrowheads) associated with the collagen fibrils. Bar: 250nm. **D)** Second harmonic generation (SHG) image of en-face section through the optic nerve head at mid-stromal depth, showing the fenestrated lamina cribrosa (LC) that supports the exiting retinal nerve axons. The collagen fibril bundles of the neighbouring peripapillary sclera (PPS) adopt a predominantly circumferential orientation in this region. Panel B taken from (Bron et al., 1997) and

reproduced with permission of Hodder Arnold. Panel C adapted from (Watson and Young, 2004) with permission of Elsevier Ltd.

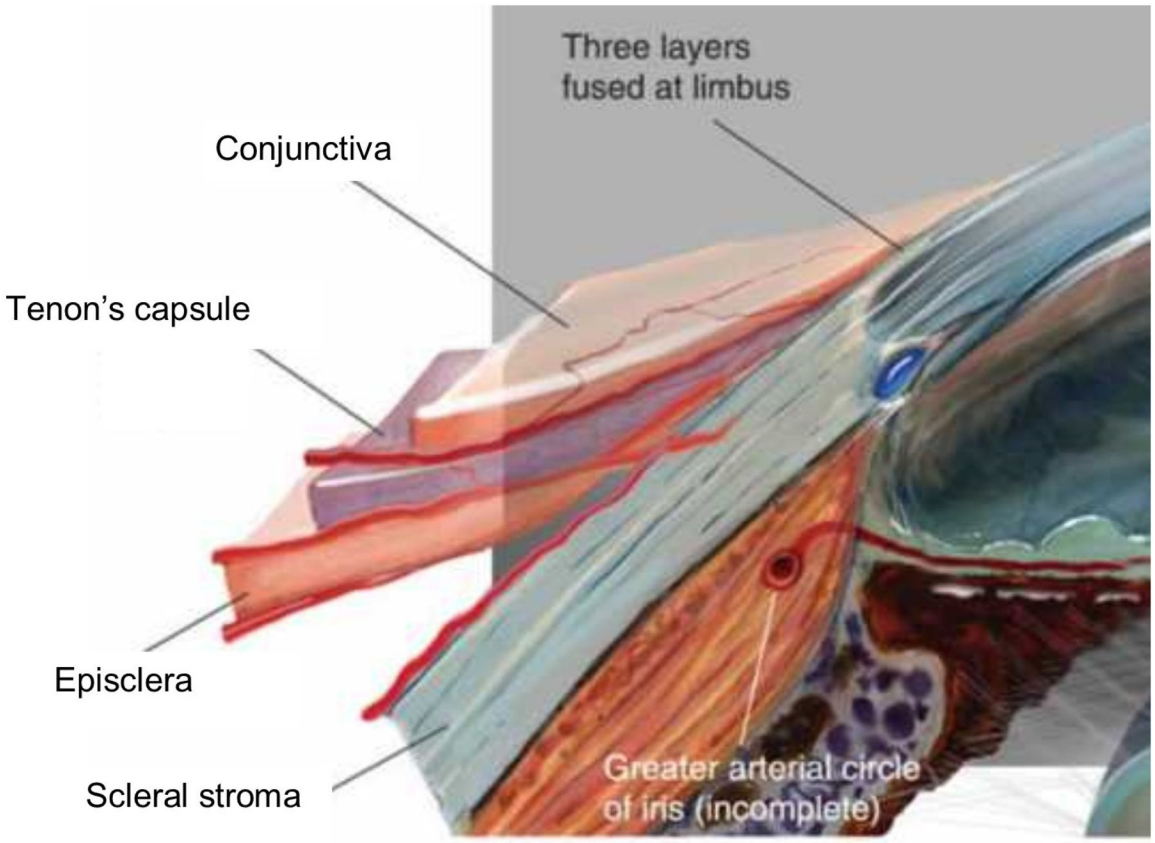

Figure 2:
Anatomy of the anterior segment of the eye, showing the various scleral tissue layers. Adapted with permission from https://eyeanatomyblog.wordpress.com/2012/10/15/the-limbus.

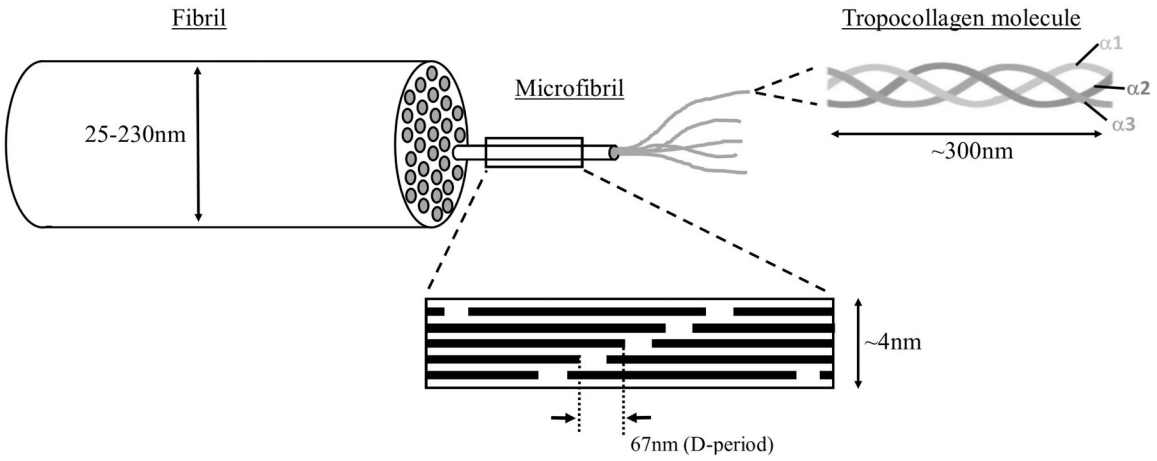

Figure 3:

The hierarchical structure of scleral collagen (not to scale). Five triple alpha-chain tropocollagen molecules assemble into microfibrils, in which the axial stagger of individual molecules leads to gap/overlap regions that define the 67nm axial D-period. Varying numbers of near-parallel microfibrils form collagen fibrils of diameters ranging from 25 to 230nm.The microfibrils are actually inclined by ~5° to the fibril axis, but this is not shown in this simplified diagram.

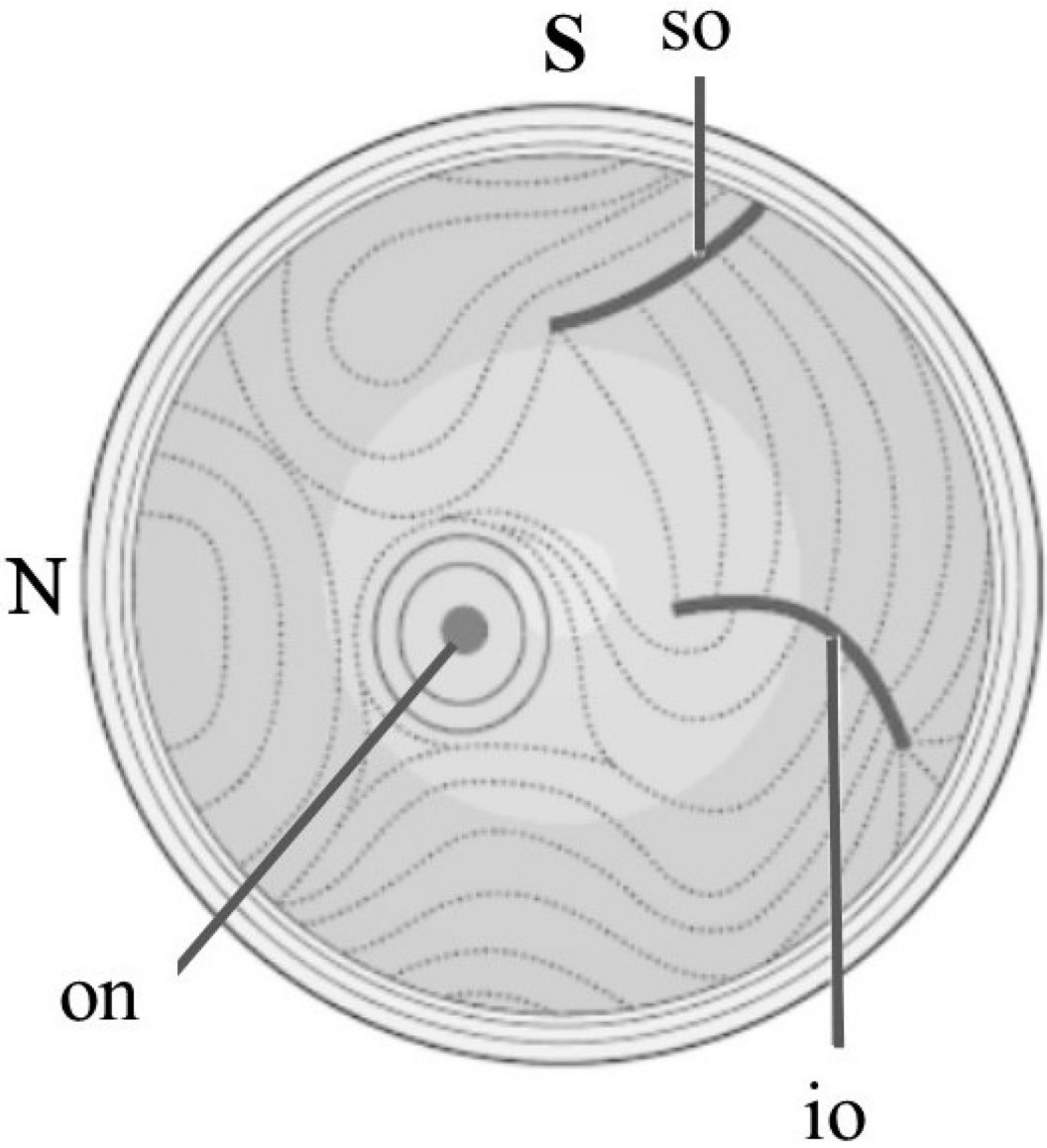

Figure 4:

Gross orientations of collagen lamellae in the posterior human sclera, as interpreted from histological examinations by Kokott (1934). Right eye shown with superior (S) and nasal (N) aspects marked. Notable features are circular orientation around the optic nerve (on) and associations with the superior oblique (so) and inferior oblique (io) muscle insertions. Figure adapted from (Watson, 2012) with permission of JP Medical Ltd.

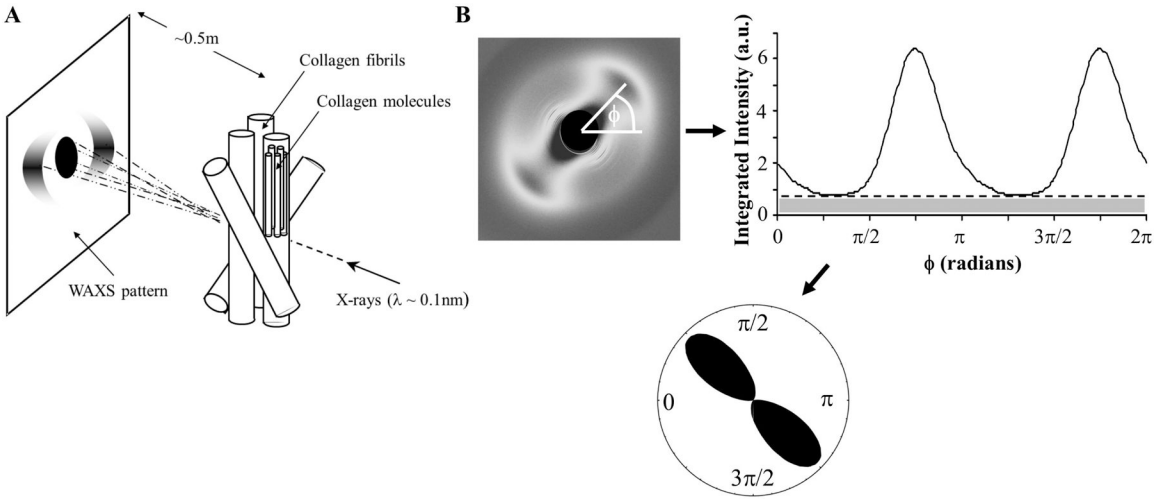

Figure 5:

Quantifying scleral collagen orientation using wide-angle X-ray scattering (WAXS). **A)** The constructive interference of forward-scattered X-rays from the regular lateral packing of constituent tropocollagen molecules aligned near-axially within the fibrils produces a Fourier transform (WAXS pattern) that is collected on a detector behind the specimen. **B)** The collagen fibril orientation distribution function is extracted from the WAXS pattern by analysing the angular spread of (radially integrated) X-ray intensity. The scatter from preferentially aligned collagen (clear region of graph above the dotted line) is displayed as a polar vector plot in which the plot shape indicates the preferential fibril orientations (in this case uniaxial), while the plot size is indicative of the degree of anisotropy.

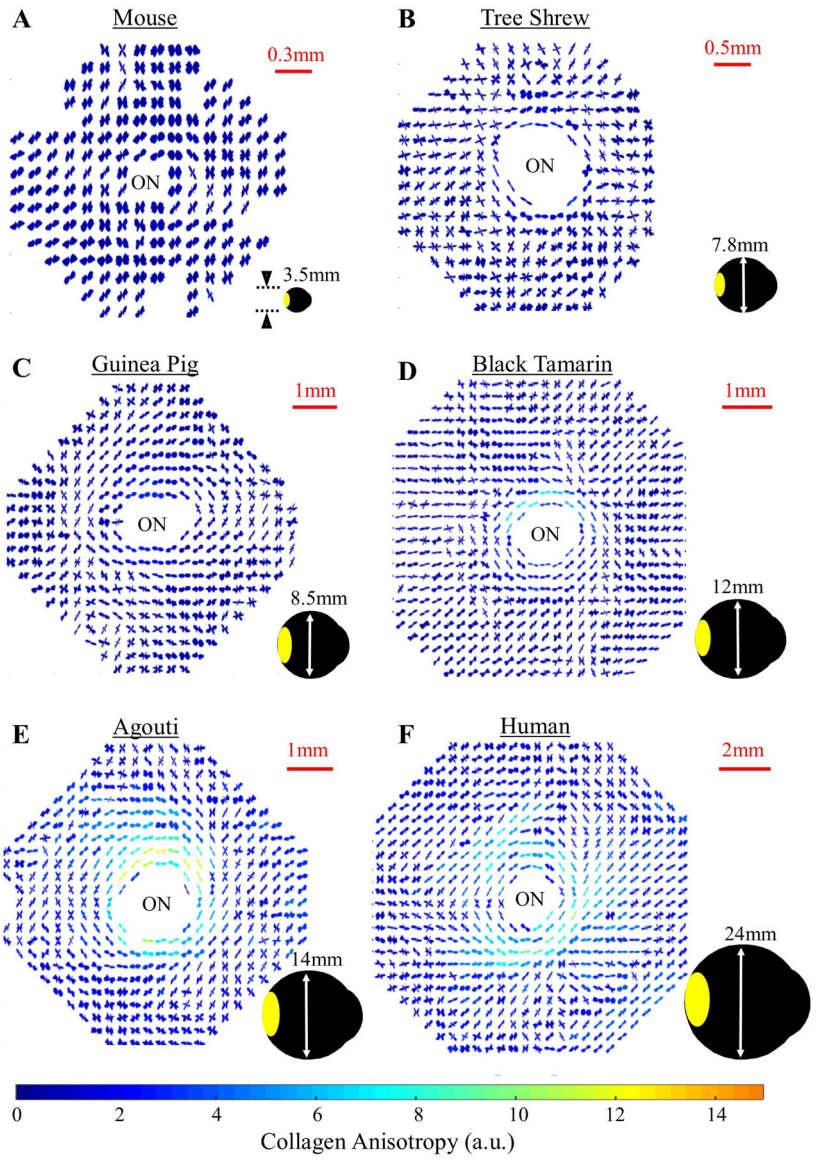

Figure 6:

Collagen microstructure of the posterior sclera across species. Polar vector plots of collagen fibril orientation in various mammal species **(A–E)** and humans **(F)**, determined using WAXS. The shape of the individual plots indicates the preferred direction of collagen fibrils at that point in the tissue, while the plot colour scaling is indicative of the degree of anisotropy. Note that the circumferential collagen structure of the peripapillary sclera bordering the optic nerve (ON) is poorly defined in smaller mammals, but becomes gradually clearer with increasing eye size. The area covered by the WAXS maps is shown in yellow on the accompanying eye shadow diagrams.

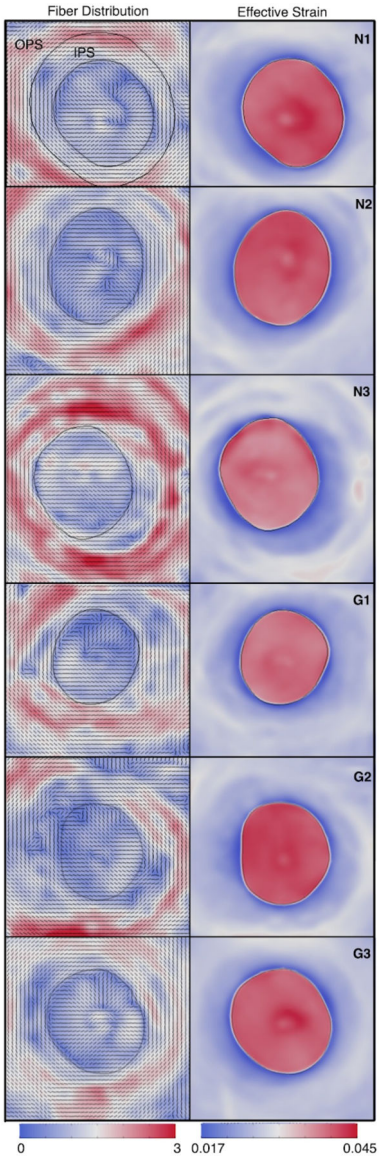

Figure 7:

SALS mapping of fibre microstructure in the peripapillary sclera (PPS) and lamina cribrosa. *Left*: Fibre maps for en-face sections from 6 human donors (3 healthy: N1–3; and 3 glaucoma: G1–3). A highly aligned (red colour) fibre ring (black vector) can be observed in the PPS (the LC boundary is shown in black). Contour colour represents the fibre concentration factor. *Right*: Simulated IOP-induced deformations (effective strain). Low deformations (blue colour) can be observed near the scleral canal boundary (a region prone to mechanical defects). Such deformations would be much higher if one were to remove the heterogenous PPS fibre ring. OPS: outer peripapillary sclera, IPS: inner peripapillary sclera. Contour colour represents the strain magnitude. Figure modified from (Zhang et al., 2015) with permission of the Association for Research in Vision and Ophthalmology.

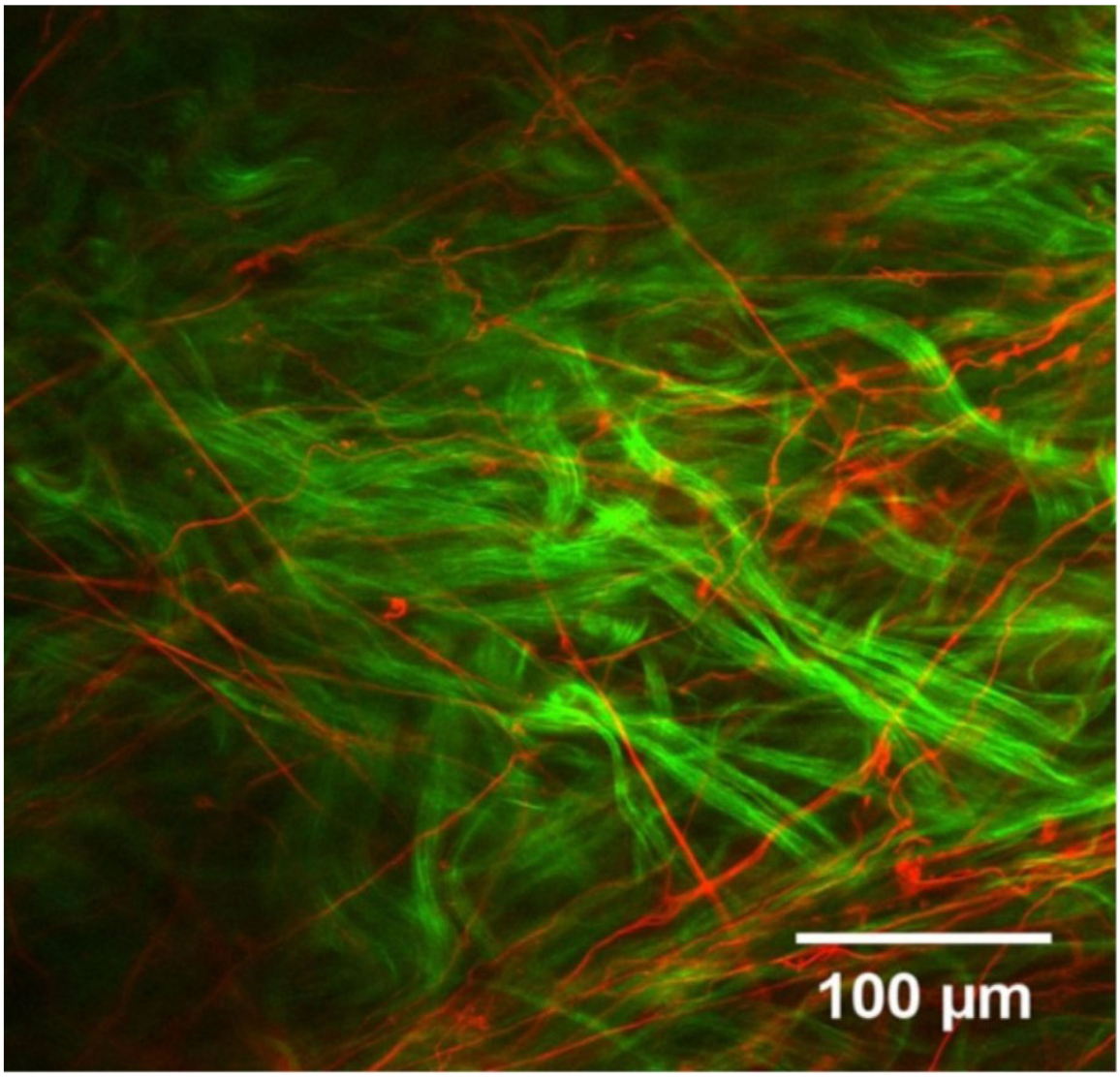

Figure 8:
Two-channel multiphoton microscopy image recorded from human episclera. The elastin fibre network (red) is revealed by TPF autofluorescence, and is shown alongside collagen fibril bundles (green) visualized concurrently with SHG imaging. Figure adapted from (Park et al., 2016) with permission of the Association for Research in Vision and Ophthalmology.

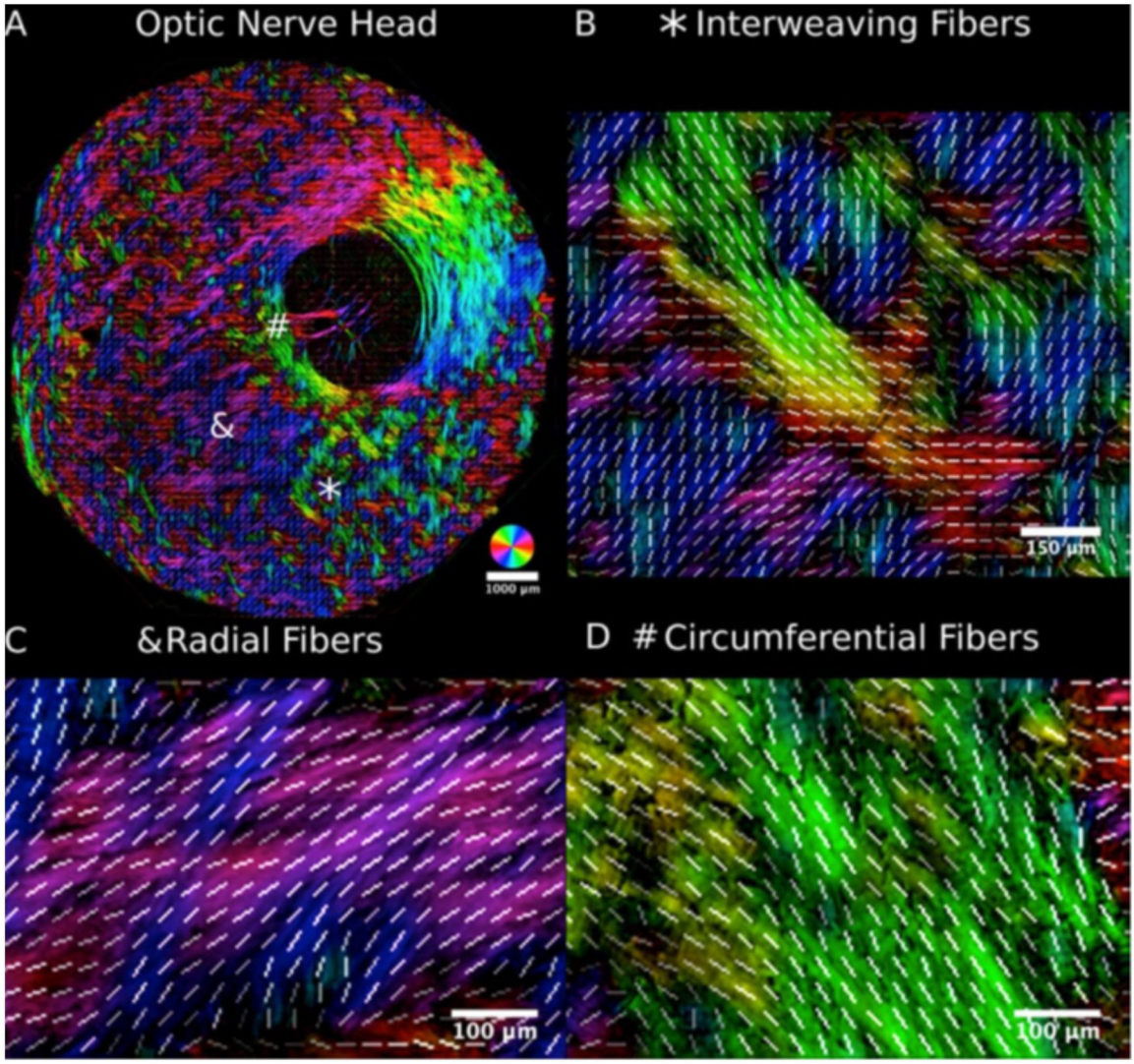

Figure 9:

A) The posterior sclera of the sheep eye visualised using PLM. Three major organizational patterns were identified and marked by an asterisk, an ampersand, and a hashtag: i) interweaving fibres that formed a basket-weave pattern (**B)** asterisk), ii) fibres oriented radially from the canal (**C)** ampersand), and iii) fibres wrapped circumferentially around the canal (**D)** hashtag). White lines representing orientation averaged over 20 × 20 μm^2 were overlaid to aid discerning the fibre organization. Figure adapted from (Jan et al., 2017b) with permission of the Association for Research in Vision and Ophthalmology.

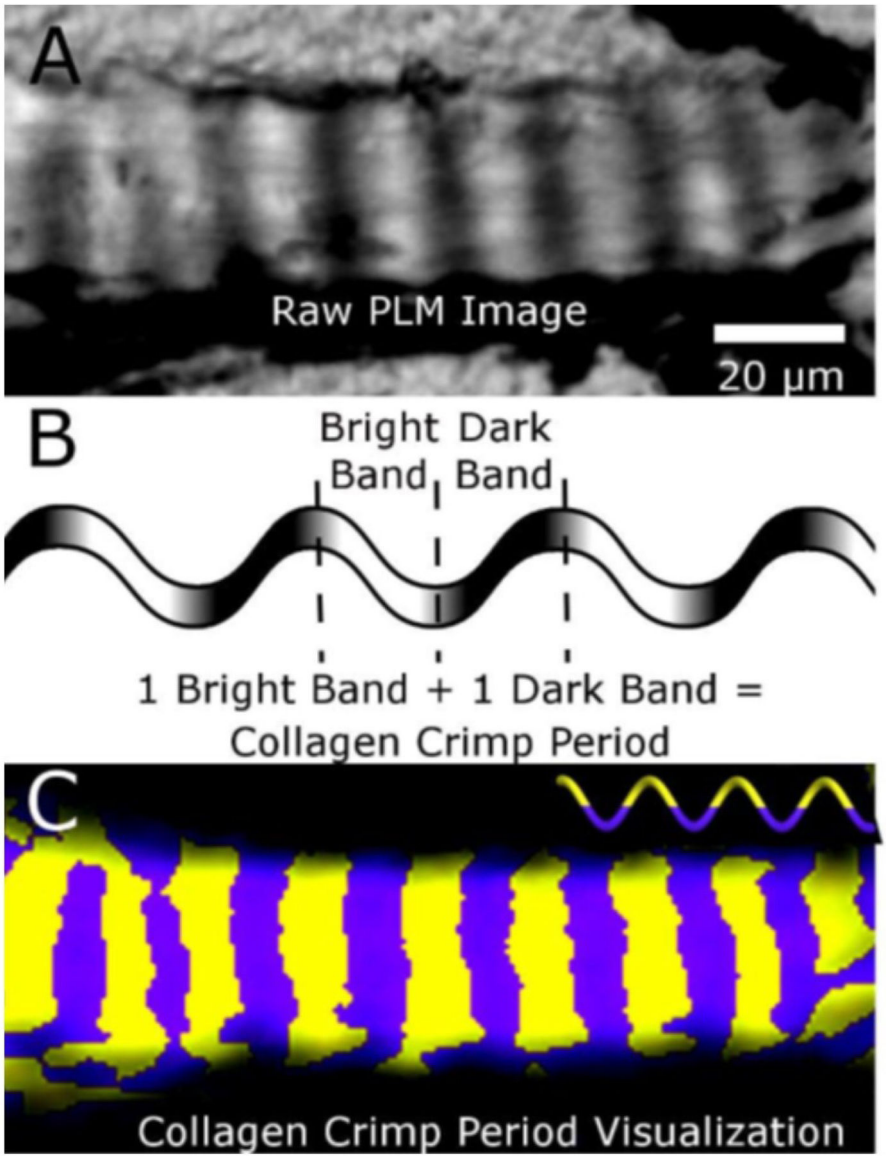

Figure 10:

Collagen crimp period visualised using PLM. **A)** An LC beam appears banded when imaged with PLM. **B)** Adding the lengths of one bright band and one dark band makes one collagen crimp period. **C)** Processing several “raw” PLM images with various filter orientations, it is possible to pseudocolour half periods as alternating yellow and purple bands that help visualize the crimp. Note that the crimp bands are fairly uniform and perpendicular to the longitudinal axis of the LC beam. This crimp pattern helps reduce shearing and torsion within the LC beam when loaded longitudinally. Note that crimp period is only one aspect of fibre crimp. Figure adapted from (Jan et al., 2017a) with permission of the Association for Research in Vision and Ophthalmology.

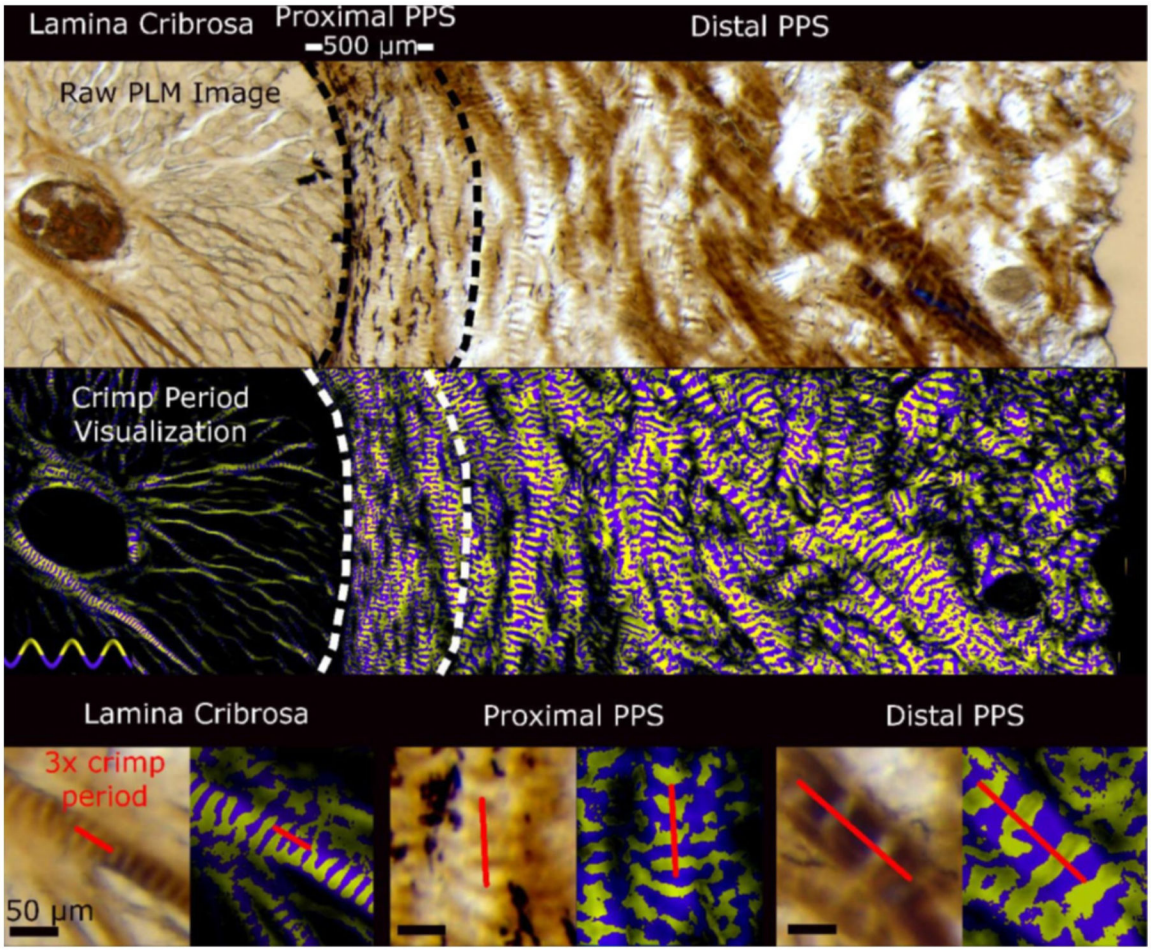

Figure 11:

Wide views spanning the LC and sclera under PLM (top) and visualised using the yellow and purple bands as described in Fig 10 to simplify discerning crimp period independent of the orientation (middle). The bottom shows pairs of raw PLM images and corresponding crimp period visualization images of close-ups of the LC (bottom left), proximal PPS (bottom center), and distal PPS (bottom right). An example line illustrating three periods is overlaid on each. It is easy to distinguish that the crimp period in the LC was small. In the proximal PPS the period was similar to that of the LC. The period increased with distance from the canal. Figure adapted from (Jan et al., 2017a) with permission of the Association for Research in Vision and Ophthalmology.

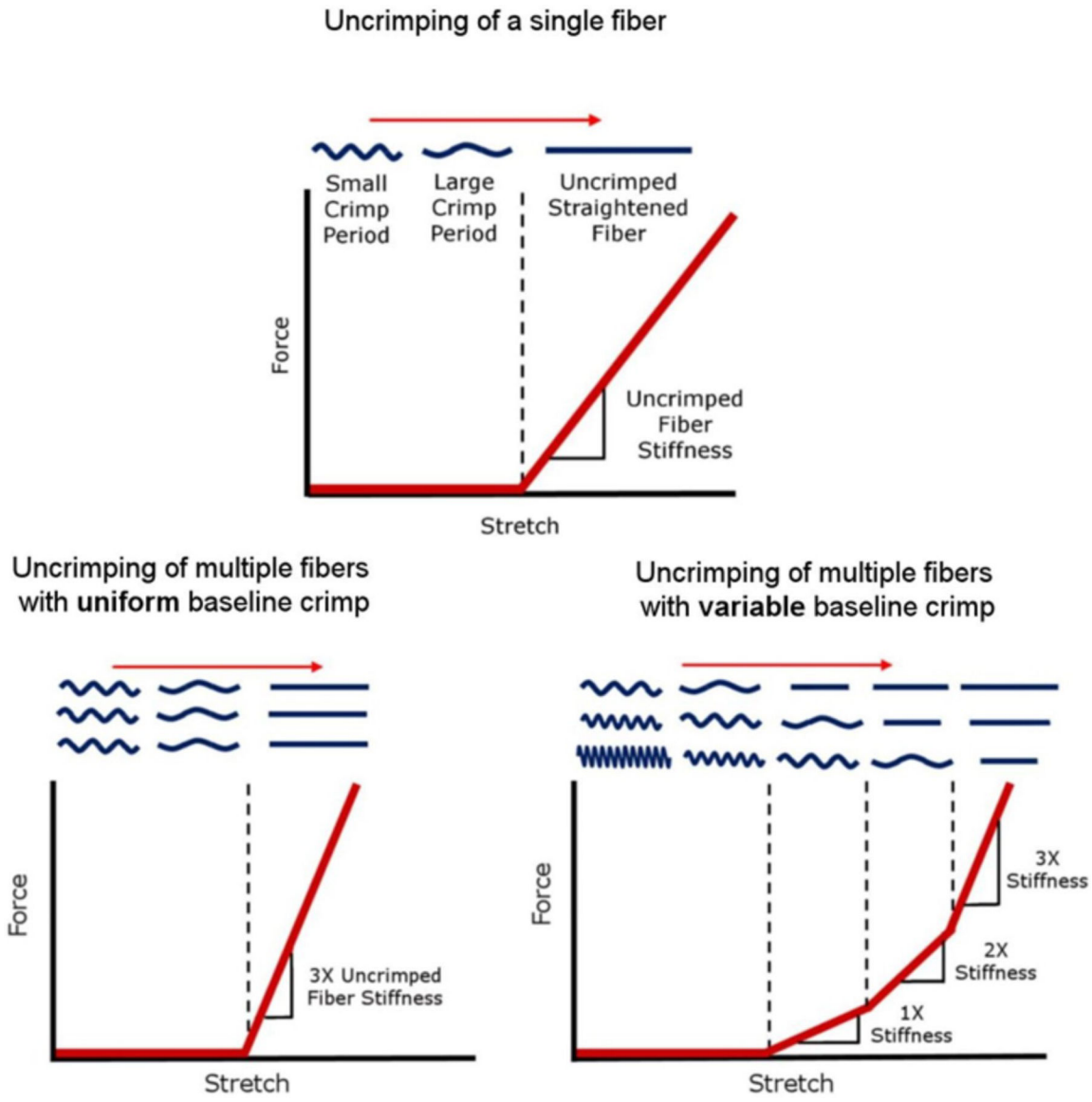

Figure 12:

Schematic of how fibre uncrimping contributes to tissue mechanical properties. (Top) As a single fibre stretches, it uncrimps, requiring relatively little force until it loses all crimp. The straightened fibre can only be stretched further by making the fibre longer, which requires an increasing force, and so the fibre appears stiffer. A fibre that has uncrimped and is bearing load is called “recruited”. The macroscopic force or stiffness of multiple fibres depends on the distribution of baseline crimp in the fibres. (Bottom row) In a region with fibres of uniform crimp, stretch leads to a macroscopic step increase in stiffness due to the simultaneous straightening of all fibres. In a region with variable crimp, stretch leads to a gradual increase in stiffness due to the progressive straightening of fibres. Fibres with less crimp are straightened and loaded (recruited) before fibres with more crimp. Figure adapted from (Jan et al., 2017a) with permission of the Association for Research in Vision and Ophthalmology.

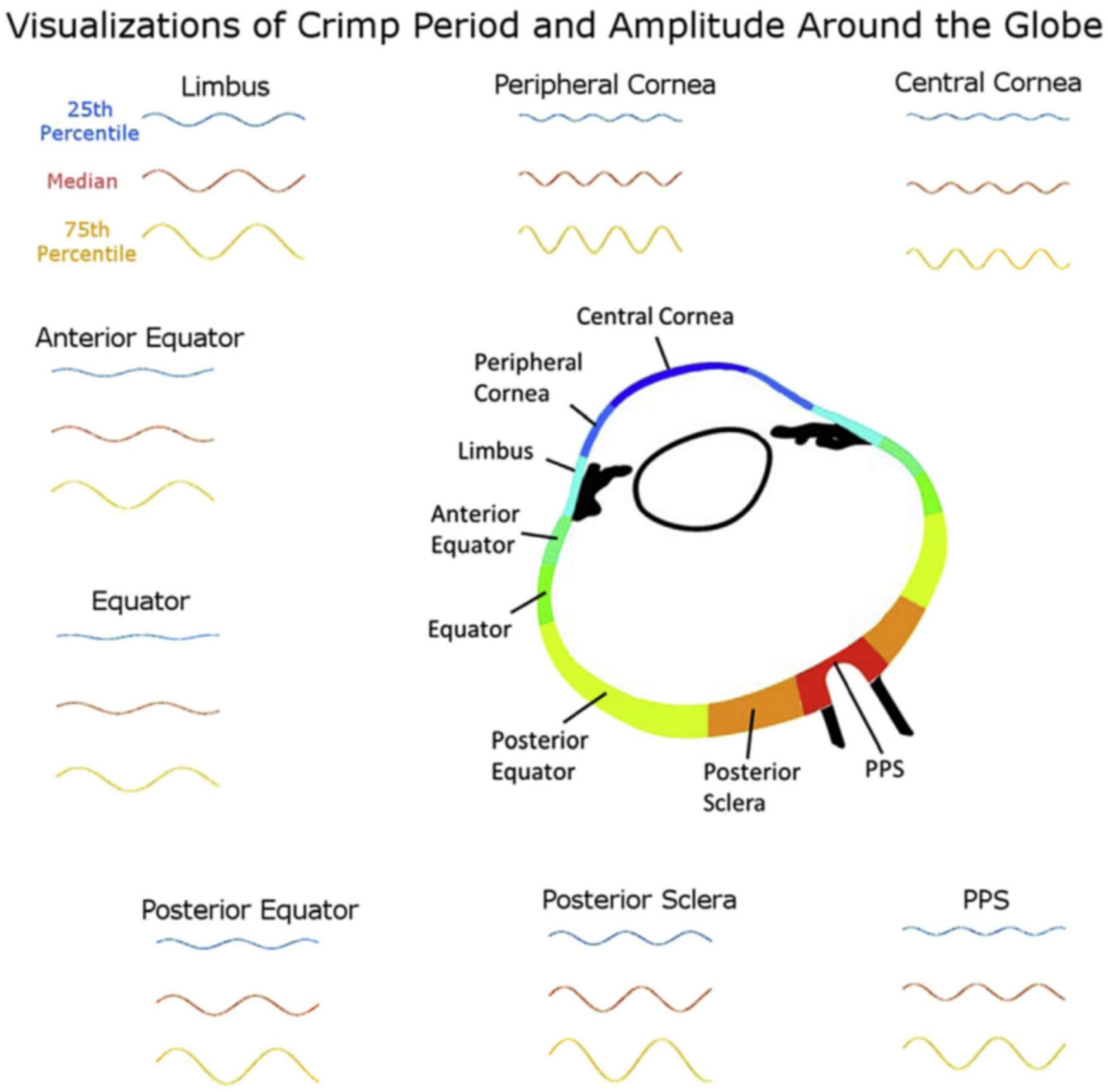

Figure 13:

Crimp characteristics vary around the globe, in consistent ways between individuals. The figure is to compare crimp period and amplitude across regions of the globe. The 25th percentile, 50th percentile (median), and 75th percentile period and amplitude values were used to generate representative fibres for each region as sinusoidals. These visualizations are not intended to represent any specific fibril, fibril bundle or lamellae, but are, instead, intended to visualise how the crimp differs between regions. In regions with more uniform crimp, all three lines would be relatively similar, whereas in regions with highly variable crimp they would vary. Figure adapted from (Jan et al., 2018) with permission of the Experimental Eye Research.

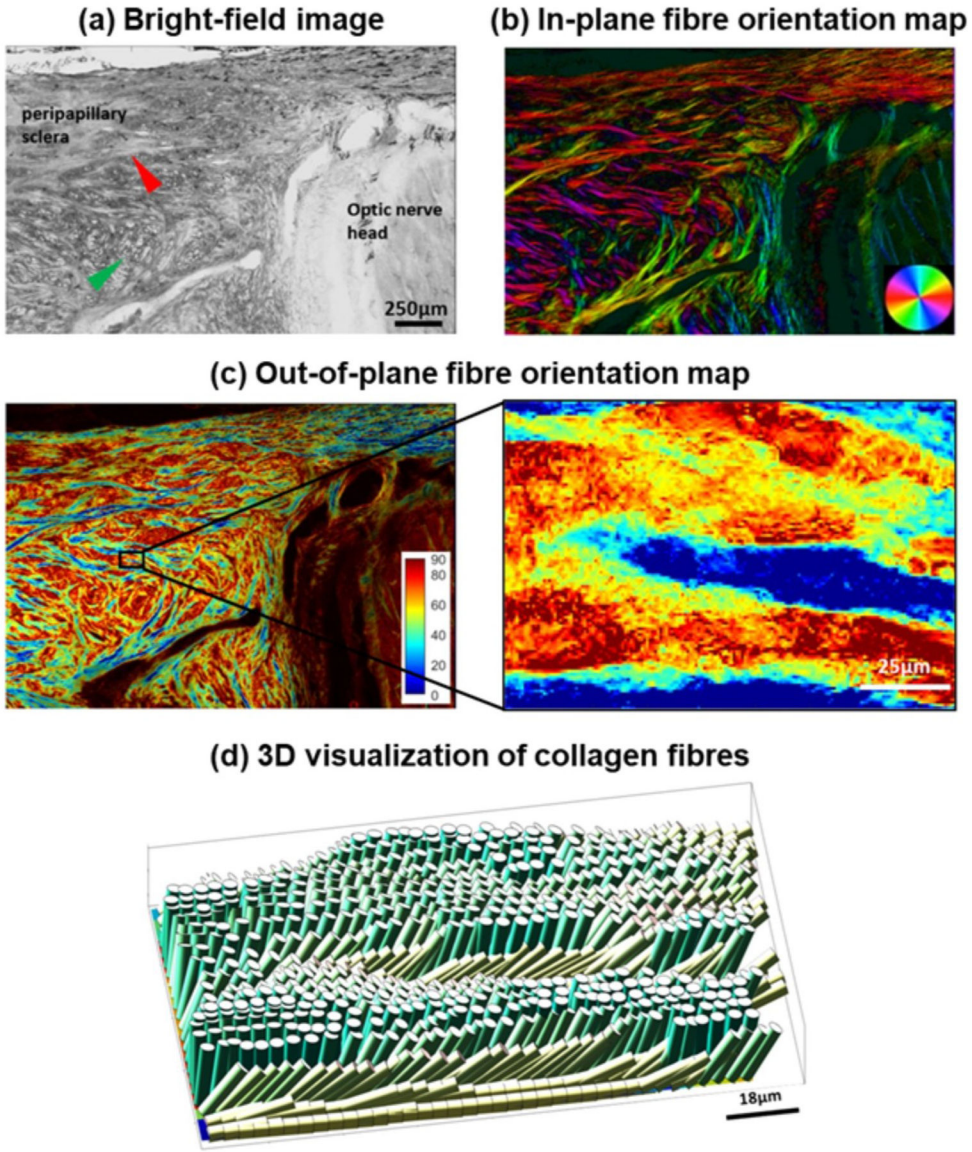

Figure 14:

Application of 3DPLM to the posterior pole of a sheep eye. The 3D orientation of the fibres can be separated into in-plane and out-of-plane orientations, where the plane is that of the section. **(a)** Bright field image of a cryosection with red and green arrowheads pointing to long in-plane fibre bundles and out-of-plane fibre bundles, respectively; **(b)** In-plane fibre orientation map showing both in-plane fibre morphology and orientation. Colours indicate the in-plane fibre orientation; **(c)** Out-of-plane fibre orientation map highlighting fibre bundles. Colours indicate the out-of-plane fibre orientation, from fully in-plane (blue) to perpendicular to the plane (maroon**); (d)** Out-of-plane fibre orientation of small region of interest shown in (c); **(e)** 3D visualization of collagen fibres. Figure adapted from (Yang et al., 2018b) with permission of the Journal of Biophotonics.

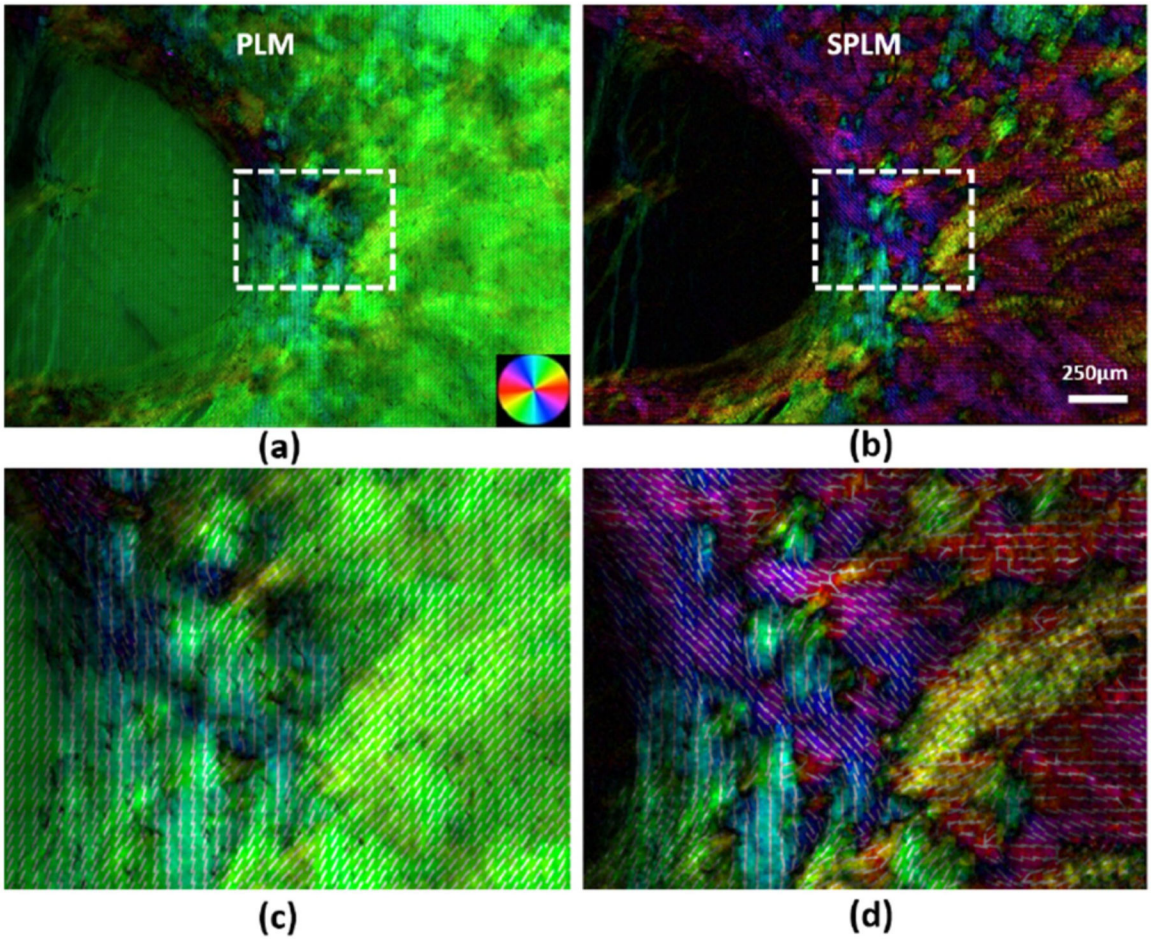

Figure 15:

Collagen fibre orientation maps in the PPS and LC region of a pig eye. The images were acquired using either PLM (a, c) or SPLM (b, d) of an uncut thick sample. **(a)** The PLM images appear green, without much detail of the known architecture of the region. **(b)** In contrast, SPLM images show a much more heterogeneous arrangement. Both circumferential and radial fibres can be identified, based on color-coded orientations; **(c)** and **(d)** show close-ups of the region marked by the dashed rectangle. Overlaid on the images are locally averaged orientation lines. Figure adapted from (Yang et al., 2018a) with permission of the SPIE.

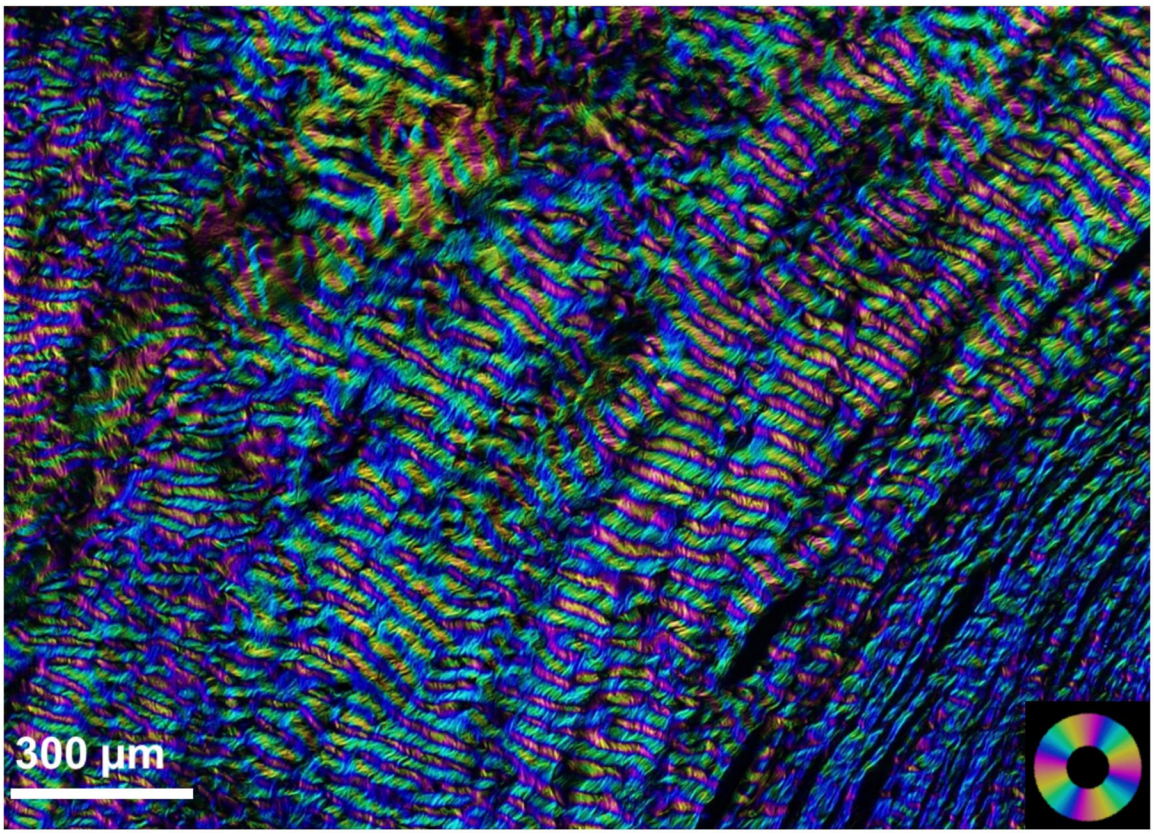

Figure 16:

Porcine PPS imaged by snapshot polarized light microscopy (Yang et al., 2019). The colors indicate the local orientation of the collagen fibres and the brightness is roughly proportional to the local collagen density. Note that the colors are obtained through optical means, and the image is not coloured digitally. The scleral canal is slightly out of frame on the bottom right corner. Clearly discernible in the image are collagen fibre bundles circumferential to the canal. The width of the region of circumferential fibres is between 20% and 40% of the canal diameter in both porcine and human eyes (Gogola et al., 2018b). It is also possible to distinguish the collagen fibres that form the bundles. The bands of color indicate collagen fibre crimp (Jan et al., 2017b). The collagen fibre bundles and the crimp of the fibres increase in size with distance from the canal (Jan et al., 2017a).

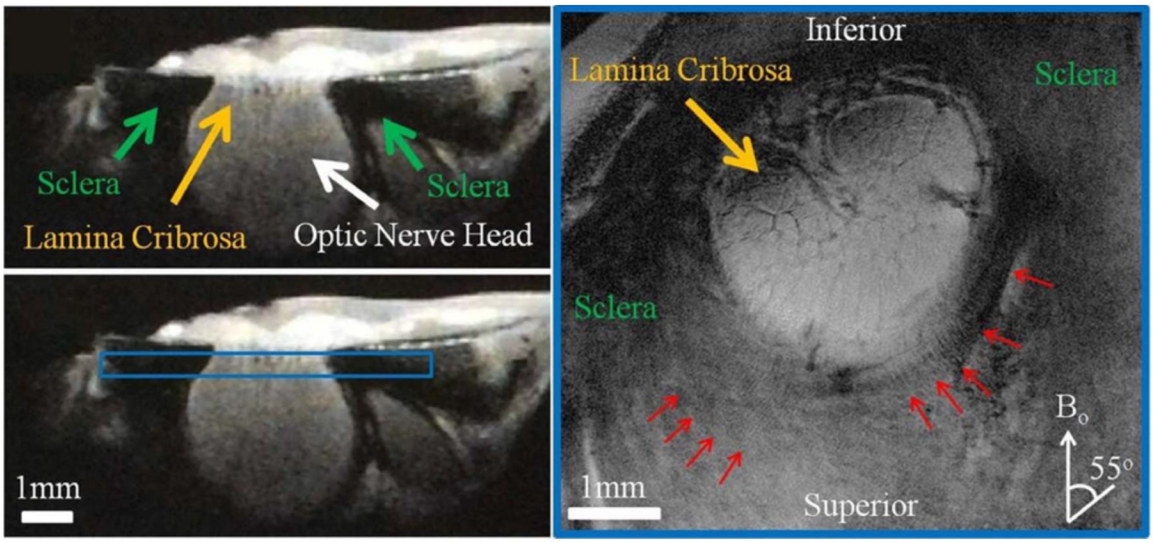

Figure 17:

High-resolution T2*-weighted MR images of the unloaded ovine sclera near the optic nerve head. The left panels show the cross-section of the sclera, optic nerve head, and lamina cribrosa in sagittal view. The right panel shows the coronal T2*-weighted image oriented as the blue box in the left panel at 16 × 16 μm^2 in-plane resolution and repetition time/echo time = 3000/9.5 ms. Details of the lamina cribrosa (yellow arrow) within the optic nerve head and the distributions of crimps (red arrows) in the scleral fibres surrounding the optic nerve head were revealed especially at orientations near the magic angle at approximately 55° to the main magnetic field (B0). Figure adapted from (Ho et al., 2014) with permission of the Association for Research in Vision and Ophthalmology.

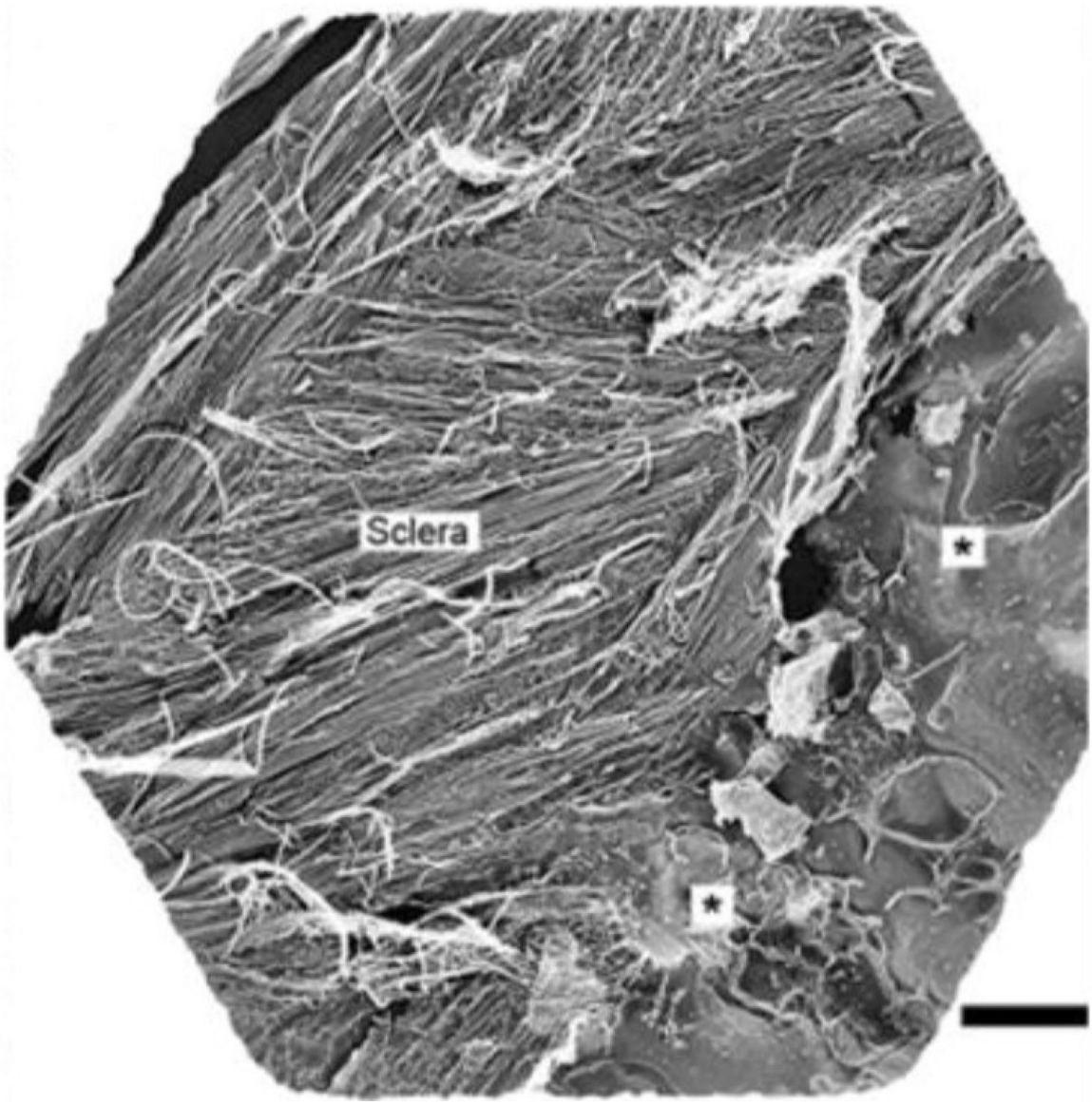

Figure 18:

Quick-freeze deep-etch (QFDE) electron microscopy image of mouse posterior sclera, revealing layers of differentially oriented collagen lamellae in 3D. On the right side of the image (*) can be seen an area of partially etched, vitrified ice - a product of the “freeze-fracture” processing that can preserve native hydrated structure more closely than is possible with conventional electron microscopy sample preparation. Scale bar: 2 μm. Figure reproduced from (Ismail et al., 2017) with permission of Elsevier Ltd.

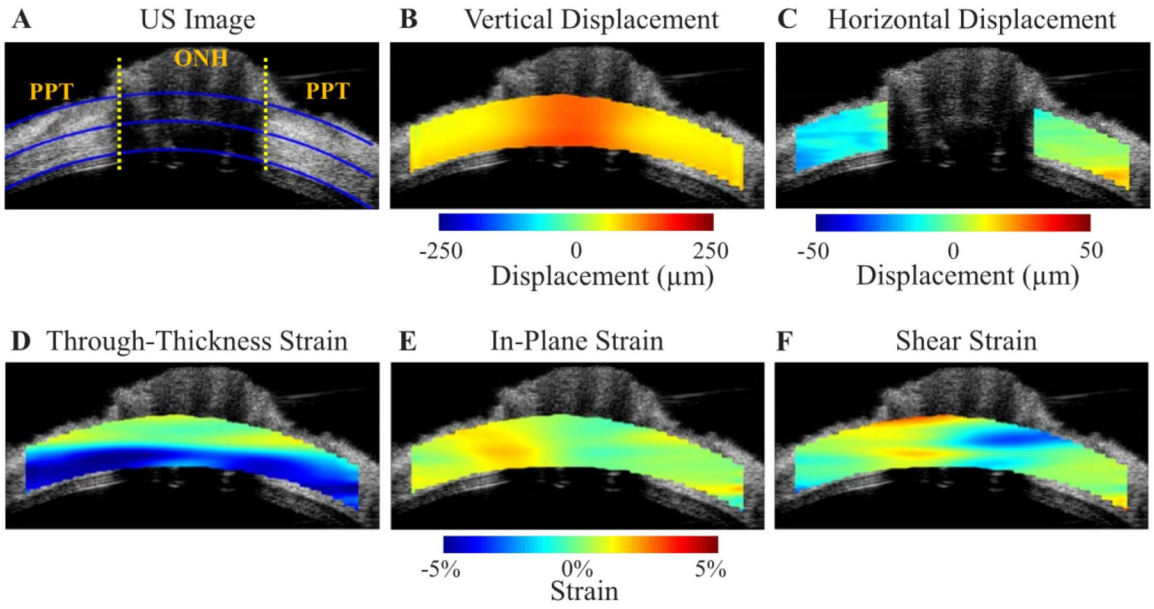

Figure 19:

Ultrasound (US) speckle tracking of scleral and ONH deformation under inflation testing. US image **A)** and colour maps of vertical displacement **B)**, horizontal displacement **C)**, and strains **(D–F)** for a representative human donor eye at 30 mm Hg. The yellow dotted lines in A) indicate the boundaries between ONH and peripapillary tissue (PPT), the inner and outer blue lines are fitted curves for demarcation of region of interest (ROI) for strain analysis, and the middle blue line is used to divide the anterior and posterior halves. Note that the retina is largely excluded from the ROI. Positive displacements = upward vertical movement or rightward horizontal movement. Vertical displacements were larger within the ONH. The horizontal displacement of PPT was negative on average on the left side of ONH and positive on the right side of ONH, indicating a small scleral canal expansion. Through-thickness compression was largest in magnitude and concentrated in the anterior half of the ONH and PPT. Reproduced from (Ma et al., 2019) with permission of the Association for Research in Vision and Ophthalmology.

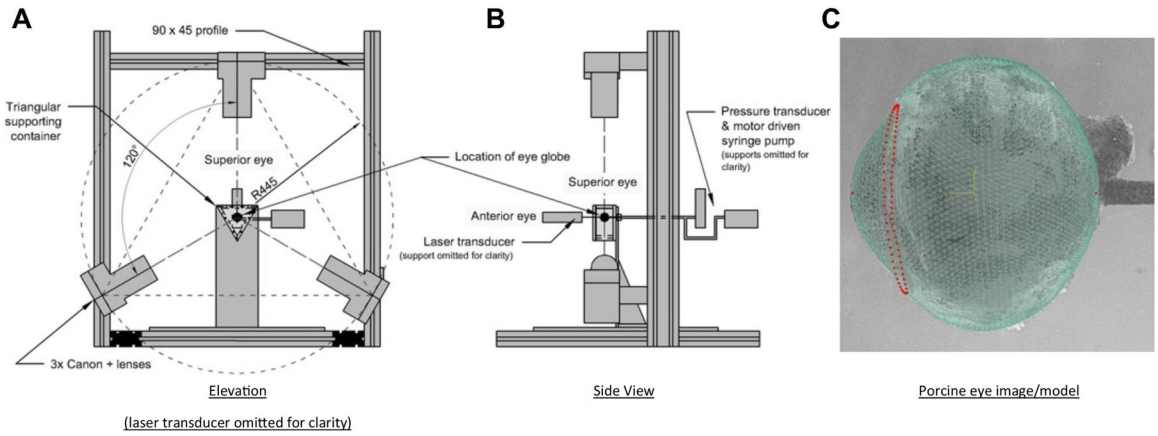

Figure 20:

Inflation testing of intact eye globe. **A)** Elevation view diagram of the whole eye globe inflation testing rig set-up. **B)** Side view of the rig set-up. **C)** Match between modelled and imaged topography of the eye globe. The FE nodes representing the corneal apex, posterior pole and limbal ring are highlighted in red. Adapted from (Whitford et al., 2016) under Creative Commons License 4.0.

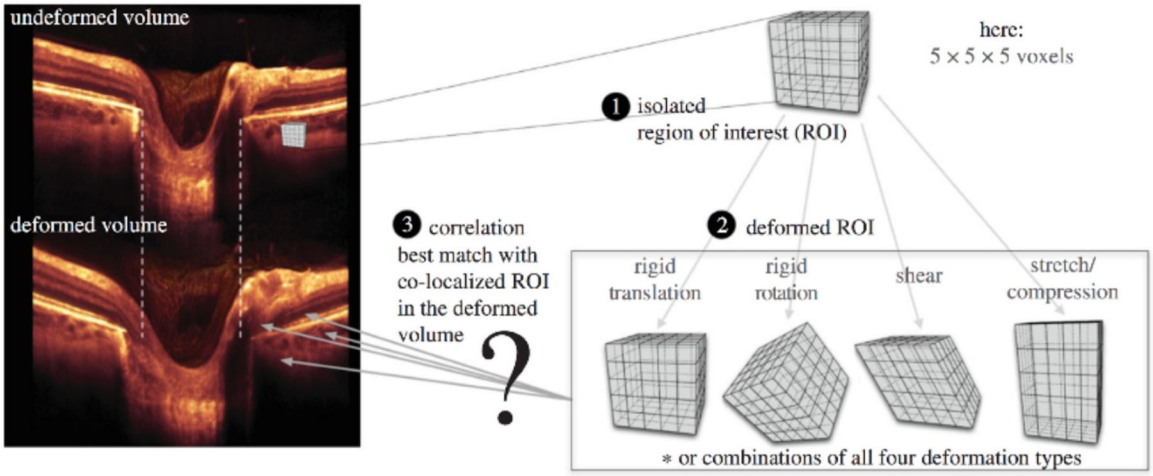

Figure 21:

Steps to track IOP-induced displacement of a single scleral point in vivo. **1)** an ROI is created in the undeformed OCT volume; **2)** The ROI undergoes a combination of affine transformations (translation, rotation, shear and stretch); **3)** a displacement vector can be extracted when the deformed ROI best matches a co-localised ROI in the deformed volume. Adapted from (Girard et al., 2013) with permission of the authors.

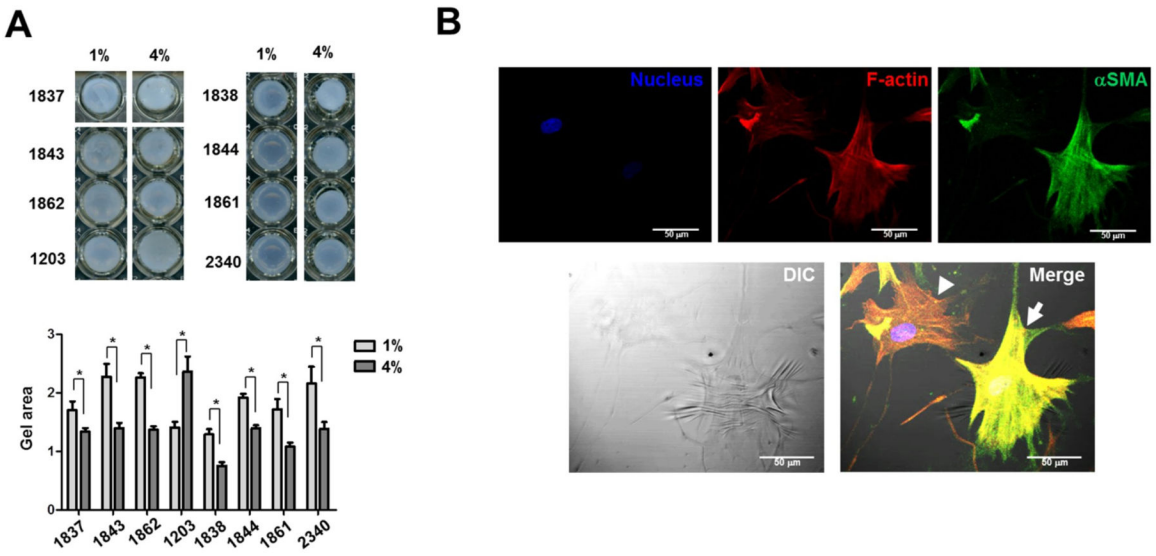

Figure 22:

Simulated IOP promotes contractility in cultured human scleral fibroblasts. **A)** Fibroblast contractility in response to 1% or 4% cyclic strain at 5 Hz for 24 hours, assessed by a 3D collagen gel–based assay. The numbers refer to cell quantities, while the vertical graph axis denotes relative gel area (a.u.) as measured in ImageJ. **B)** Phase-contrast and confocal immunofluorescent images overlaid to show the correlation between expression of intracellular contractile apparatus (αSMA and F-actin) and wrinkle formation. Arrow indicates a wrinkle-forming myofibroblast. Arrowhead indicates a non–wrinkle-forming fibroblast. Red: F-actin, Green: αSMA, Blue: DAPI. Scale bar: 50 μm. Reproduced from (Qu et al., 2015) with permission of the Association for Research in Vision and Ophthalmology.

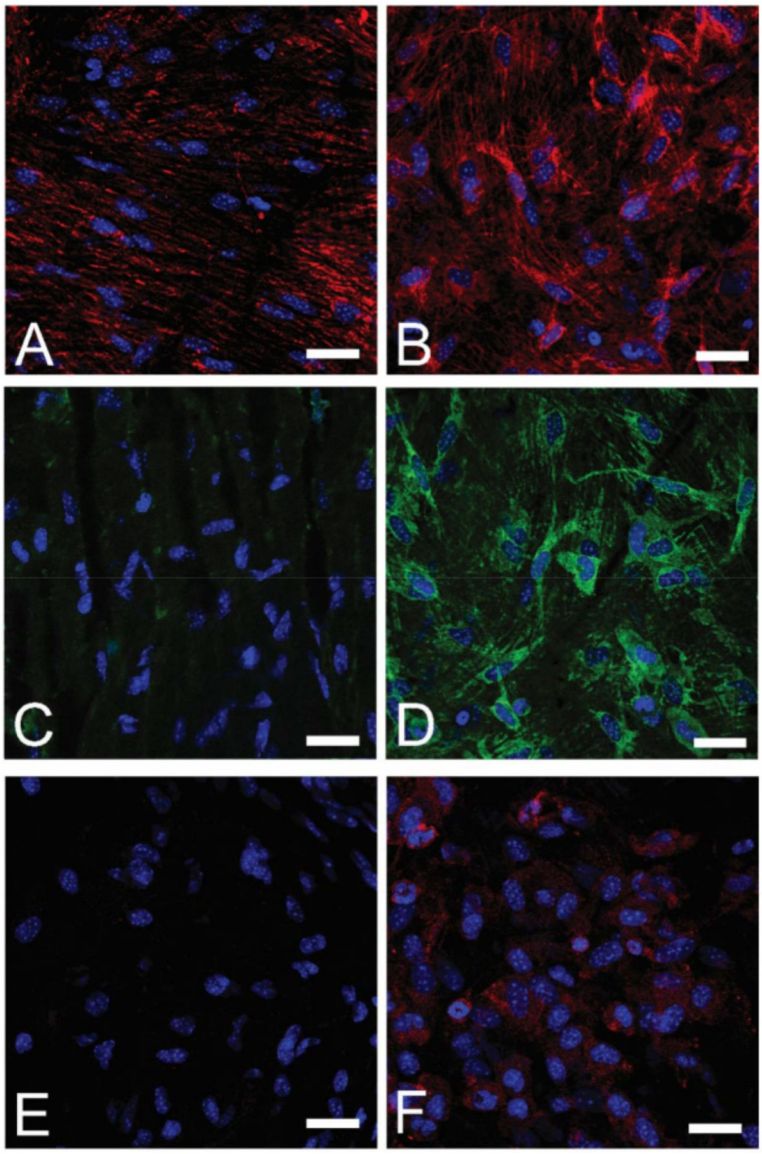

Figure 23:

Experimental glaucoma increases cell proliferation and myofibroblast differentiation in mouse sclera. *Top row*: Immunohistochemical labelling of vimentin (red) in **A)** control and **B)** 3-day glaucoma scleral wholemounts. *Middle row*:→SMA labelling (green) in **C)** control and **D)** 3-day glaucoma. *Bottom row*: cell adhesion molecule →actinin labelling (red) in **E)** control and **F)** 3-day glaucoma. DAPI nuclear counterstain is shown in blue in all panels. Scale bars = 20um. Reproduced from (Oglesby et al., 2016) with permission of Molecular Vision.

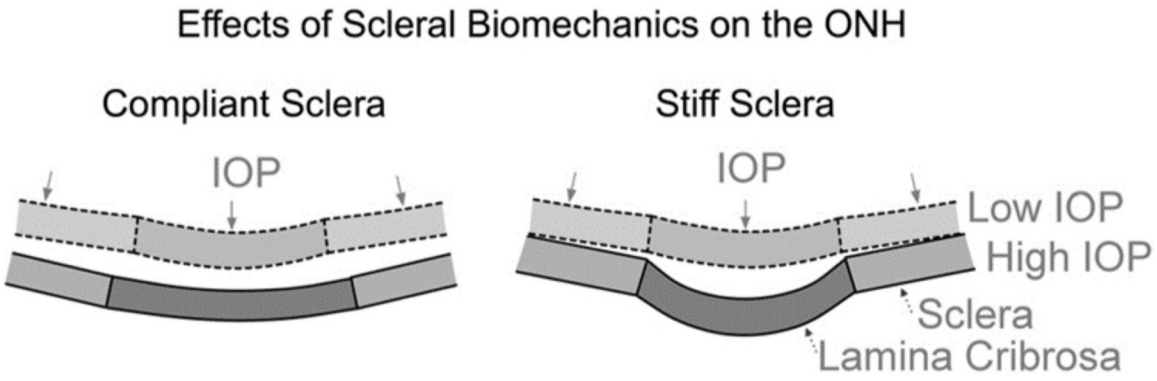

Figure 24:

A schematic illustration of how the stiffness of the sclera affects the IOP-induced ONH deformations. In the case of a compliant sclera (left), an increase in IOP induces large scleral deformations, which are transmitted to the scleral canal, resulting in a large scleral canal expansion that pulls the lamina taut. Conversely, a stiff sclera deforms little under IOP (right), with a small scleral canal expansion, allowing the lamina to be displaced posteriorly by the action of IOP on its anterior surface. Figure adapted from (Sigal et al., 2011b) with permission of the Association for Research in Vision and Ophthalmology.

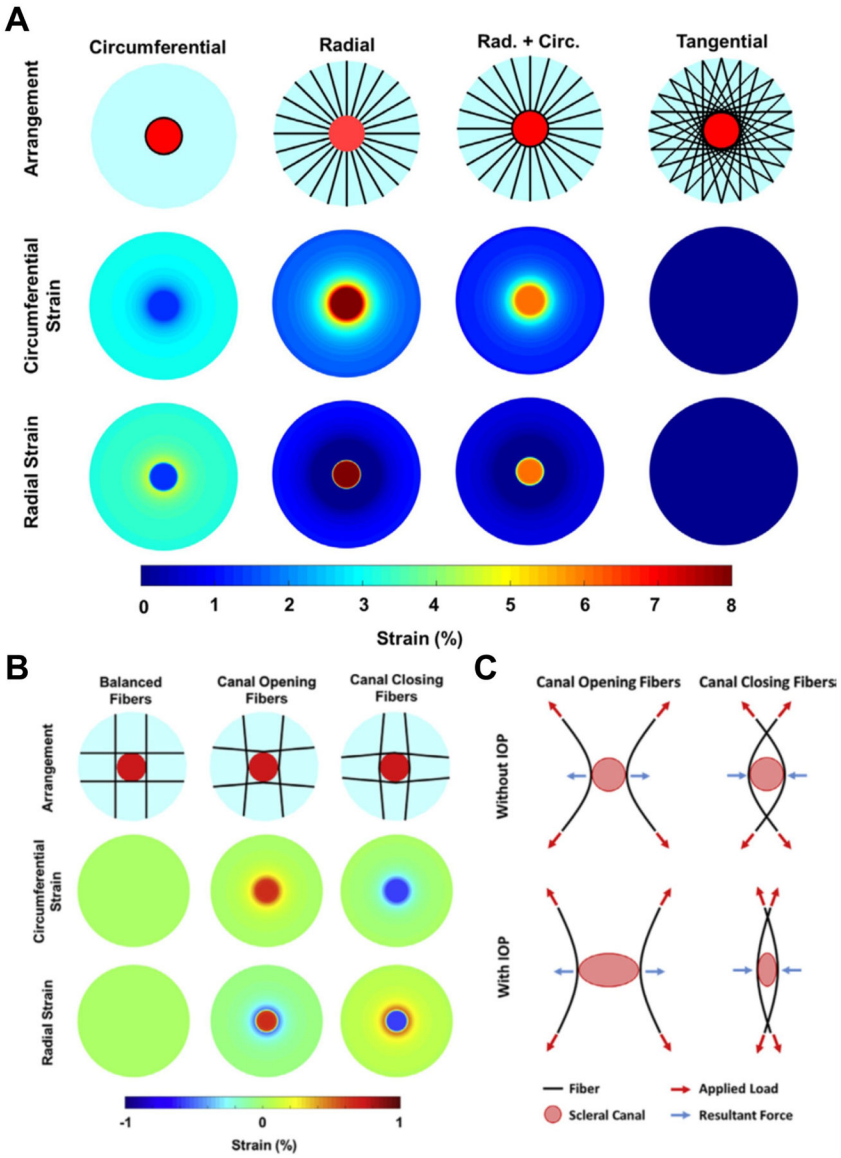

Figure 25:

A) Computational models used to simulate the biomechanical behavior of four theoretical collagen fibre arrangements (top row). Shown in light blue is the posterior sclera, with the scleral canal as a red disc. The black lines represent the collagen fibres. On the middle and bottom row are shown contour levels of the magnitude of the deformations (strain) due to an IOP elevation of 50 mmHg. A simple reinforcement of the canal with circumferential fibres limited the strain in the lamina due to IOP but did provide support to the sclera. Conversely, a radial arrangement of fibres reduced the strain in the sclera, but lead to high strains within the lamina. The combination of radial and circumferential fibres still caused high strains in the lamina. A tangential arrangement of fibres provided the best reinforcement for both the sclera and the lamina, reducing the strains to near zero-levels. Depending on the fibre curvature, long fibres tangential to the canal can have substantially different responses to IOP increases. **B)** Maps of IOP-induced strain for three different fibre curvatures. When the

fibres were concave to the canal (Canal Closing Fibers), increased IOP caused the canal to close, and lamina compression. When the fibres were convex (Canal Opening Fibers), increased IOP caused the canal to open and the lamina to stretch. Note that the models incorporated many fibres. For simplicity, only a few are shown. **C)** Diagram of the mechanism of action of long tangential fibres. For concave fibres, the load from IOP results in an outward tensile force at the canal boundary as the fibres straighten. For convex fibres, the load from IOP results in an inward compressive force at the canal boundary as the fibres straighten. Figure adapted from (Voorhees et al., 2018) with permission of Acta Biomaterialia.

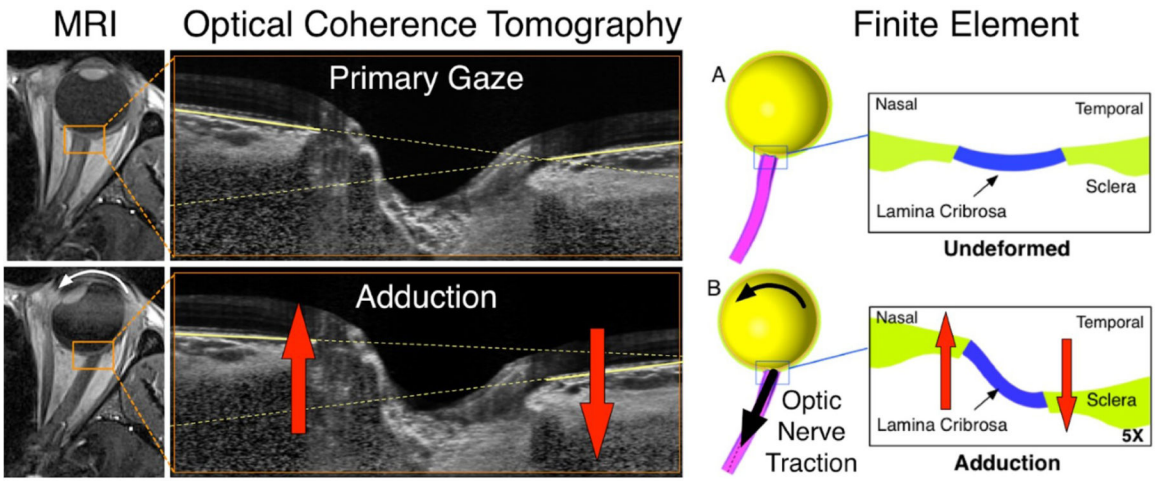

Figure 26:

Magnetic resonance imaging (left), optical coherence tomography imaging (centre), and finite element modelling (right) all strongly suggest that the optic nerve applies a traction force onto the back of the eye during eye movements. The net result is shearing of the optic nerve head tissues (red arrows). Note that deformations were magnified 5 times in the finite element models to aid visual interpretation. Adapted from Wang et al., 2016a and Wang et al., 2017 with permission of the Association for Research in Vision and Ophthalmology.

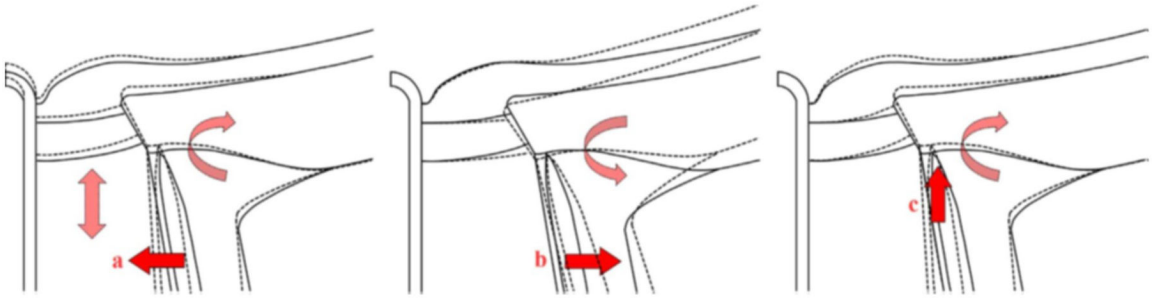

Figure 27:

A schematic description of three mechanisms by which increases in CSFP cause ONH deformations. Undeformed ONH is shown with continuous lines, and deformed ONH with dashed lines. **(a)** CSFP acts inwardly compressing the pia mater and the retrolaminar neural tissue within. Due to the Poisson effect, lateral compression may cause expansion in the axial direction, increasing retrolaminar pressure (Morgan et al., 1995) “pushing” anteriorly on the lamina and causing clockwise rotation of the PPS. **(b)** CSFP acts outwardly on the dura mater away from the pia mater, causing the known distension of the dural sheath, (Killer et al., 2003) rotating the PPS counterclockwise, and displacing the periphery of the lamina posteriorly. **(c)** CSFP “pushes” the PPS anteriorly, causing flattening of the globe and clockwise rotation of the PPS, and displacing the periphery of the lamina anteriorly. Figure adapted from (Hua et al., 2018) with permission of the Association for Research in Vision and Ophthalmology.

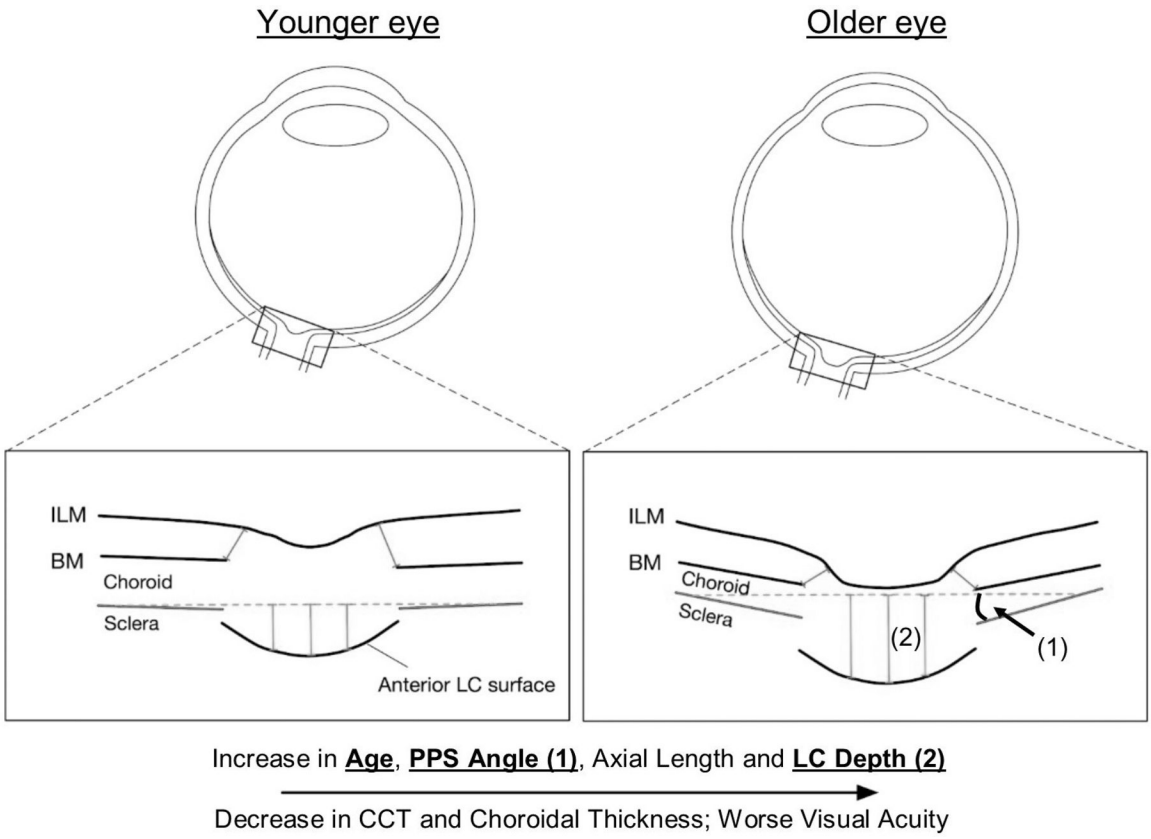

Figure 28:

Determinants of the peripapillary sclera (PPS) angle in healthy eyes. An increase in the v-shaped configuration of the peripapillary sclera (PPS) is associated with increasing age, longer axial length, thinner central corneal thickness (CCT), thinner choroidal thickness, worse vision and an increase in lamina cribrosa (LC) depth. Adapted from (Tun et al., 2019) with permission of the Association for Research in Vision and Ophthalmology.

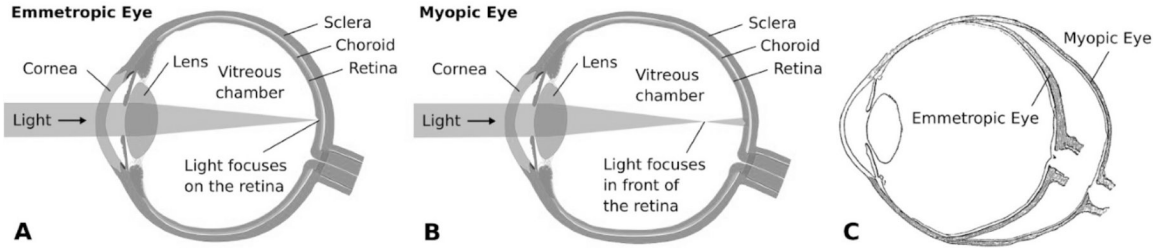

Figure 29:

Effect of myopia on eye shape. **A)** Emmetropia is the visual condition of the normal eye with clear vision. This condition is achieved when the axial length of the eye matches the refractive power of the cornea and lens, such that light rays are focused exactly on the retina. **B)** A myopic eye is too long for its optical components and light focuses in front of the retina causing faraway objects to appear blurry. **C)** Overlaid histologic sections of the emmetropic eye and the contralateral, highly myopic eye of the same donor showing the extended posterior segment of the myopic eye. The anatomy of the anterior segment is nearly identical in both eyes. In contrast, the posterior segment of the myopic eye is elongated compared to the emmetropic eye, causing the typical increase in axial length seen in myopia. Reproduced from (Grytz, 2018) with permission of Kugler Publications.

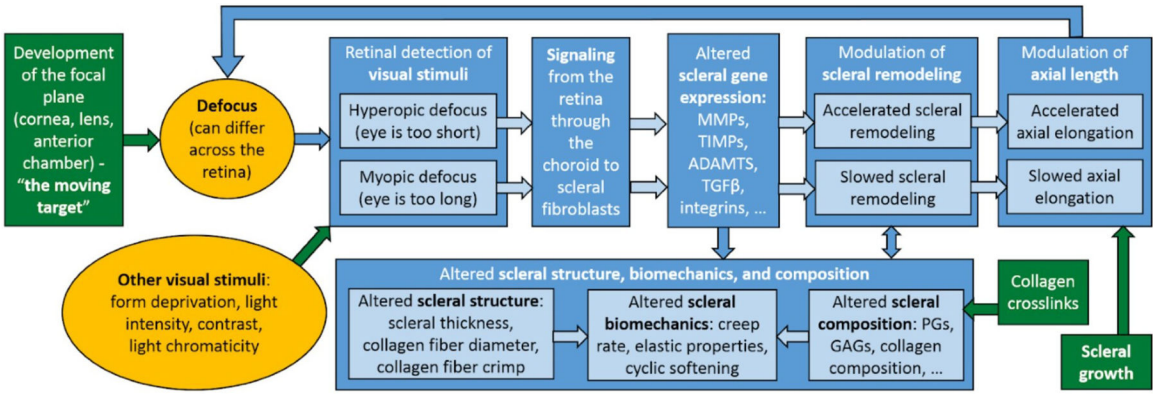

Figure 30:

The emmetropization process and factors that impact the refractive development of the eye. Mechanisms highlighted in yellow represent visual stimuli and environmental factors that impact the refractive development of the eye. Mechanisms highlighted in blue are thought to be involved in the feedback mechanism. Mechanisms highlighted in green are believed to impact the refractive development of the eye without modulation by the feedback mechanism. Reproduced from (Grytz, 2018) with permission of Kugler Publications.

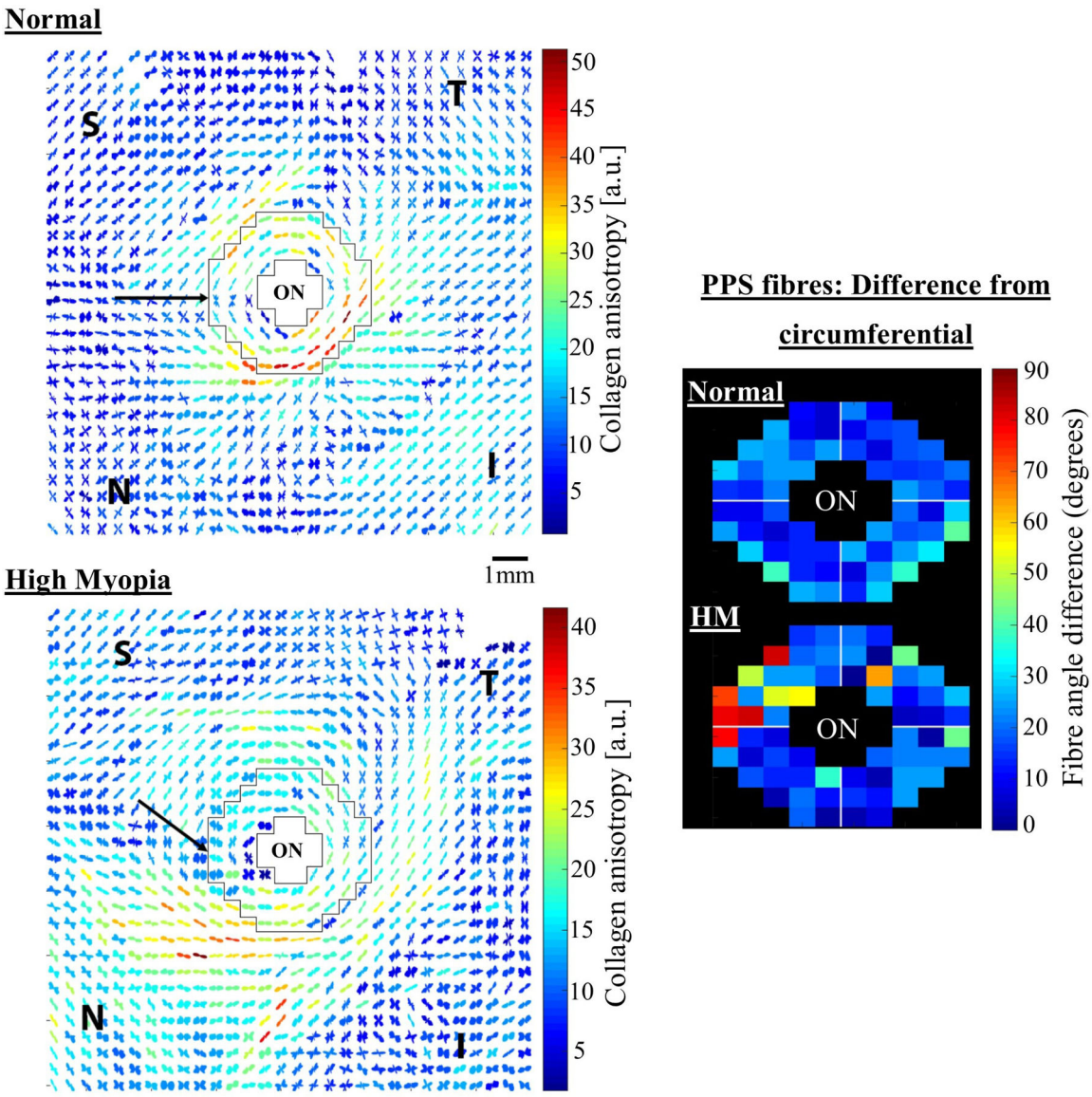

Figure 31:

Bulk collagen microstructural changes in human high myopia. *Left panel*: WAXS polar vector maps of collagen orientation in (top) a normal and (bottom) a high myopia flat-mount human posterior sclera. The peripapillary sclera, bordering the optic nerve, is shown bounded in black. Note myopic alteration to collagen directions in this region. The normal sclera features a predominantly circumferential pattern, with only a slight interruption in the superior (S)-nasal (N) aspect. However the S-N interruption is far more widespread in the highly myopic eye (arrows), suggesting an unravelling of the normal structure in high myopia. *Right panel*: fibre displacement angle from perfect circumferential alignment in (top) average of 7 normal specimens and (bottom) the high myopia specimen. ON: optic nerve. Figure adapted from (Markov et al., 2018) with permission of Molecular Vision.

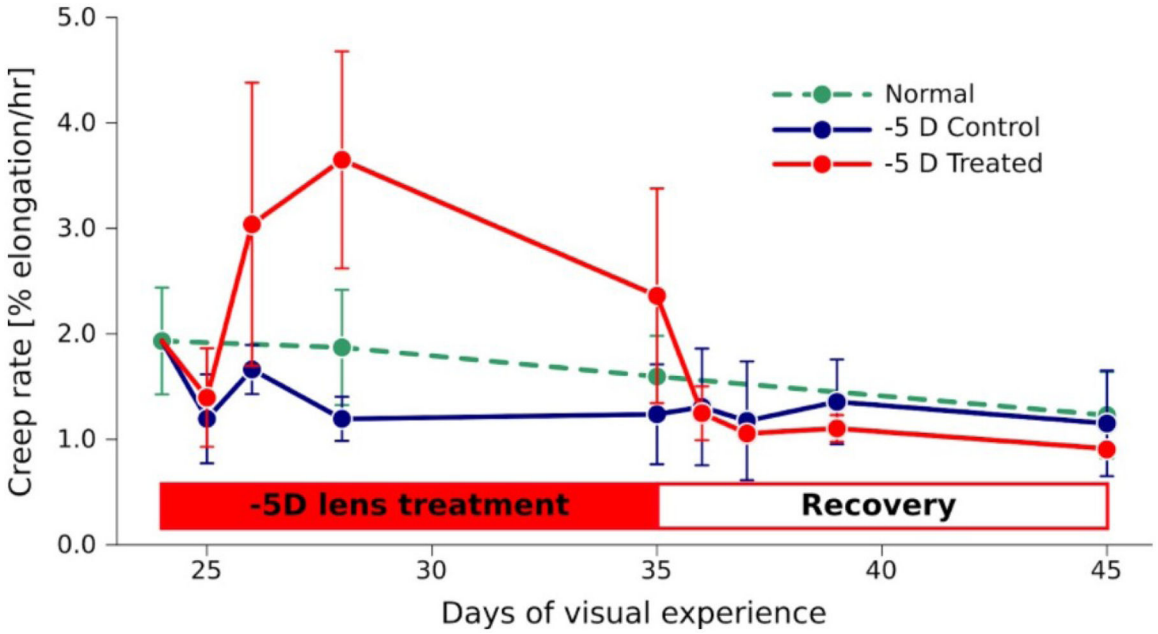

Figure 32:

Regulation of scleral creep rate in tree shrews during experimentally induced myopia (−5D lens treatment) and recovery. Axial elongation was accelerated in the treated eye during monocular - 5D lens treatment and slowed during recovery from −5D lens wear (lens removal). Creep rate increased/decreased in the treated eye during lens treatment/recovery. The creep rate of the control eye and normal animals without lens treatment are shown for comparison. Reproduced from (Grytz, 2018) with permission of Kugler Publications.

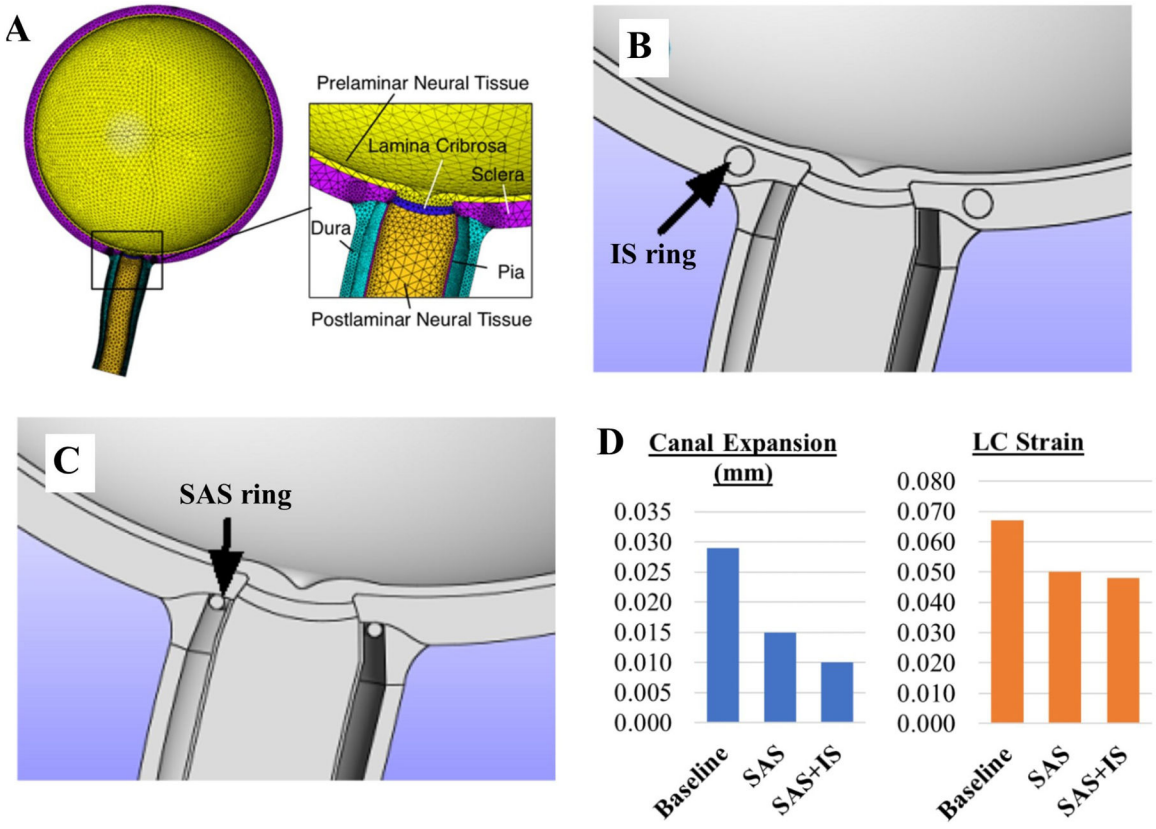

Figure 33:

Computational modelling of theoretical posterior segment ring implants as a potential glaucoma therapy. **A)** Generic human eye model geometry and FE mesh. **B)** Proposed intrascleral (IS) ring implant (implant material stiffness = 200GPa). **C)** Alternative ring implant (200GPa stiffness) located in the subarachnoid space (SAS). **D)** Effect of SAS and IS+SAS combination implants on calculated ONH deformation behaviour, under a simulated IOP of 50mmHg. A maximum 66% reduction in scleral canal expansion and a 28% reduction in LC strain are predicted by the model under the double ring combination implant strategy. Adapted from (Soh, 2016) under Creative Commons License 4.0.

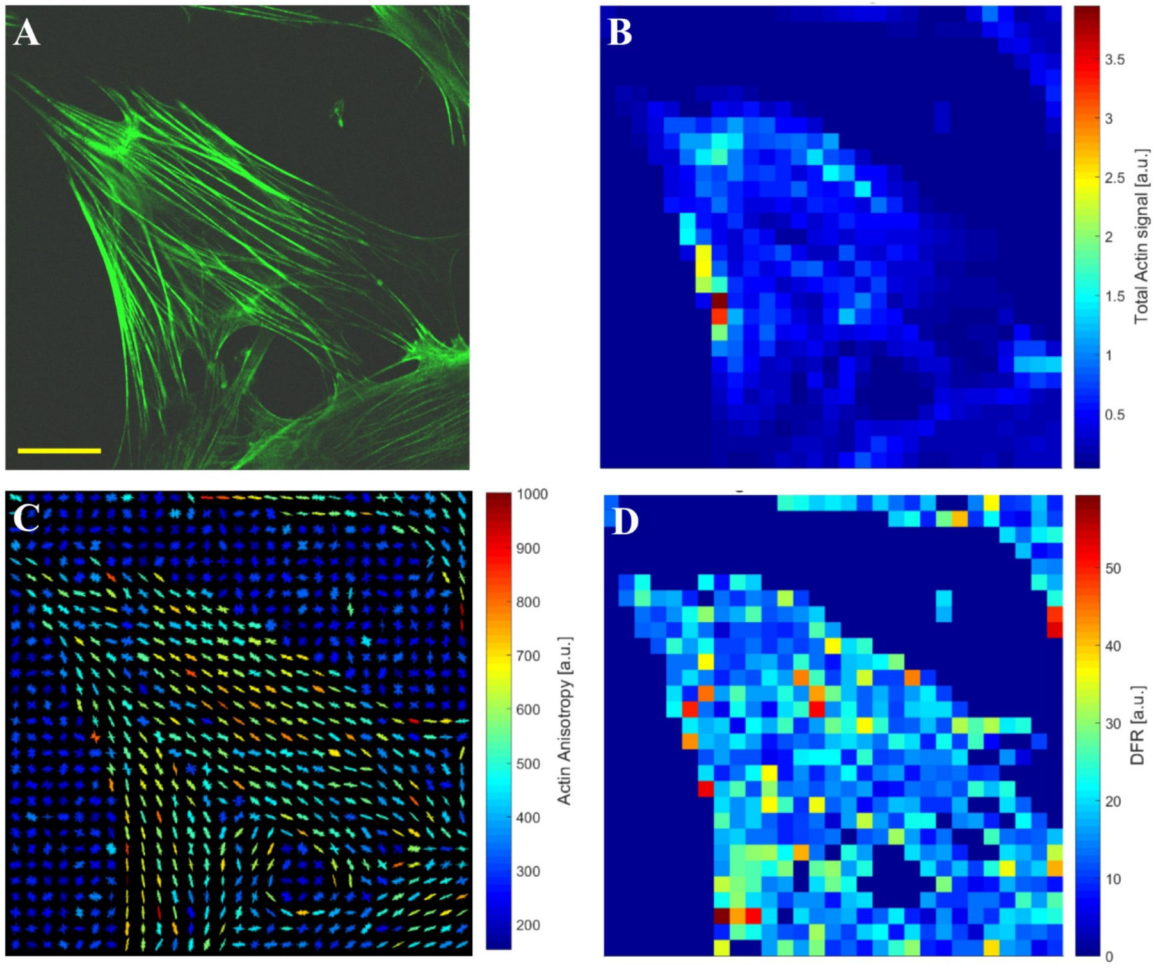

Figure 34:

Fourier analysis of mechanical load-induced F-actin stress fibre networks in cultured bovine scleral fibroblasts. **A)** Confocal image showing green cytoskeletal stress fibres of F-actin, stained with Alexa-488® phalloidin (bar = 25um). **B)** Map of integrated actin signal, sampled every 5um. **C)** Polar vector map of actin fibre orientation from analysis of Fourier power spectrum. **D)** Map of degree of fibre recruitment (DFR) around the principal fibre direction. Reproduced from (Pijanka et al., 2019) with permission of the Journal of Biophotonics.

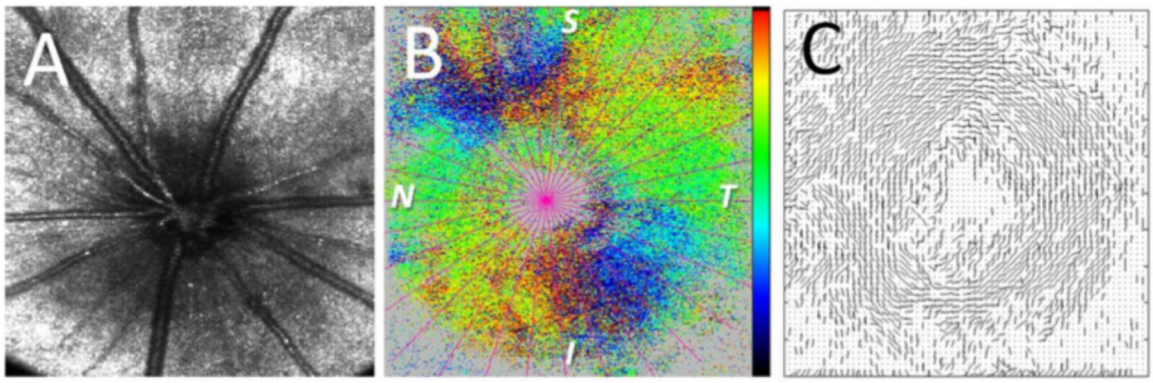

Figure 35:

A) Fundus image of the rat ONH. **B)** Collagen fibre orientations (colour map) in the peripapillary sclera about 160 um posterior to the retinal pigment epithelium. Colour scale: −90 to 90 degrees. S, T, I, N: superior, temporal, inferior, nasal. **C)** Preferred collagen fibre orientations in the peripapillary sclera showing a ring pattern. Adapted from (Baumann et al., 2014) with permission of the Association for Research in Vision and Ophthalmology.

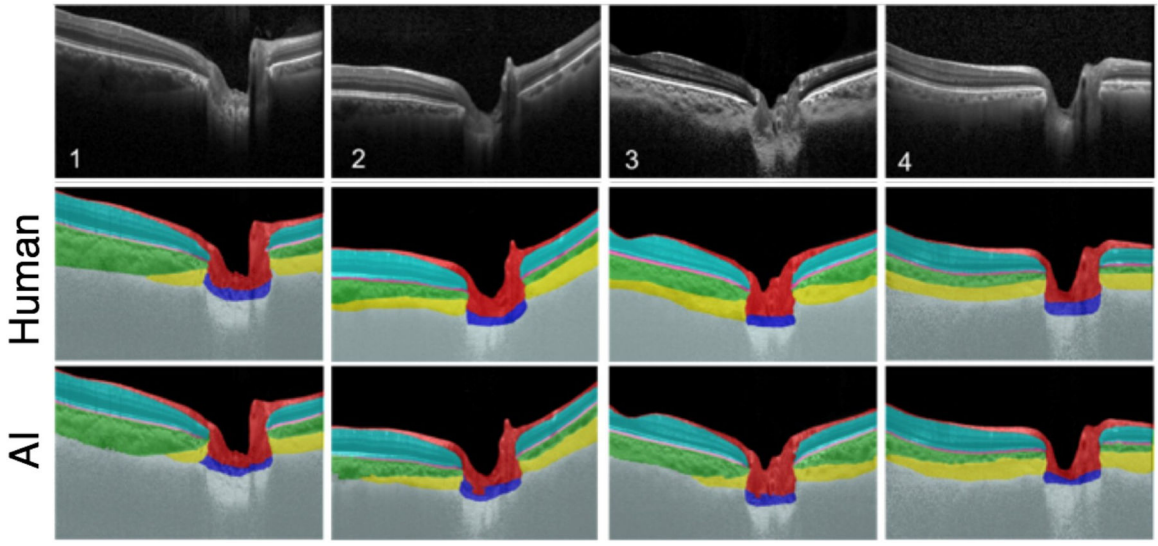

Figure 36:

Automated segmentation of ONH connective and neural tissues using artificial intelligence (AI) computing. The peripapillary sclera is shown in yellow. The performance of AI is now similar to that of a human expert.

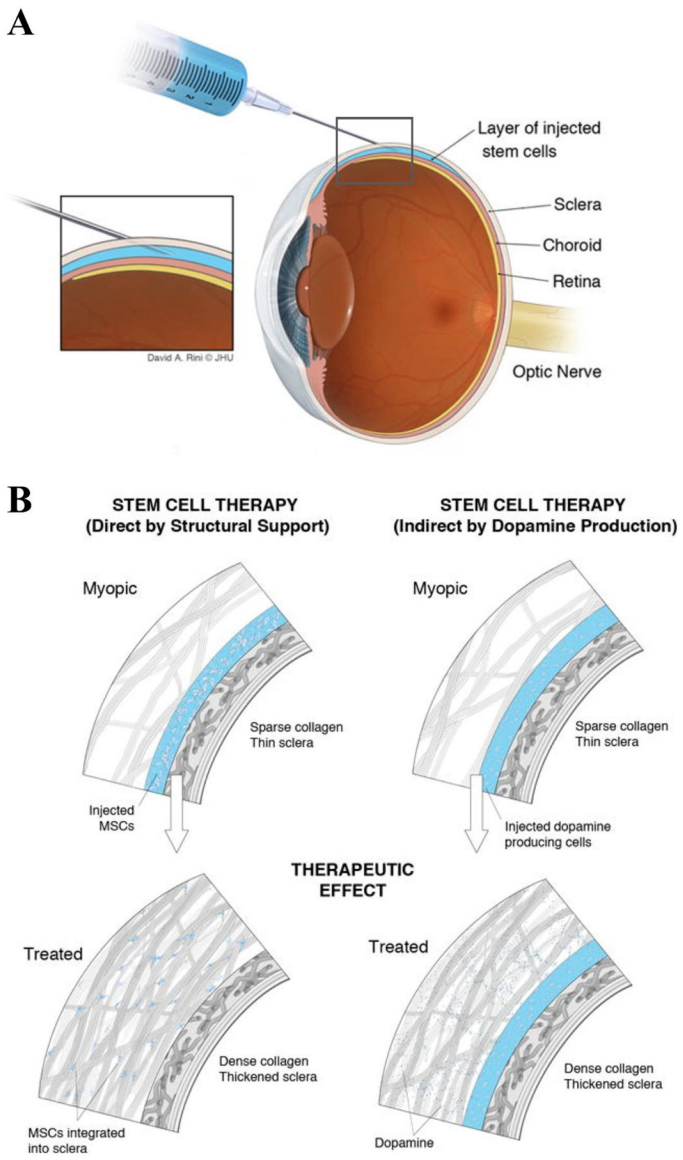

Figure 37:

Potential stem cell treatment for progressive myopia. **A)** Injection of a mesenchymal stem cell suspension into the subscleral space. **B)** Dual mechanisms for the possible prevention of myopic eye elongation. *Left*: Integration of stem cells into the scleral stroma for direct mechanical support. *Right*: Indirect stimulation of the scleral tissue via dopamine production. Adapted from (Janowski et al., 2015) with permission of AlphaMed Press.

Table 1:

Approximate composition of the human sclera.

Component	% of wet weight
Water	68
Collagens	28
Other proteins (including cell components)	<3
Proteoglycans	<1
Elastin	0.6